WWW.OEAW.AC.AT

ÖAW ÖSTERREICHISCHE AKADEMIE DER WISSENSCHAFTEN

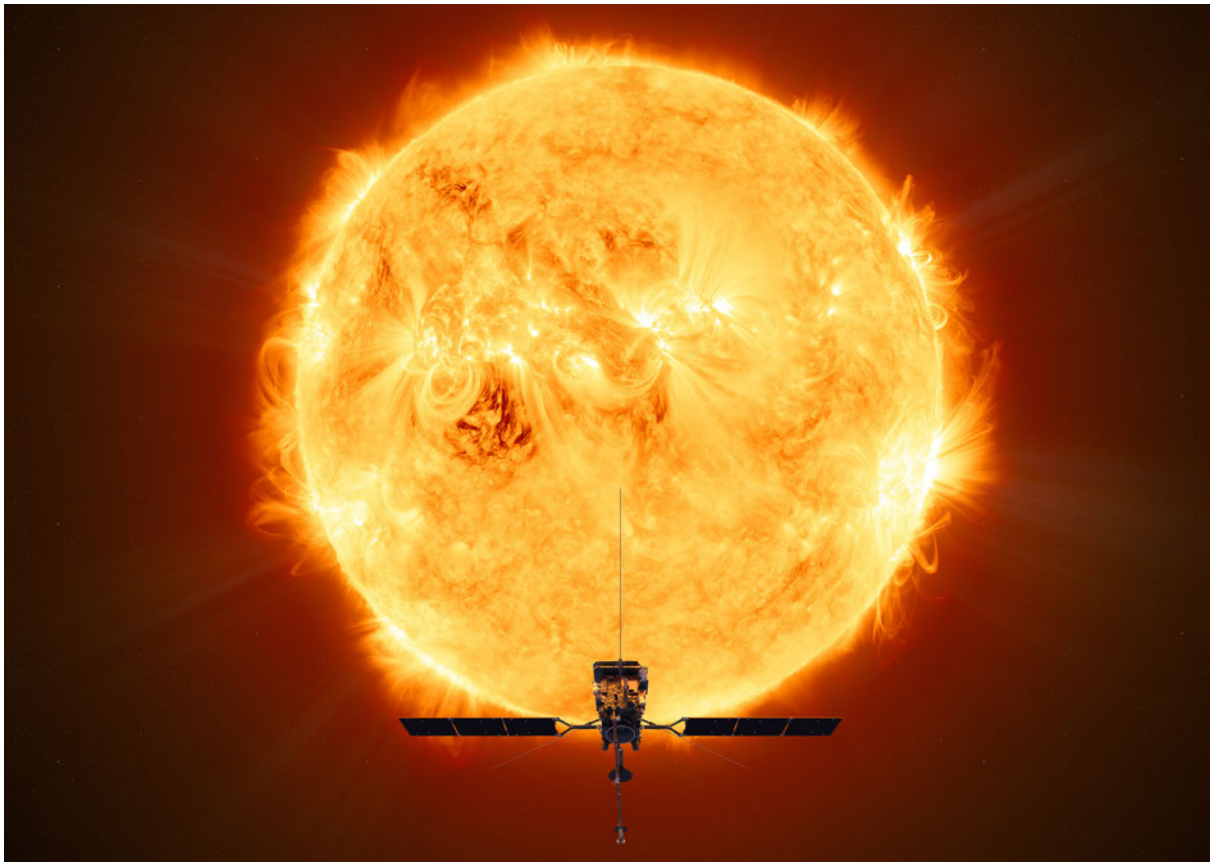

ANNUAL REPORT 2020

IWF INSTITUT FÜR WELTRAUMFORSCHUNG

WWW.OEAW.AC.AT/IWF

ÖAW ÖSTERREICHISCHE AKADEMIE DER WISSENSCHAFTEN

IWF INSTITUT FÜR WELTRAUMFORSCHUNG

COVER IMAGE

Artist's impression of ESA's *Solar Orbiter* mission, which will face the Sun from within the orbit of Mercury at its closest approach (© ESA/ATG medialab).

TABLE OF CONTENTS

INTRODUCTION

The Space Research Institute (Institut für Weltraumforschung, IWF) in Graz focuses on the physics of our solar system and exoplanets. With about 100 staff members from 20 nations it is one of the largest institutes of the Austrian Academy of Sciences (Österreichische Akademie der Wissenschaften, ÖAW).

IWF develops and builds space-qualified instruments and analyzes and interprets the data returned by them. Its core engineering expertise is in building magnetometers and on-board computers, as well as in satellite laser ranging, which is performed at a station operated by IWF at the Lustbühel Observatory. In terms of science, the institute concentrates on dynamical processes in space plasma physics, the upper atmospheres of planets and on exoplanets.

IWF cooperates closely with space agencies all over the world and with numerous other national and international research institutions. A particularly intense cooperation exists with the European Space Agency (ESA).

The institute is currently involved in twenty-one active and future international space missions; among these:

- The *Cluster* mission celebrated its 20th anniversary in 2020 and still provides unique data to better understand space plasma.
- For already five years, the four *MMS* spacecraft explore the acceleration processes that govern the dynamics of the Earth's magnetosphere.
- The first China Seismo-Electromagnetic Satellite *(CSES-1)* has studied the Earth's ionosphere since 2018. *CSES-2* will follow in 2022.
- On its way to Mercury, *BepiColombo*, had gravity assist maneuvers at Earth (March) and Venus (October). It will investigate the planet, using two orbiters, one specialized in magnetospheric studies and one in remote sensing.
- In its first operational year, *CHEOPS (CHaracterizing ExOPlanets Satellite)* has already provided significant results about the characteristics of exoplanets orbiting bright stars.
- Along its innovative trajectory, ESA's *Solar Orbiter* flew by Venus in December to change its orbit around the Sun.

A United Launch Alliance (ULA) Atlas V rocket carrying *Solar Orbiter* lifts off on 9 February 2020 at 11:03 p.m. EST (© ULA).

- ESA's *JUpiter ICy moons Explorer (JUICE*, launch: 2022) will investigate Jupiter and three of its largest moons, Ganymede, Callisto, and Europa.
- *FORESAIL-2* (launch: 2023) is one of three CubeSats to characterize the variability of ultra-low frequency waves in the inner magnetosphere.
- *SMILE* (launch: 2023) is designed to study the interaction between the solar wind and Earth's magnetosphere.
- *PLATO (*launch: 2026) is a space-based observatory to search for planets orbiting alien stars.
- *Comet Interceptor* (launch: 2029) will characterize in detail, for the first time, a dynamically-new comet or interstellar object.

HIGHLIGHTS IN 2020

- The successful launch of *Solar Orbiter* marked the highlight at the beginning of the year. The Chinese *Tianwen-1* mission followed in July.
- Two studies in the "Journal of Geophysical Research" and "Geophysical Research Letters" explained the origin of bead-like structures in the aurora.
- In "Astronomy & Astrophysics" the first measurement results from *CHEOPS* were presented, characterizing the exoplanet WASP-189b in detail.
- In "Nature Communications" the first successful daylight space debris laser ranging was published.

THE YEAR 2020 IN NUMBERS

Members of the institute published 168 papers in refereed international journals, of which 42 were first author publications. During the same period, articles with authors from the institute were cited 7089 times in the international literature. In addition, 26 talks (11 invited) and 33 posters were presented (virtually) by IWF members at international conferences. Last but not least, institute members were involved in the organization of four international meetings.

IWF STRUCTURE AND FUNDING

The institute is led by Director Wolfgang Baumjohann. Werner Magnes serves as Deputy Director.

IWF is structured into six research groups:

- Exoplanets (Lead: Luca Fossati)
- Planetary Atmospheres (Lead: Helmut Lammer)
- Space Plasma Physics (Lead: Rumi Nakamura)
- On-Board Computers (Lead: Manfred Steller)
- Magnetometers (Lead: Werner Magnes)
- Satellite Laser Ranging (Lead: Georg Kirchner)

Most financial support is given by ÖAW. Significant support is also provided competitively by other national institutions, in particular the Austrian Research Promotion Agency (FFG) and the Austrian Science Fund (FWF). Furthermore, European institutions like ESA and the European Union contribute substantially.

Tianwen-1 was launched aboard a Long March 5 rocket from the Wenchang Space Center on 23 July 2020 (© CNSA).

NEAR-EARTH SPACE

Near-Earth space is a most suitable place to study fundamental space plasma processes through advanced, in-situ measurements of the charged particles together with electric and magnetic fields at high cadence. In particular, multi-point spacecraft missions enable to advance our understanding of complex plasma processes by differentiating spatial structure from temporal changes. IWF has been participating in a number of Near-Earth space missions from the planning and proposal phase, by developing and building new hardware, and by operating and calibrating the instruments. Data taken from these missions have been extensively analyzed at IWF with different methods and by theoretical modeling to compare with the observations.

New studies dealing with the interaction of the solar wind with the Earth's magnetosphere were completed using the data from the missions to which IWF contributes. Also theoretical and numerical studies helped to interpret the mission data. Among different results one of this year's highlights is the first 3D fully kinetic particle-in-cell simulation of a plasma instability called Kelvin-Helmholtz instability performed for a specific (i.e., southward) interplanetary magnetic field orientation. The simulation showed how the instability drives fast magnetic reconnection, which is the main scientific target of the *Magnetospheric Multi-Scale (MMS)* mission. The results will also significantly support the physical interpretation of *MMS* observations.

While *MMS* studies micro-scale processes, observations from the *Time History of Events and Macroscale Interactions during Substorms (THEMIS)* multi-spacecraft mission are suited for meso-scale magnetospheric boundary processes such as dipolarization fronts. This magnetic feature is considered to be produced in association with the interaction of plasma jets and the ambient magnetic field and is a major energy conversion region in the magnetotail. A detailed comparison between the *THEMIS* observations and a computer model of the plasma instability called interchange instability, unveiled detailed mechanisms how a localized magnetic field front structure is formed. The obtained knowledge from the near-Earth space observations contribute to enhancing our understanding of space plasma processes in other plasma environments within our solar system and beyond.

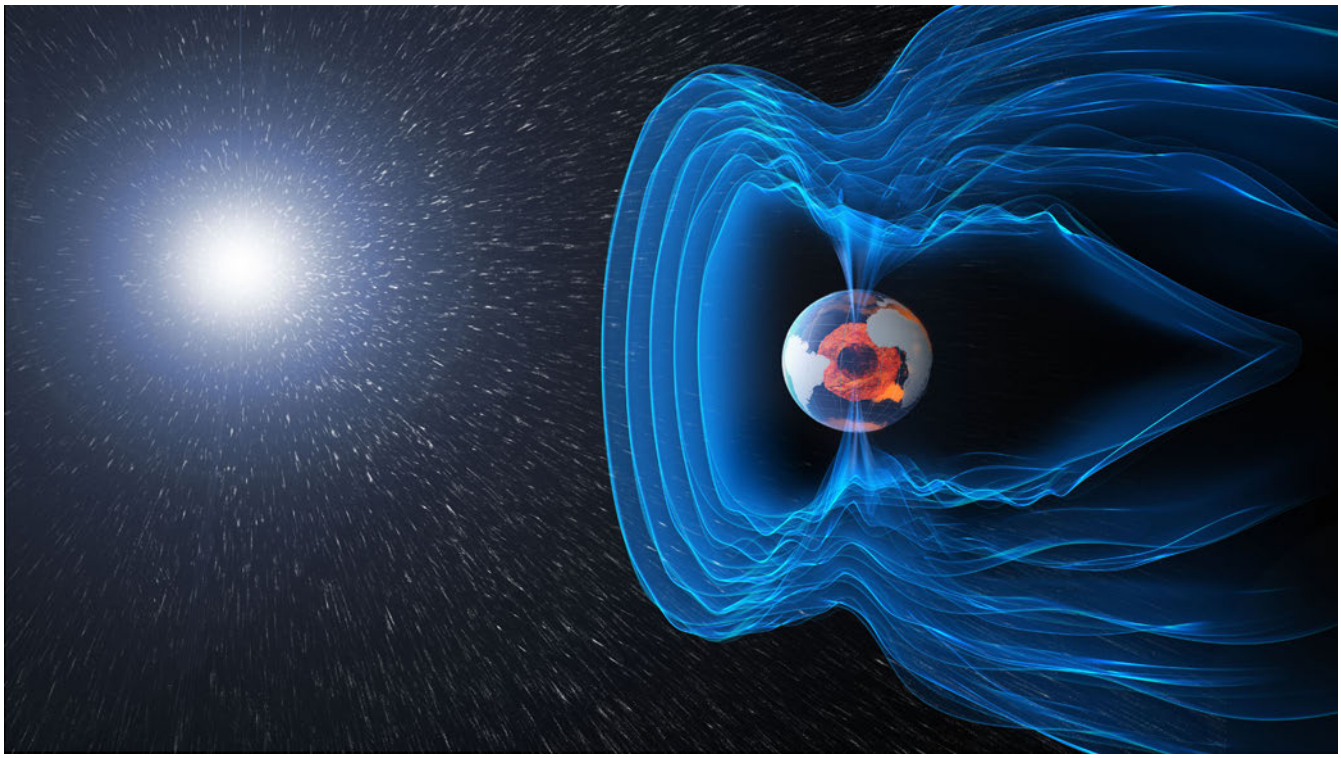

Artist's impression of the solar wind interaction with the Earth's magnetosphere (© ESA/AOES Medialab).

CLUSTER

ESA's *Cluster* mission is designed to study different plasma processes created by the interaction between the solar wind and the Earth's magnetosphere. This first four-spacecraft mission has been successfully operating for twenty years starting from its launch in August 2000 and is currently planned to be extended until 2022. IWF is Principal and/or Co-Investigator (PI/Co-I) of five instruments and has contributed to data archiving activities at the *Cluster Science Archives (CSA)* in addition to the science data analysis.

THEMIS/ARTEMIS

NASA's five-spacecraft mission *THEMIS (Time History of Events and Macroscale Interactions during Substorms)*, was launched in 2007. In 2010, the two outer spacecraft were renamed *ARTEMIS (Acceleration, Reconnection, Turbulence and Electrodynamics mission)* and put in orbit around the Moon. Both missions were extended until 2022. As Co-I of the magnetometer, IWF is processing and analyzing data.

MMS

NASA's *Magnetospheric Multi-Scale (MMS)* mission, launched in 2015, explores the dynamics of the Earth's magnetosphere and the underlying energy transfer processes. Four identically equipped spacecraft carry out measurements in the Earth's magnetosphere with highest temporal and spatial measurements ever flown in space. *MMS* investigates the small-scale basic plasma processes, which transport, accelerate and energize plasma in thin boundary and current layers. Extension of *MMS* has been approved until 2022.

IWF has taken the lead for the *Active Spacecraft POtential Control* of the satellites *(ASPOC)* and is participating in the *Electron Drift Instrument (EDI)* and the *Digital FluxGate magnetometer (DFG)*. In addition to the operation of these instruments and the scientific data analysis, IWF is contributing in inflight calibration activities and also deriving a new data product such as the density using controlled spacecraft potential.

A spacecraft in a plasma becomes charged due to a number of different processes. The two most important are photoelectron emission from the sunlit surfaces of the spacecraft and the collection of thermal electrons by the spacecraft. For the regulation of the spacecraft potential on *MMS* an *ASPOC* instrument was included, which reduces the potential by emitting a current.

If the photoelectron emission can be modelled, then the spacecraft potential can be used to obtain a measurement of the electron density. This has the advantage of an increased time resolution over direct measurements with plasma instruments. However, large external electric fields can accelerate lower energy photoelectrons that would not have energy to escape the spacecraft. This can cause the spacecraft potential to follow fluctuations in the electric field decreasing the quality of determination of the electron density from the spacecraft potential.

To correct for this effect, the following methodology was developed: The contribution of the electric field to the change in potential was determined empirically and then removed. An example from the *MMS* spacecraft of the corrected density estimation is shown in the figure below, where the measured potential is depicted in black and the corrected potential in red. The corrected potential determination matches well with other estimates of the electron density.

Roberts et al., J. Geophys. Res., 125, e2020JA027854, 2020.

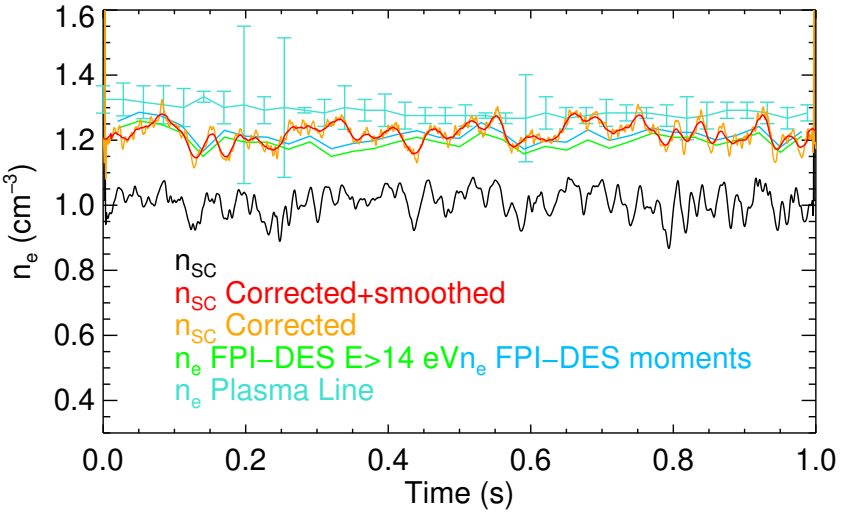

Several estimations of the electron density: the spacecraft potential not corrected for the electric field (black), the estimation where the electric field effect has been corrected and smoothed (red/orange). This agrees well with the estimates from the *Fast Plasma Investigation (FPI*, green) and the plasma frequency line (cyan).

CSES

The *China Seismo-Electromagnetic Satellites (CSES)* are scientific missions dedicated to the investigation and monitoring of varying electromagnetic fields and waves as well as plasma parameters and particle fluxes in the near-Earth space, which are induced by natural sources on ground like seismic and volcanic events.

After the successful launch of the first satellite *CSES-1* in February 2018, the second satellite *CSES-2* is scheduled for launch in 2022. It will be in the same Sun-synchronous circular low Earth orbit as *CSES-1*, with a local time of the descending node at 2 pm, but with a phase difference of 180 degrees. The combined observations of both satellites will double the detection probability of natural hazard-related events and will help to separate seismic from non-seismic events.

The *CSES* magnetometers, which are nearly identical on both spacecraft, have been developed in cooperation between the National Space Science Center (NSSC), the Institute of Experimental Physics of Graz University of Technology (TUG), and IWF. NSSC is responsible for the dual sensor fluxgate magnetometer, the instrument processor and the power supply unit, while IWF and TUG participate with the newly developed absolute scalar magnetometer, called *Coupled Dark State Magnetometer (CDSM).*

Throughout 2020, the magnetometer sensors of *CSES-1* operated continuously in good health. The data from the scalar sensor were e.g. used to derive its absolute error. This was done by comparing the measurements to magnetic field models, measurements from other satellite missions, and through a comprehensive study of the integrity of its own data. The latter was based on the comparison of all available instrument parameters in flight with the verification measurements performed on ground before launch. This led to a maximum uncertainty in the measurement of 1.1 nT as shown in the figure below.

Pollinger et al., Geosci. Instrum. Method. Data Syst., 9, 275-291, 2020.

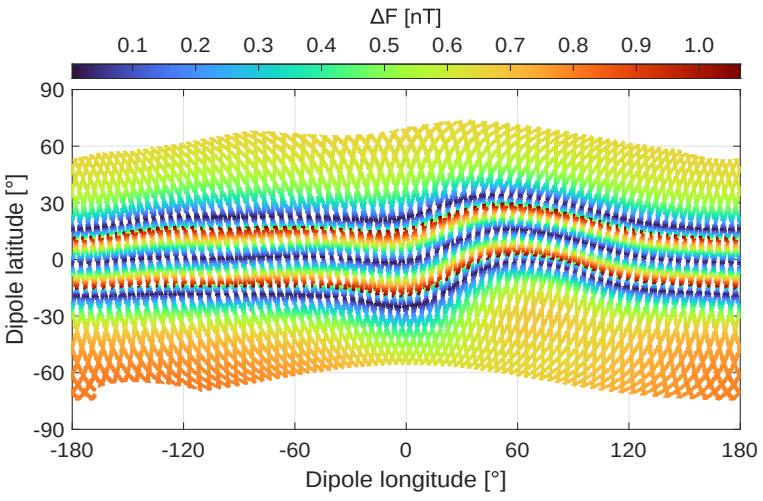

The worst case uncertainty of the magnetic field measurement by the scalar sensor aboard *CSES-1* as a function of geomagnetic coordinates.

GEO-KOMPSAT-2A

GEO-KOMPSAT-2A (GEOstationary KOrea Multi-Purpose SATellite-2A) is a South Korean meteorological and environmental satellite in geostationary orbit at 128.2° East, which also hosts a space weather environment monitoring system. The Korean Meteorological Administration managed the implementation of the satellite, launched in 2018, and the necessary ground segment. The space weather observations aboard *GEO-KOMPSAT-2A* are performed by the Korean Space Environment Monitor (KSEM), which was developed under the lead of the Kyung Hee University. It consists of a set of particle detectors, a charging monitor and a four-sensor *Service Oriented Spacecraft MAGnetometer (SOSMAG).*

The *SOSMAG* development was initiated and conducted by ESA as part of the Space Situational Awareness Programme and built by the *SOSMAG* consortium: IWF, Magson GmbH, Technische Universität Braunschweig, and Imperial College London. The *SOSMAG* instrument is a "ready-to-use" magnetometer avoiding the need of imposing magnetic cleanliness requirements onto the hosting spacecraft. This is achieved through the use of two high quality fluxgate sensors on an approximately one meter long boom and two additional magneto-resistive sensors mounted within the spacecraft body. The measurements of the two spacecraft sensors together with the inner boom sensor enable an automated correction of the outer boom sensor measurement for the dynamic stray fields from the spacecraft.

During the second year of operation, flight data verification, in-flight calibration and operation support were continued. Furthermore, the *SOSMAG* ground processor software was finished. It has been integrated in the Space Weather Service Network of ESA's Space Safety program in the second half of 2020 for a real time release of the *SOSMAG* data to the space weather community.

Magnes et al., Space Sci. Rev., 216, 119, 2020.

FORESAIL-2

FORESAIL is a CubeSat program conducted by Aalto University in the frame of the Finnish Centre of Excellence in Research of Sustainable Space. *FORESAIL-2*, as the second mission in this program, is planned for launch into a geostationary transfer orbit (GTO) in 2023. The technology demonstration goal of this mission is to survive the harsh radiation of the Van Allen belt using low cost components and a fault-tolerant software approach. In addition, a Coulomb-drag experiment shall demonstrate safe de-orbiting from orbits with high apogee.

The characterization of the variability of ultra-low frequency (ULF) waves and their role in energizing particles in the inner magnetosphere are the core scientific objectives of *FORESAIL-2*. This shall be achieved by in-situ measurements of the magnetic field as well as relativistic electrons and protons.

In cooperation with the Institute of Electronics of Graz University of Technology, IWF contributes a miniaturized magnetometer, which will be based on a newly developed microchip for the readout of the triaxial magnetic field sensor. During the reporting year, the preliminary design of the magnetometer has been settled and the design and simulation of the prototype microchip has been nearly finalized.

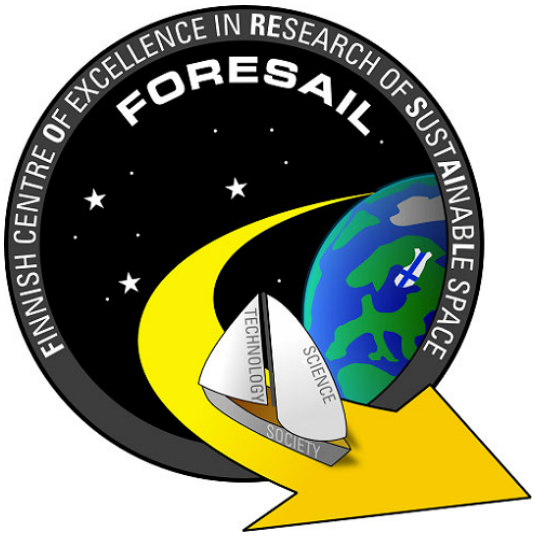

CubSats will set sail to investigate the Earth's magnetosphere.

SMILE

The *Solar wind Magnetosphere Ionosphere Link Explorer (SMILE)* is a joint mission between ESA and the Chinese Academy of Sciences (CAS), scheduled for launch in 2023. It aims to build a more complete understanding of the Sun-Earth connection by measuring the solar wind and its dynamic interaction with the magnetosphere. IWF is Co-I for two instruments: the *Soft X-ray Imager (SXI)*, led by the University of Leicester, and the magnetometer *(MAG)*, led by CAS.

The institute, in close cooperation with international partners, contributes the instrument's control and power unit *EBOX* for *SXI*. IWF is coordinating the development and design of the Digital Processing Unit (DPU) and is responsible for the mechanical design and the tests at box level. In 2020, ESA changed its philosophy and requested to get rid of all electronic components, which need a US export license. Thus IWF had to do a complete redesign of the DPU, using European semiconductors only. The component selection and the design process has been completed, but the printed circuit board layout activity is still ongoing. In parallel, the structural and thermal model of the *EBOX* has been designed and manufactured. All components are in house and the assembly has started.

Another activity was the design of the *SXI* simulator, which will be provided to Airbus instead of an Engineering Model. The simulator is based on a commercial Raspberry Pi enhanced by an in-house developed SpaceWire extension board.

In addition to the hardware activities, IWF is participating in the modeling and science working group activities.

SMILE SXI simulator to be used at spacecraft level instead of an Engineering Model (© ÖAW/IWF/Steller).

DECAY OF KELVIN-HELMHOLTZ VORTEX AT THE EARTH'S MAGNETOPAUSE

When the magnetic field is oriented nearly perpendicular to the direction of the plasma shear flow, the flow easily satisfies the super-Alfvénic unstable condition for the Kelvin-Helmholtz Instability (KHI). When the Interplanetary Magnetic Field (IMF) is strongly northward or southward, this configuration is realized at the Earth's low-latitude magnetopause across which the velocity shear between the magnetosheath (shocked solar wind) and magnetosphere persistently exists. Indeed, clear signatures of the KH waves and vortices have been frequently observed during periods of strong northward IMF. However, these signatures have been much less frequently observed during southward IMF. The first 3D fully kinetic Particle-In-Cell (PIC) simulation of the magnetopause KHI under pure southward IMF conditions is illustrated below. The simulation demonstrates that fast magnetic reconnection, driven by the magnetic shear between the Earth's northward magnetic field and the southward IMF, grows in the direction nearly perpendicular to the KHI k-vector (the shear flow). It is induced at multiple locations along the vortex edge in an early non-linear growth phase of the KHI. The reconnection outflow jets significantly disrupt the flow of the non-linear KH vortex, while the disrupted turbulent flow strongly bends and twists the reconnected field lines. The resulting coupling of the complex field and flow patterns within the magnetopause boundary layer leads to a quick decay of the vortex structure, which may explain the difference in the observation probability of the KH waves and vortices between northward and southward IMF conditions.

Nakamura T. et al., Geophys. Res. Lett., 47, e2020GL087574, 2020.

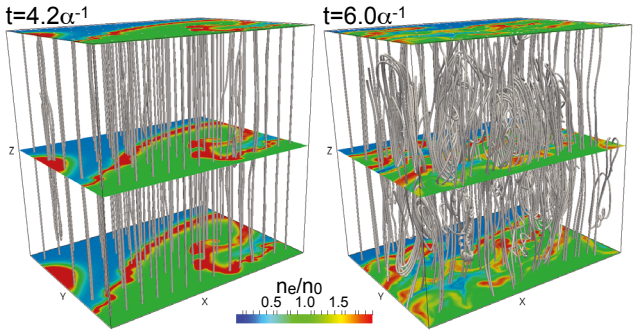

3D fully kinetic simulation results of the Kelvin-Helmholtz instability (KHI) at the magnetopause at two time slices in the early non-linear growth phase of the KHI. Plots show 3D views of magnetic field lines with the 2D contours of electron density in the X-Y plane at Z=0, Lz/2 and Lz. The non-linearly rolled-up KH vortex structure (seen in the left panel) quickly decays by turbulent evolution of magnetic reconnection.

RECONSTRUCTION OF THE RECONNECTION KERNEL ZONE

Magnetic reconnection is one of the key processes inherent to plasma physics, responsible for the topological reconfiguration of magnetic fields, plasma heating and acceleration. While, in general, reconnection is substantially a three-dimensional, time-dependent process, in some cases the problem is simplified due to the configuration symmetry and quasi-stationary regime. Then, in the nearest vicinity of the reconnection X-point the reconstruction problem is reduced to a two-dimensional Poisson equation for scalar potential of the in-plane magnetic field. In incompressible plasma this equation turns to the Grad-Shafranov (GSH) equation.

With boundary conditions, specified at some unclosed curve (e.g., the satellite trajectory), the GSH equation yields an ill-posed problem. The solution for this problem is to imply some regularization procedure. For the case of a compressible plasma, two regularization techniques were compared on a benchmark reconstruction of particle-in-cell simulation data. The reconstruction error sources were investigated. It was found that the transition from the exact Poisson to the modeling GSH equation is the major contributor to the reconstruction inaccuracy, shrinking the reconstruction domain cross-size to several electron inertial lengths. Within this domain the so-called "boundary layer approximation" provides for the simplest and the most accurate method for the problem regularization.

Korovinskiy et al., Phys. Plasmas, 27, 082905, 2020.

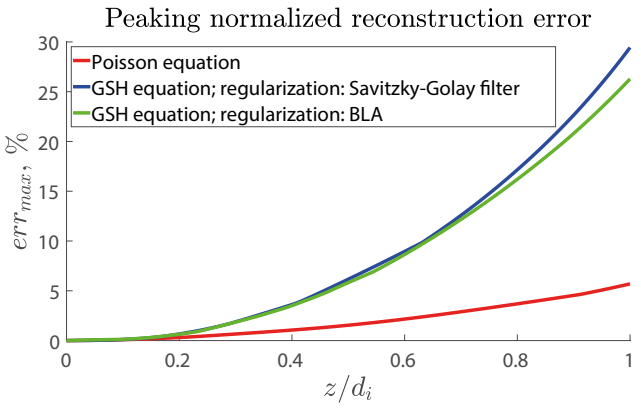

Peaking normalized reconstruction error, in %, versus the reconstruction domain cross-size normalized to the ion inertial length, d_i, where $d_i = 16\ d_e$. The error is evaluated as $err = (|A_{data}-A_{rec}|)/(\max|A_{data}|)$, where A is the scalar potential of the in-plane magnetic field and subscripts "data" and "rec" stand for data and reconstruction, respectively.

KINETIC ALFVÉN WAVE MECHANISM REVEALED IN SPACE PLASMAS

In the 1980s, numerical linear Vlasov theory showed a peculiar behavior that kinetic Alfvén waves change the polarization sense from left-hand to right-hand rotation around the mean magnetic field as the propagation direction approaches nearly perpendicular to the mean field.

The mechanism of polarization reversal remained a problem in space plasma physics. It was finally revealed by tracking the dielectric response of plasmas analytically. The wave electric field is determined by different motions between electrons and ions (Hall current), causing the left-hand polarization. At nearly perpendicular propagations, however, thermal motions of electrons and ions dominate the system (by diamagnetic current), and the polarization flips into right-hand rotation.

Narita et al., Front. Physics, 8, 166, 2020.

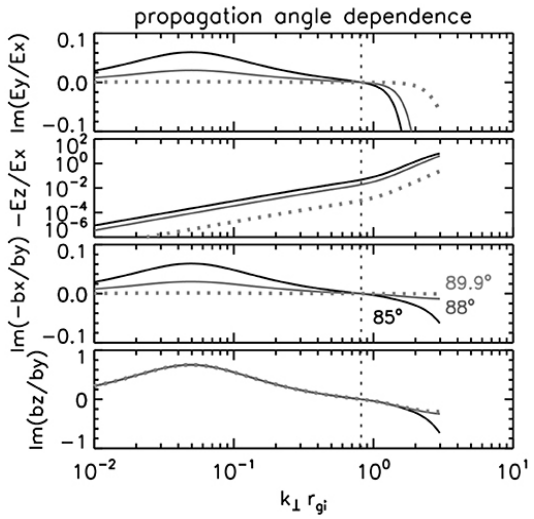

Field rotation sense of wave electric and magnetic field (panel 1 and 3) and compressive sense of electric and magnetic field parallel to the mean magnetic field (panel 2 and 4) as function of wave numbers normalized to the ion gyro-radius. Three different propagation scenarios are shown.

VLF/LF RADIO PROPAGATION

Frequency-banded wave emission has been recorded near the Earth's equatorial region by the *DEMETER* satellite. This emission occurs on the night side in the frequency range from few kHz up to 800 kHz when the satellite's magnetic latitude mainly varies between -30° and +20°. This emission exhibits different spectral behavior before and after the crossing of the magnetic equator. Two spectral components have been investigated, one appears as frequency bands continuous in time between a few kilohertz and up to 50 kHz, and the other one is from 50 to 800 kHz.

The first component exhibits positive and negative frequency drift rates in the Southern and Northern Hemisphere, at latitudes between -40° and 20°. The second one displays multiple spaced frequency bands as shown in the figure below. Such bands mainly occur near the magnetic equatorial plane with a particular enhancement of the power level when the satellite latitude is close to the magnetic equatorial plane. It is important to note that the number of parallel narrow bands is found to be different from one event to another. In addition, the enhanced banded frequencies above 200 kHz, may be considered harmonic components of a fundamental frequency appearing around 140 kHz. The power distribution of such emissions shows restrained and extended deployment around the equatorial magnetic plane. Hence, the latitudinal beam is found to be about 40° when the frequency is, on average, less than 100 kHz. Above this limit and up to about 800 kHz, the latitudinal beam is decreasing and found to be about 20°.

Boudjada et al., Ann. Geophys., 38, 765-774, 2020.

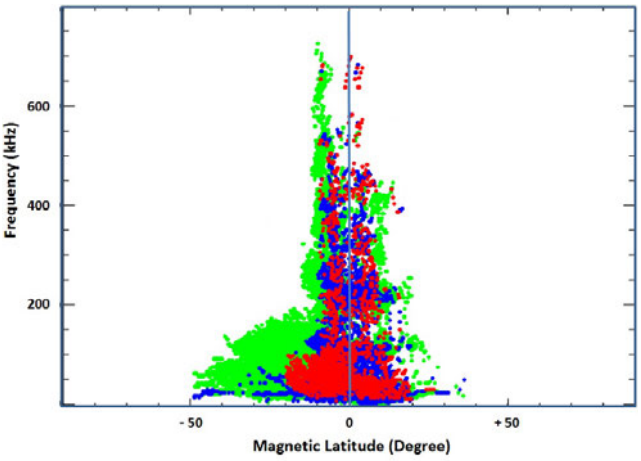

Variation of the power levels versus the frequency and the magnetic latitude for all events. The red, blue and green colors indicate the intense, moderate and weak frequency-banded emissions.

S/C TRAJECTORIES THROUGH INTERCHANGE HEADS

The terrestrial magnetic field lines on the anti-sunwardside of the Earth form an elongated structure (the magnetotail), which is periodically disrupted by magnetic reconnection. An instability was recently found to produce azimuthally narrow heads that intrude into the dipole region from the near-Earth magnetotail. At the developed stages of the instability, it was predicted that localized plasma structures, which have narrow heads and contain enhanced northward magnetic fields (dipolarization front), grow toward the Earth that may cause a full-scale disruption of the magnetotail.

By combining high-performance computing plasma simulations with multi-point in-situ observations by *THEMIS*, it is shown that under the right magnetotail conditions the dipolarization fronts can also be generated by this instability at about ten Earth's radii downtail in the transition region between the geomagnetic dipole and tail fields.

Panov et al., J. Geophys. Res., 125, e2020JA027930, 2020.

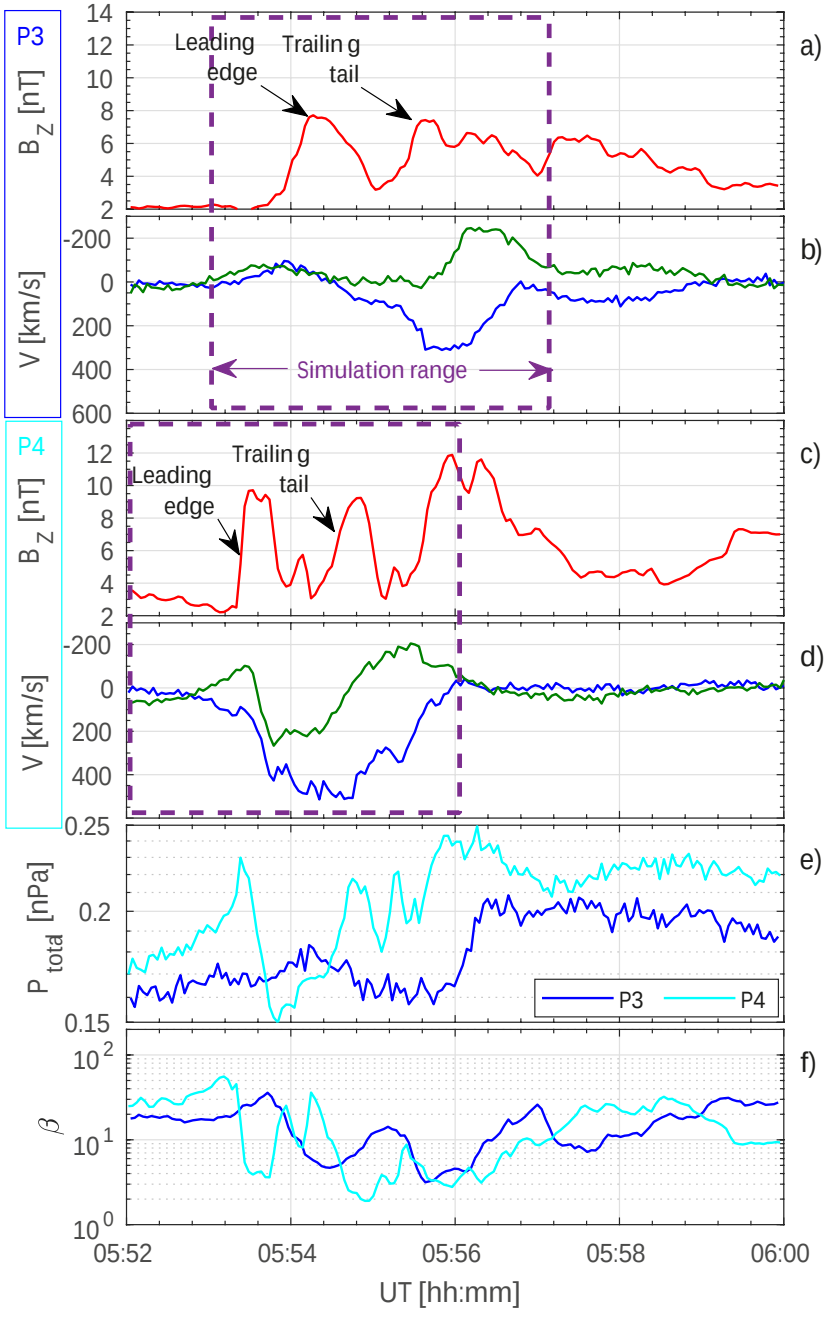

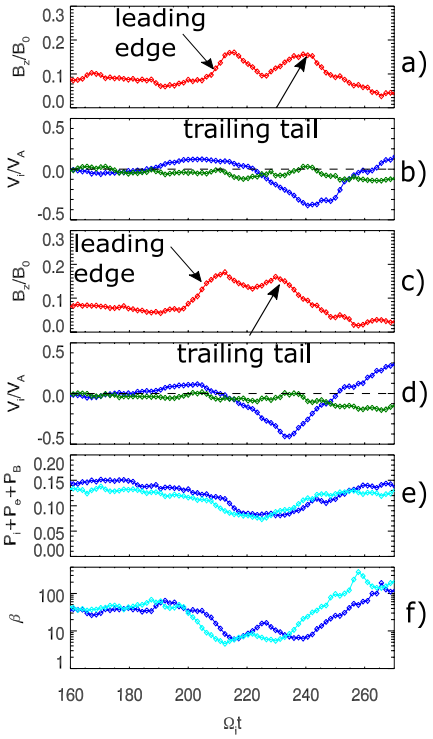

Left: *THEMIS* P3 (a, b, e, and f) and P4 (c–f) observations during dipolarization front crossing on 26 February 2009 between 5:52 and 6:00 UT: GSM B_Z magnetic field component (a, c), GSM V_X (blue), and V_Y (green) ion velocity components (b, d) (note that the ordinates are reversed in the ion velocity panels (facing downward), the sum of the ion, electron and magnetic field pressures (e), and the ratio of the plasma pressure to the magnetic field pressure (plasma-β) (f). Top: corresponding virtual spacecraft observations predicted by the particle-in-cell simulations.

ALIGNMENT OF JET VELOCITY AND MAGNETIC FIELDS

Jets in the subsolar magnetosheath are localized enhancements in dynamic pressure that are able to propagate all the way from the bow shock to the magnetopause. Due to their excess velocity with respect to their environment, they push slower ambient plasma out of their way, creating a vortical plasma motion in and around them. Simulations and case study results suggest that jets also modify the magnetic field in the magnetosheath on their passage, aligning it more with their velocity. Based on *MMS* jet observations and corresponding superposed epoch analyses of the angles Φ between the velocity and magnetic fields, it was confirmed that this suggestion is correct.

However, while the alignment is more significant for faster than for slower jets, and for jets observed close to the bow shock, the overall effect is small: typically, reductions in Φ of around 10° are observed at jet core regions, where the jets' velocities are largest. Furthermore, time series of Φ pertaining to individual jets significantly deviate from the superposed epoch analysis results. They usually exhibit large variations over the entire range of Φ: 0 to 90°. This variability is commonly somewhat larger within jets than outside, masking the systematic decrease in Φ at core regions of individual jets.

Plaschke et al., Ann. Geophys., 38, 287-296, 2020.

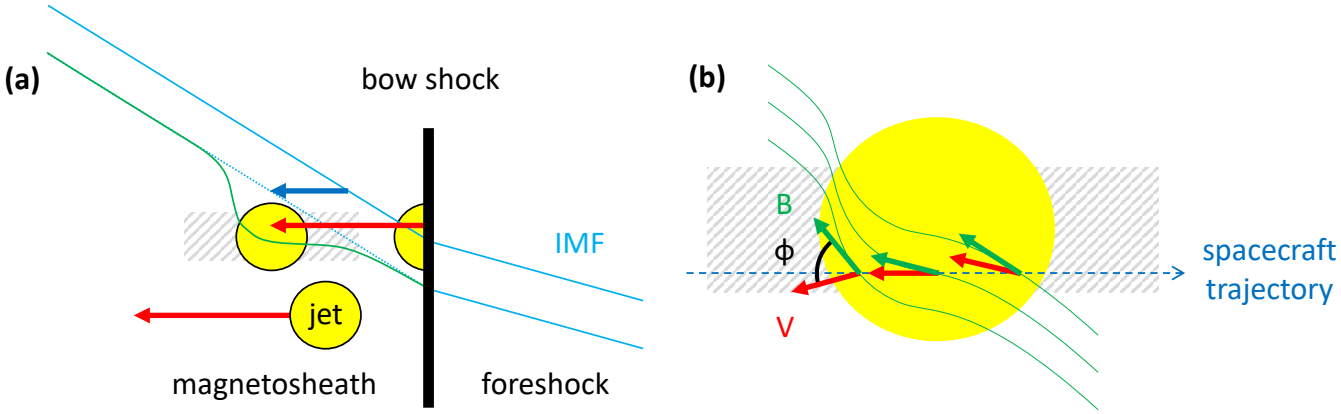

(a) Sketch of how magnetic fields in the magnetosheath may be modified by the motion of fast plasma jets. Velocities of jets and ambient plasmas are illustrated by red and blue arrows, respectively. (b) Close-up on a jet. Green and red arrows show local directions of the magnetic field B and velocity V measured by a spacecraft on its trajectory through the jet. The angle between B and V is Φ.

SOLAR SYSTEM

IWF is engaged in many missions, experiments and corresponding data analysis addressing solar system phenomena. The physics of the Sun and the solar wind, its interaction with solar system bodies, and various kinds of planetary atmosphere/surface interactions are under investigation.

SUN & SOLAR WIND

The Sun's electromagnetic radiation, magnetic activity, and the solar wind are strong drivers for various processes in the solar system.

2020 marks the beginning of a new era of investigating the Sun and solar wind with the launch of *Solar Orbiter* in February. The remote sensing instruments got a first chance to make measurements in June, when the spacecraft surrounded the Sun for the first time at a distance of about 0.5 AU. Further scientific observations were made by the *Solar Orbiter* payload during the first Venus flyby in December 2020.

Artist's impression of *Solar Orbiter* making a flyby at Venus (© ESA/ATG medialab).

SOLAR ORBITER

Solar Orbiter is an ESA space mission to investigate the Sun. Flying a novel trajectory, with partial Sun-spacecraft corotation, the mission plans to investigate in-situ plasma properties of the inner solar heliosphere and to observe the Sun's magnetized atmosphere and polar regions. Gravity assist from Venus and Earth will be used to reach the operational orbit, a high elliptical orbit with perihelion at 0.28 AU.

IWF has built the Digital Processing Unit (DPU) for the *Radio and Plasma Waves (RPW)* instrument and has calibrated the *RPW* antennas, using numerical analysis and anechoic chamber measurements. Furthermore, the institute has contributed to the fluxgate magnetometer.

RPW will measure the magnetic and electric fields at high time resolution and will determine the characteristics of magnetic and electrostatic waves in the solar wind from almost DC to 20 MHz. Besides the 5 m long antennas and the AC magnetic field sensors, the instrument consists of four analyzers: the thermal noise and high frequency receiver, the time domain sampler, the low frequency receiver, and the bias unit for the antennas. The control of all analyzers and the communication will be performed by the DPU.

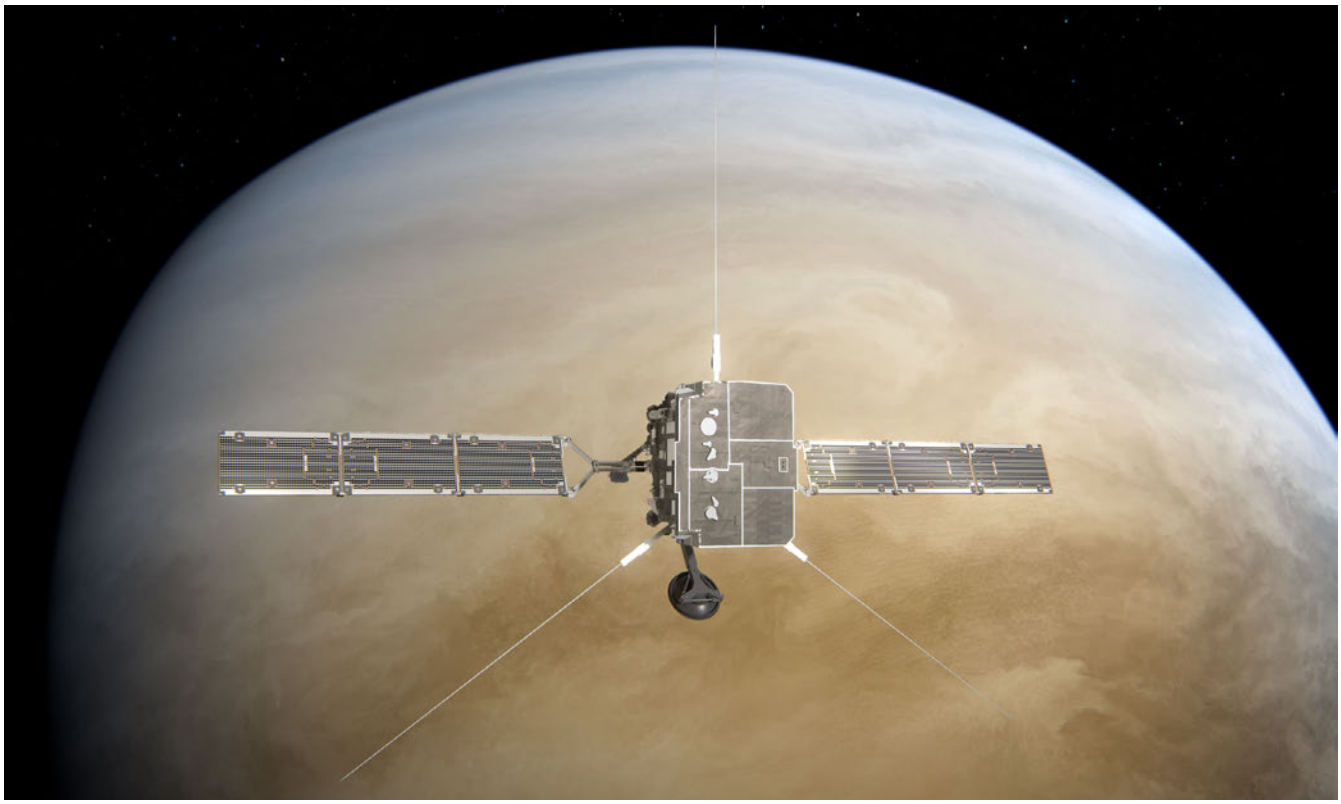

SOLAR CORONA MHD SIMULATIONS

Realistic models of the Sun's atmosphere, the corona, require knowledge of the real situation on the solar surface, because this reshapes the magnetic field in the corona. The evolution of the magnetic fields lead to electric currents in the corona that heat the plasma to temperatures even above 1 million Kelvin. The mechanism for this heating has been a riddle for a long time and computer models now allow to analyze the plasma processes in the corona much better than only by observing the corona with telescopes. However, a realistic driving of such three-dimensional magneto-hydrodynamic (3D MHD) models requires careful numerical methods to impose the observed state at the solar surface, the photosphere, but at the same time let the rest of the model evolve as freely as possible. Novel methods have been used to extrapolate the observed magnetic field into the interior of the Sun and allow the plasma to flow horizontally and to braid the magnetic field due to the convection motion that emerges from the solar interior. The boundary condition of the model also allows for a compressible lower atmosphere, the chromosphere, so that downflows from the corona are softly damped, before reaching the surface, as it is also the case on the real Sun. Using high-performance computers, like the institute's LEO system, new models were run for different solar phenomena, like sunspots and full active regions.

Bourdin et al., Geophys. Astro. Fluid Dyn., 114, 235-260, 2020.

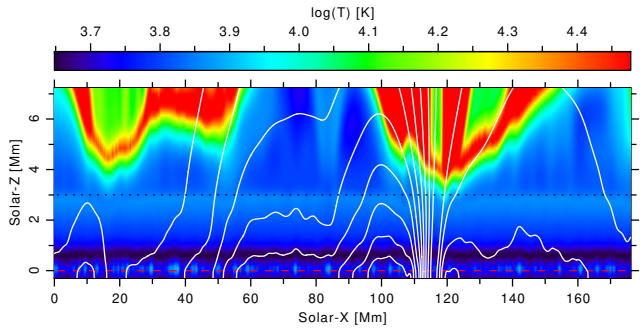

Logarithmic temperature in Kelvin from a vertical cut through the solar atmosphere, starting from the photosphere (red dashed line) to the transition region (horizontal dotted line) that forms the base of the corona (above the dotted line). Red color indicates hot temperatures above 30000 K, while blue color shows plasma below 8000 K. The white lines indicate the magnetic field, which is vertical over strong flux concentrations; see at X=110–120 Mm. Below the photosphere, the novel boundary condition allows for a flexible magnetic field and for compressible horizontal plasma flows.

MAGNETIC HOLES IN THE SOLAR WIND BETWEEN MERCURY AND VENUS

The Interplanetary Magnetic Field (IMF) shows various kinds of structures and discontinuities on different scales, one of which is the Magnetic Hole (MH). This structure is characterized by a decrease in magnetic field strength and an increase in plasma density and/or temperature. Two special cases of MHs are discussed, the Linear MH (LMH) and Pseudo MH (PMH) where the magnetic field rotates less than 10° over the structure and between 10° and 45°, respectively.

The *MESSENGER* magnetometer data during the cruise phase from Venus to Mercury were used and the occurrence rate of MHs was determined as a function of radial distance from the Sun and categorized by the magnetic field rotation over the MH.

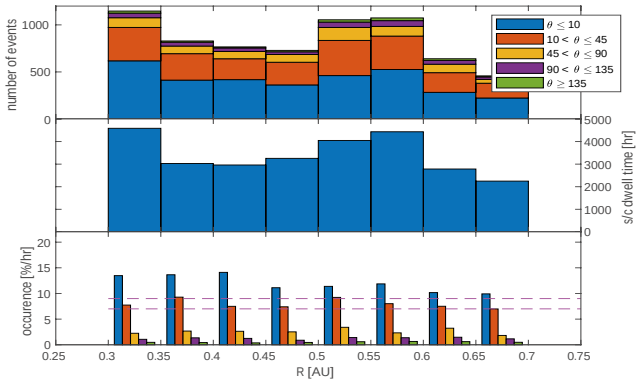

Histogram of the occurrence rate of MHs as a function of radial distance and color coded after the rotational bins as given in the legend. The two dashed magenta lines in the bottom panel show the average occurrence rates from *Helios* data.

The occurrence rate of LMHs (blue) and PMHs (dark orange) does not change much between Mercury and Venus. The small difference between the occurrence rates over the observation interval rules out the "dilution" or "parametric decay" of the structures. The narrow range of widths between ~4 and ~30 s, assuming Bohm-like diffusion of the structures happen, which would make them larger, would argue for a constant creation and diffusion and (stochastic) decay of these structures between Mercury and Venus.

Volwerk et al., Ann. Geophys., 38, 51-60, 2020.

INTERPLANETARY CME RATE IN SOLAR CYCLE 25 & PSP DOUBLE CROSSINGS

The *Solar Orbiter* and *Parker Solar Probe (PSP)* missions are destined to make groundbreaking observations of the Sun and interplanetary space in this decade. Through simulations with the semi-empirical flux rope model (3DCORE), a particularly interesting case of a possible coronal mass ejection (CME) observation by *PSP* was found, which may happen when a CME erupts during times when *PSP* is near its aphelion (<0.1 AU). The same magnetic flux rope inside a CME was observed in-situ by *PSP* twice, by impacting its nose or front part and its leg or side part. In order to look at the odds of this unprecedented observing situation to happen, the in-situ CME rate valid for Earth as well as at *PSP* and *Solar Orbiter* was calculated, based on two predictions for the sunspot number (SSN, peak at 115 and 232). On the order of 1 to 10 possible *PSP* flux rope double crossings were found, which holds considerable promise to determine the structure of CMEs in the solar corona. A double crossing is essentially a multi-point in-situ CME observation very close to the Sun. Ideally, *Solar Orbiter* would image the event from a vantage viewing point or detect the same CME in-situ, further constraining the 3DCORE simulations. For the higher sunspot number prediction, during the next solar maximum around 2025, about five CMEs would impact Earth per month on average, which would form the strongest space weather impacts since the early 1990s.

Möstl et al., Astrophys. J., 903, 92, 2020.

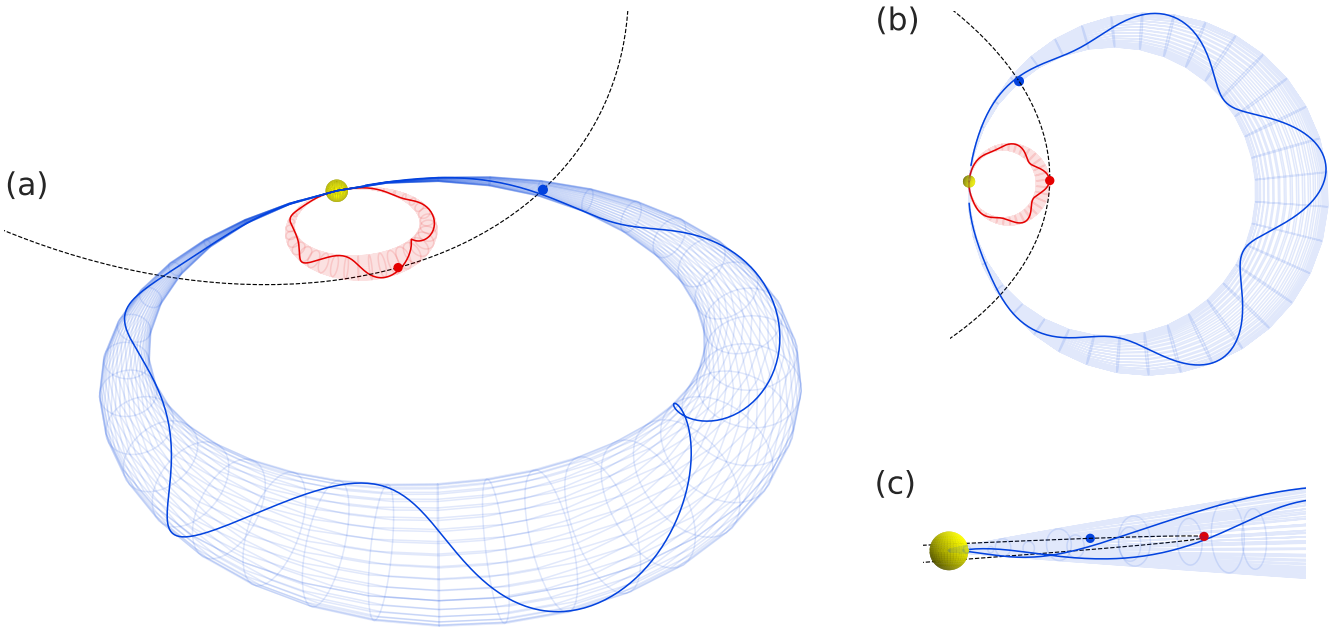

Simulation of a *PSP* CME double crossing from different viewing angles (a-c). Red: 3DCORE model flux rope at simulation time of +4 hours. Blue: model flux rope at +26 hours. Dashed line: *PSP* trajectory. Further imaging and in-situ observations may be provided by *Solar Orbiter*, *STEREO-A*, *SOHO*, *Wind*, and *BepiColombo*.

MERCURY

Mercury is in the center of attention because of the ESA/JAXA *BepiColombo* mission. The planet has a weak intrinsic magnetic field and develops a mini-magnetosphere, which strongly interacts with the solar wind.

In 2020, *BepiColombo* experienced its first two planetary flybys: Earth in April and Venus in October.

BEPICOLOMBO

The European-Japanese spacecraft, launched 2019, is on its way to Mercury. *BepiColombo's* trajectory is bent towards the Sun and its velocity is decreased during nine gravity-assist manoeuvers (GAM) such, that the spacecraft finally can reach its Mercury orbit insertion point at the end of 2025. GAMs - also known as flybys, swingbys or gravitational slingshots - use the gravitation of a planet or other astronomical objects to alter the path and speed of a spacecraft without using thrusters and propellant.

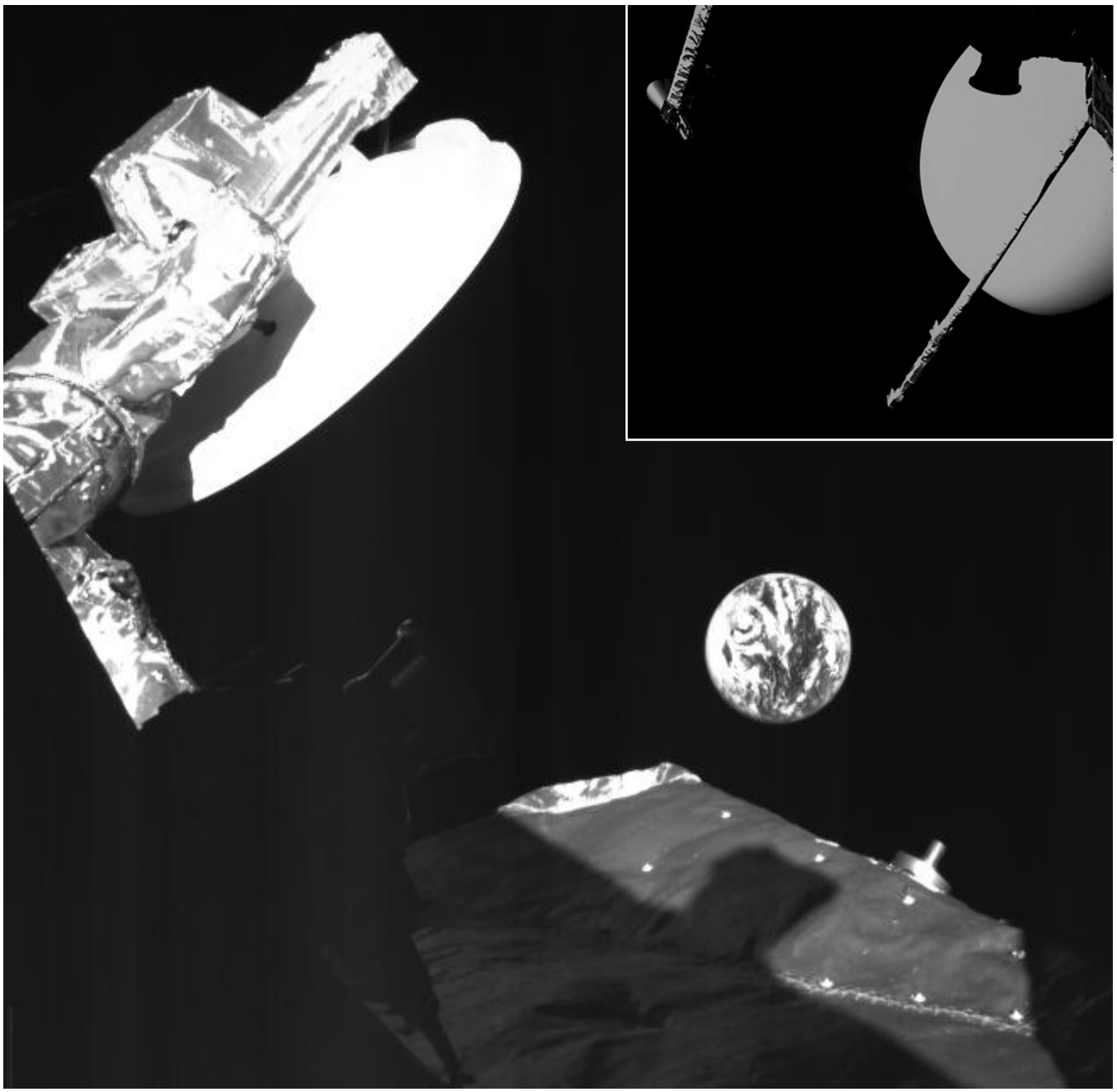

Selfies taken by the camera of *BepiColombo's Mercury Transfer Module (MTM)* as the spacecraft neared Earth and passed Venus (inset) during its gravity-assist manoeuvers in April and October (© ESA/*BepiColombo/MTM*, CC BY-SA 3.0 IGO).

The first and only Earth flyby took place in April, with the closest approach at a distance of 12,677 km from the Earth's surface on 10 April, 04:45 UTC. Half a year later *BepiColombo* visited Venus for the first of two times around 15 October. Many sensors use the flybys for further calibration activities and for the first science measurements, including the three sensors with an IWF hardware contribution on both the European *Mercury Planetary Orbiter (MPO)* and the Japanese *Mercury Magnetospheric Orbiter (MMO)*.

The *MMO-MGF* (IWF PI-ship) magnetometer with its two sensors on the still stowed boom was switched on during the flybys and a number of other constellation and instrument check-out campaigns. The Earth flyby has been used for an evaluation of the scale factors and the exact orientation of the stowed sensors.

MPO-MAG (IWF technical management) has been monitoring the magnetic field almost continuously. Apart from the instrument calibration during the Earth flyby, *MPO-MAG* data have already been widely used for scientific evaluation of magnetospheric features during the two planetary flybys and interesting structures of the solar wind like a specific Coronal Mass Ejection which could be measured in concert with the Solar Orbiter spacecraft.

PICAM (IWF sensor PI-ship), the ion mass spectrometer with imaging capability as part of the *SERENA* instrument suite on *MPO*, was operated in different science modes for about 20 hours near Earth and for 27 hours at Venus. The campaigns brought the first real science measurements, which significantly aid in the calibration and flight software update activities.

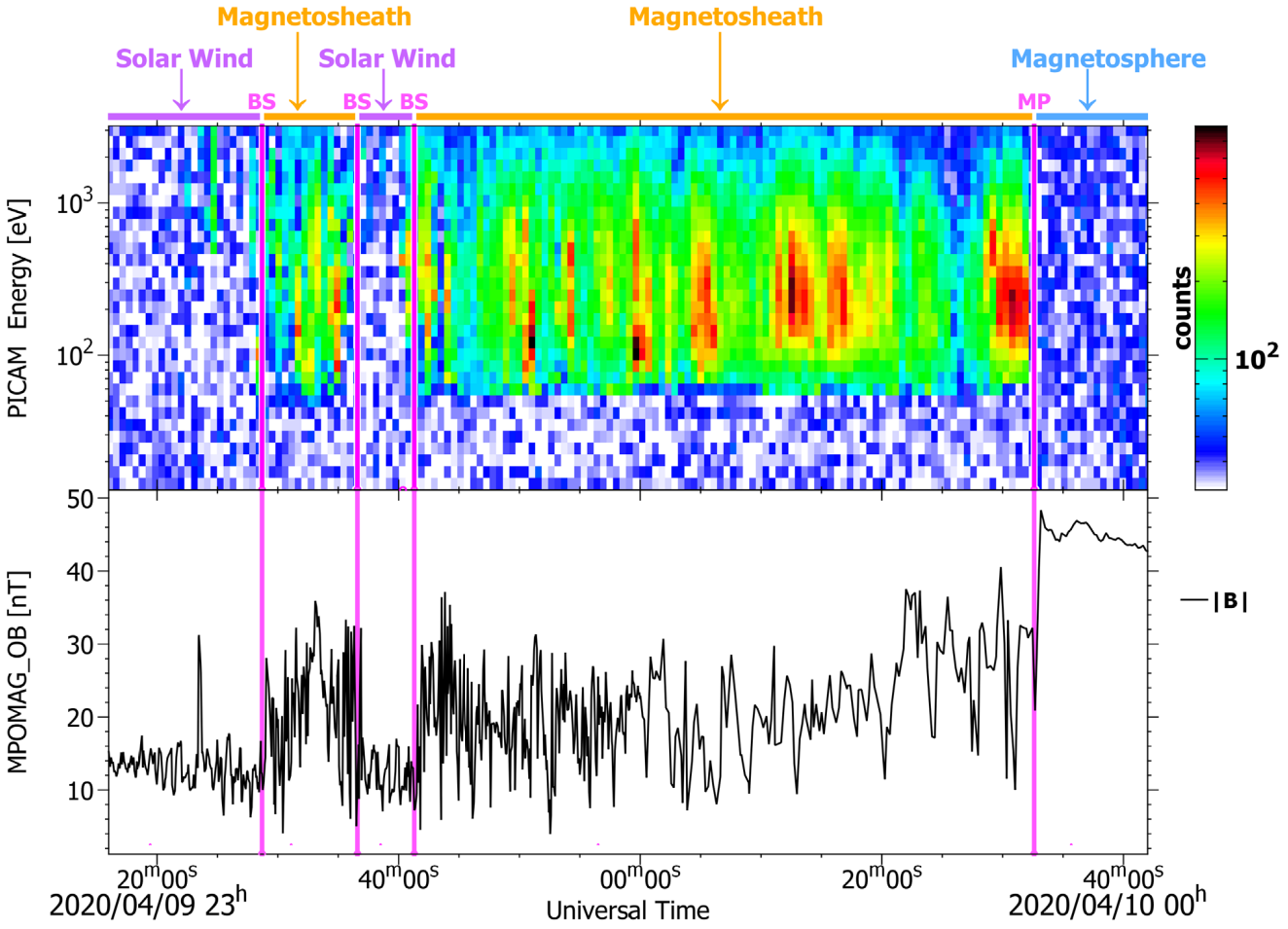

An example of *BepiColombo* observations during its Earth flyby. The top panel shows the ion spectrogram from *PICAM* and the bottom panel the total magnetic field from *MPO-MAG*. *BepiColombo* successfully captured the dynamics of plasma at the moment of entry from the interplanetary space to the Earth's magnetosphere.

DETERMINING MAGNETOMETER OFFSETS IN HERMEAN ENVIRONMENT

The offsets of a magnetometer are usually evaluated from observations of Alfvénic fluctuations in the pristine solar wind, if available. While *BepiColombo's MMO* orbit will indeed partially reside in the solar wind, *MPO* will remain within the magnetosphere at most times during the main mission phase. An alternative offset determination method, based on the observation of highly compressional fluctuations, the so-called mirror mode technique, becomes important in such orbit conditions.

To evaluate the method performance in the Hermean environment four years of *MESSENGER* magnetometer data were analyzed. They were calibrated by the Alfvénic fluctuation method and compared with the accuracy and error of the offsets determined by the mirror mode method in different plasma environments around Mercury. It is shown that the mirror mode method yields the same offset estimates and thereby confirms its applicability. Furthermore, the spacecraft observation time within different regions necessary to obtain reliable offset estimates is evaluated.

Although the lowest percentage of strong compressional fluctuations were observed in the solar wind, this region is most suitable for an accurate offset determination with the mirror mode method. 132 hours of solar wind data are sufficient to determine the offset to within 0.5 nT, while thousands of hours are necessary to reach this accuracy in the magnetosheath or within the magnetosphere.

It is concluded that in the solar wind the mirror mode method might be a good complementary approach to the Alfvénic fluctuation method to determine the (spin-axis) offset of the *MMO* magnetometer. However, although the mirror mode method requires considerably more data within the magnetosphere, it might also be the most valuable scheme for *MPO* to determine the offsets accurately.

Schmid et al., Ann. Geophys., 38, 823-832-, 2020.

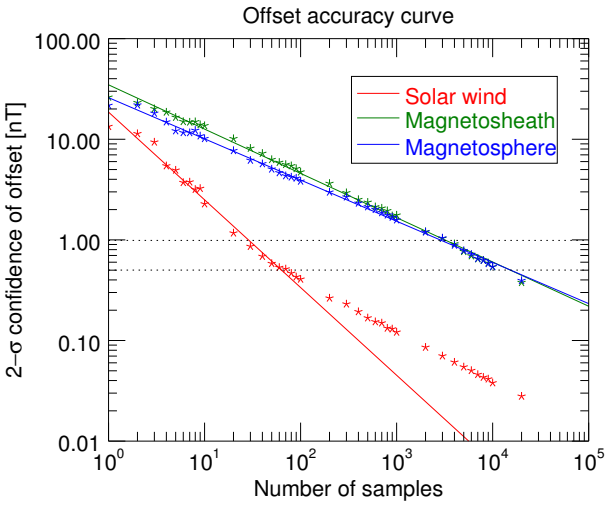

Relationship between the best-estimate offset and the number of samples to obtain this value with 95% confidence. The time interval to take one sample is 30 s. The solid lines represent the linear least squares fits of the offsets above 0.5 nT.

VENUS AND MARS

Venus and Mars are the Earth's nearest inner and outer planetary neighbors, respectively. Venus orbits the Sun at 0.7 AU in 224 days, has a radius slightly smaller than the Earth, and has a very dense atmosphere. Mars orbits the Sun at 1.5 AU in 687 days, has about half the radius of the Earth, and has a very tenuous atmosphere. Both planets do not have an internal magnetic field, although Mars does show remnant surface magnetization, which might indicate that the planet used to have a functioning dynamo. Through their interaction with the solar wind, however, a so-called induced magnetosphere is created.

2020 was a busy year for exploring the Red Planet. Three missions lined up for launch: NASA's *Perseverance*, the Emirate's *al-Amal (Hope)*, and China's *Tianwen-1*.

TIANWEN-1

China's Mars orbiter, lander, and rover mission will conduct a comprehensive remote sensing of the Red Planet, as well as surface investigation. IWF contributed to a magnetometer aboard the orbiter.

INSIGHT

NASA's *InSight (INterior exploration using Seismic Investigations, Geodesy and Heat Transport)* landed on Mars in 2018. The *Heat flow and Physical Properties Probe (HP³)* was designed to measure the internal heat flux of the planet as well as the thermal and mechanical properties of the regolith. The hammering of the "Mole" into Martian ground got stuck, caused by lacking friction of the regolith.

With the numerical model developed at IWF it could be demonstrated that the first half meter is the most difficult part of the insertion process. Throughout 2020 the "Mole" penetration attempts were further supported with the Instrument Deployment Arm and finally the hole that was formed around the "Mole" was filled in. At the same time due to seasonal effects and an increased dust load on the solar panels the energy situation of *InSight* became critical. Therefore, in February 2021 it was decided to discontinue the *HP³* deployment attempts.

The Tianwen-1 team with the spacecraft (© CNSA).

EARLY EVOLUTION OF EARTH AND VENUS

The atmospheric $^{36}Ar/^{38}Ar$, $^{20}Ne/^{22}Ne$, $^{36}Ar/^{22}Ne$, noble gas isotope and elemental bulk ratios on Venus and Earth provide important information on their origin and evolution. For reproducing Earth's and Venus's present atmospheric isotope ratios, hydrodynamic upper atmosphere escape and smooth particle hydrodynamics impact models were applied to study losses of captured H_2-dominated primordial atmospheres for different proto-planetary masses. Additionally, a wide range of possible solar EUV evolution tracks and initial atmospheric compositions based on mixtures of captured nebula gas, outgassed and delivered material from planetary building blocks was added to the modeling of growing proto-planets. It was found that for outgassed noble gases and rock-forming elements from planetary building blocks with masses that are less than that of Earth's Moon the gravity is too weak so that all outgassed elements will escape immediately to space. For these bodies the loss rates of noble gases Ar and Ne are so high that there will be no fractionation of their isotopes. The studied planetary embryos, even though not isotopically fractionated, are strongly depleted in noble gases and moderately volatile elements.

Depending on the disk lifetime and the composition of accreted building blocks after disk dispersal, it was found from the reproduction of today's atmospheric Ar, Ne, and some bulk elemental ratios (see figure below), that early Earth's evolution can be explained if it had accreted masses of up to 0.58 M_{Earth} by the time the gas disk dissipated (top panel, figure below). If proto-Earth would have accreted a higher mass during this early period the Earth's present atmospheric Ar and Ne isotope ratios cannot be reproduced and for masses > 0.75 M_{Earth}, Earth would have ended as an H_2/He-dominated sub-Neptune. It was also discovered that if proto-Venus captured a primordial atmosphere from the gas disk it should have grown to masses between 0.85 - 1.0 M_{Venus} until the disk dissipated (bottom panel, figure below). However, in the case of Venus, a future spacecraft to our inner neighbor should carry out new precise re-measurements of atmospheric noble gases that will better constrain the material that was involved in the planet's accretion history and possibly also the EUV activity evolution of the young Sun.

Lammer et al., Space Sci. Rev., 216, 74, 2020.
Lammer et al., Icarus, 339, 113551, 2020.

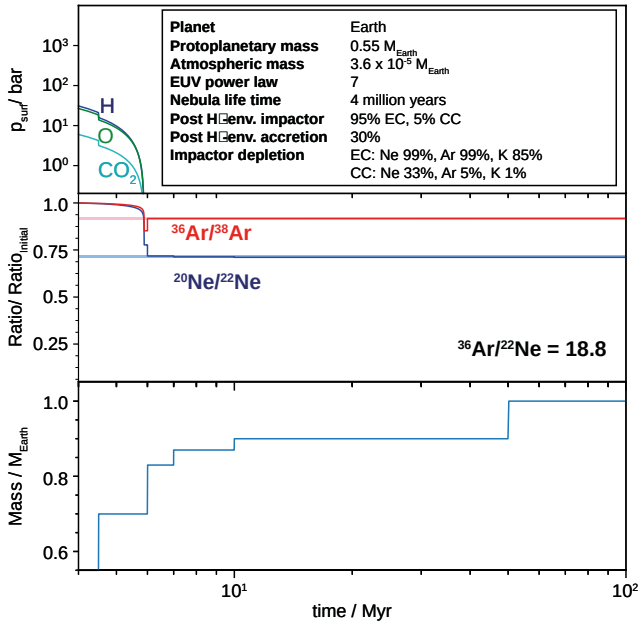

Reproduction of Earth's present atmospheric Ar and Ne isotope ratios by assuming a composition based on the analysis of isotopic data from lithophile-siderophile elements.

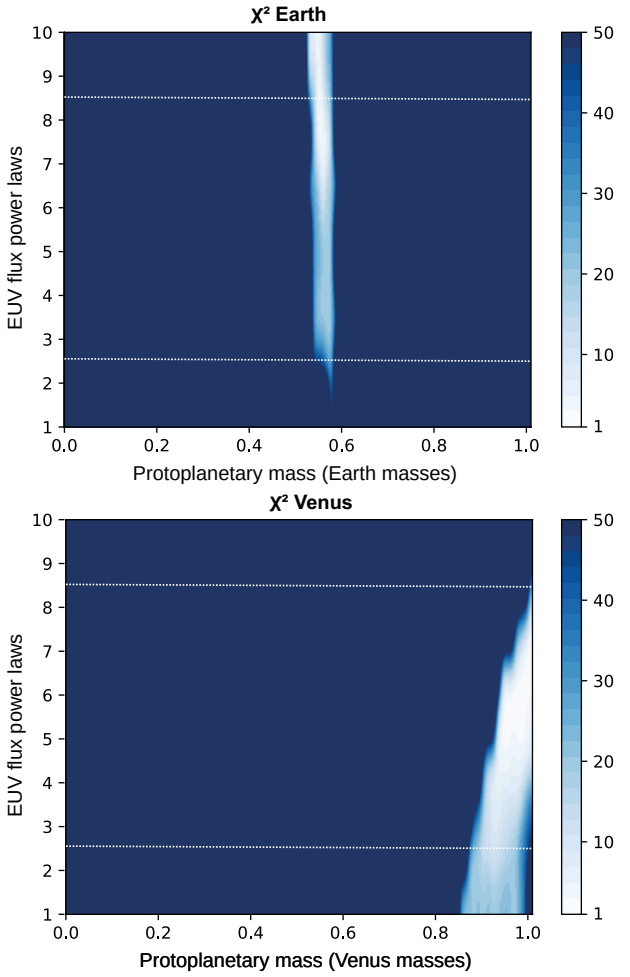

Statistical χ^2 parameter study of the isotope evolution for proto-Earth and -Venus. Today's ratios of both planets can be reproduced within the white areas if the young Sun was between a slow (EUV power laws: 1-5) and a moderate rotating young G star (EUV power laws (>5-10). The EUV fluxes within the two horizontal lines can reproduce both planets simultaneously.

JUPITER AND SATURN

Jupiter and Saturn, the two largest planets in our solar system, both have several dozens of moons. For Jupiter, the most prominent moons are the four Galilean satellites, and three of them will be visited frequently by the future *JUICE* spacecraft. For Saturn, Titan is clearly the most prominent satellite with its dense atmosphere consisting of nitrogen and methane.

Although *Cassini* had 126 close Titan flybys, no signs of lightning have been detected. On the hardware side, the *MAGSCA* sensor for *J-MAG* was delivered to Imperial College London for integration.

JUICE

ESA's first large (L-class) mission *JUpiter ICy moons Explorer (JUICE)* is planned to be launched in June 2022 and to arrive at Jupiter in late 2029, starting a 3.5 years discovery mission. It will make detailed observations of the gas giant and three of its largest moons, Ganymede, Callisto, and Europa. These three moons are thought to have water oceans below their icy surfaces. Towards the end of the mission *JUICE* will orbit Jupiter's largest moon Ganymede. In 2020, ESA and the prime contractor Airbus have begun with the assembly of the flight spacecraft in Friedrichshafen, Germany.

The *Jupiter MAGnetometer (J-MAG)* is led by Imperial College London (ICL) and will measure the magnetic field vector and magnitude in the bandwidth DC to 64 Hz in the spacecraft vicinity. It is a conventional dual sensor fluxgate configuration combined with an absolute scalar sensor based on more recently developed technology. Science outcome from *J-MAG* will contribute to a much better understanding of the formation of the Galilean satellites, an improved characterization of their oceans and interiors, and will provide deep insight into the behavior of rapidly rotating magnetic bodies. IWF supplied the atomic scalar sensor *(MAGSCA)* for *J-MAG*, which was developed in collaboration with TU Graz.

In 2020, the qualification sensor needed to be reworked due to a problem with the optics at the very low qualification temperature of -160 °C and the flight model was assembled, tested and delivered to ICL for integration into the *J-MAG* instrument. The *Particle Environment Package (PEP)* is a plasma package with sensors to characterize the plasma environment of the Jovian system and the composition of the exospheres of Callisto, Ganymede, and Europa. IWF participates in the *PEP* consortium on Co-Investigator basis in the scientific studies related to the plasma interaction and exosphere formation of the Jovian satellites.

IWF was also responsible for the calibration of the radio antennas of the *Radio and Plasma Wave Investigation (RPWI)*. In August 2020, the *RPWI* instrument was completed and shipped to Airbus in Friedrichshafen for implementation on the spacecraft.

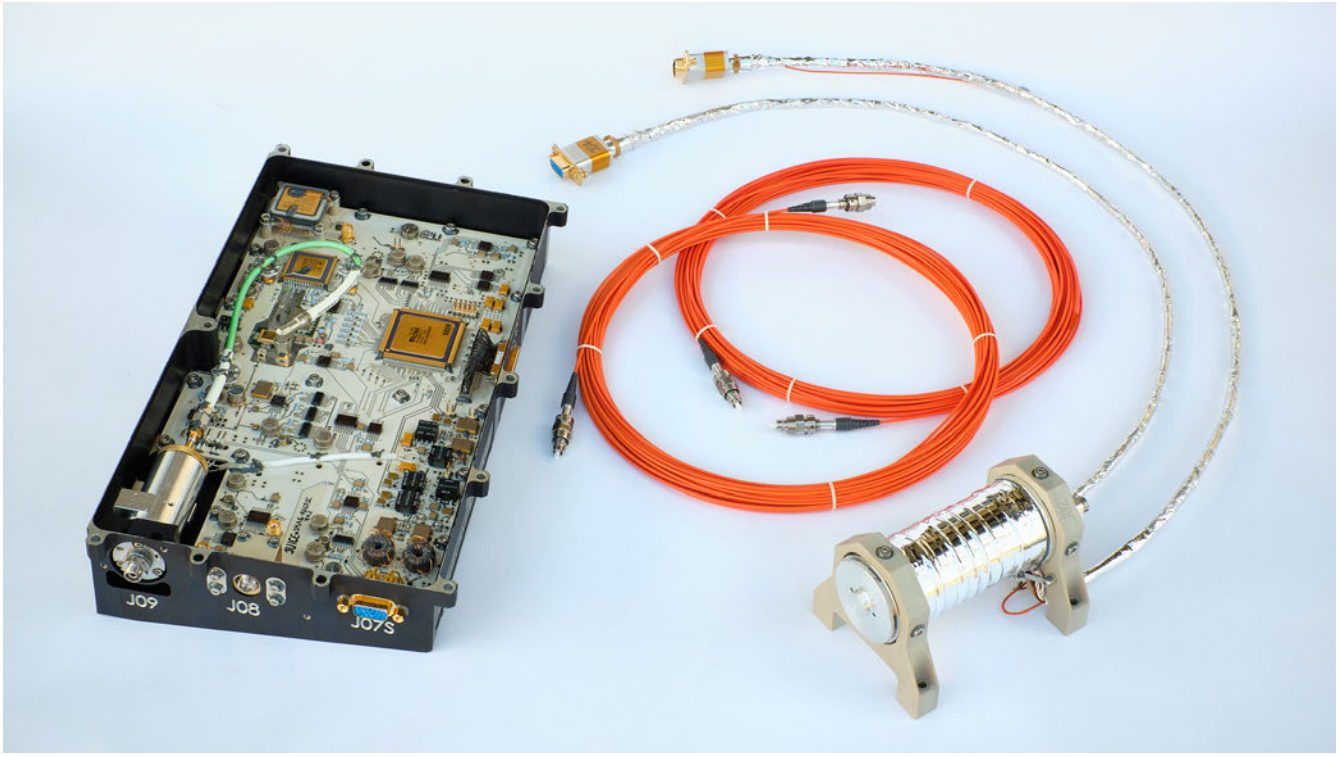

Flight model of the atomic scalar sensor together with the related front-end electronics and the optical fibers (with orange jacket), which connect sensor and electronics (© Andreas Pollinger/IWF/ ÖAW, CC-BY 4.0).

NO LIGHTNING ON TITAN

The Saturn-orbiting *Cassini* spacecraft completed 126 close Titan flybys from 2004 until the end of the mission in September 2017. During almost all of them the *Radio and Plasma Wave Science (RPWS)* instrument was turned on to search for radio emissions from Titan lightning. However, a careful inspection has revealed no corresponding emissions. This puts new and strong constraints on the permissible flash energy and flash rate of potential Titan lightning, as detailed in the figure below.

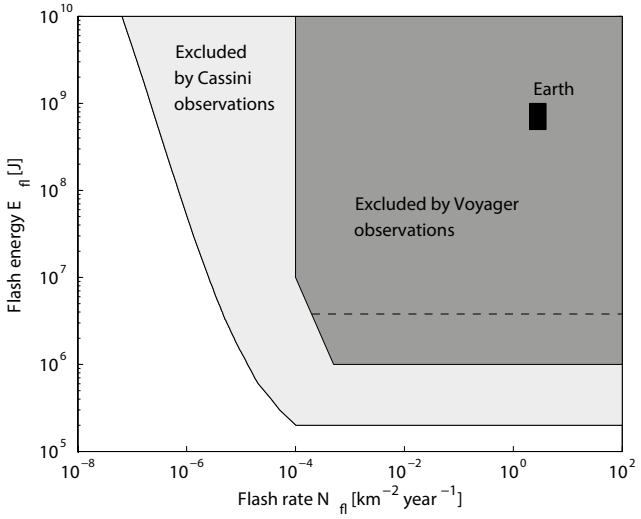

Flash energy of potential Titan lightning versus its rate; various regions excluded by *Voyager 1* and *Cassini* observations are shown as gray areas.

In this figure, the black square shows the flash energy and rate of typical Earth lightning. The dark gray region was excluded by the single *Voyager 1* observation in 1980. The light gray region is the additional region to be excluded after the non-detection of Titan lightning by *Cassini*. The white region marks the flash energy and rate combinations which are left for potential Titan lightning. This means that any lightning on Titan must be either very weak (5000 times weaker than typical Earth lightning), very rare (just ~80 flashes per year all over Titan), or does not exist at all. The latter could be due to cloud electric fields being too low to initiate a discharge. This finding has important implications for the prebiotic chemistry of Titan's atmosphere.

Fischer G. et al. J. Geophys. Res., 125, e2020JE006496, 2020.

NITROGEN ATMOSPHERES OF THE ICY BODIES IN THE SOLAR SYSTEM

Titan is the only body in the solar system, besides Earth, that holds a substantial N_2-dominated atmosphere, but its origin and evolution is still debated. A 1D upper atmosphere model and simple scaling laws were used to study thermal and non-thermal escape of nitrogen over Titan's history. It was found that, depending on whether the Sun was a slow, moderate, or fast rotator, Titan could have lost between 0.5 and 16 times the present-day atmospheric N_2-reservoir. This indicates that if the Sun were no slow rotator, Titan's atmosphere must have outgassed later-on in its history, otherwise it could not have been maintained until the present day. These simulations also show that Titan's present-day atmospheric ratio of $^{14}N/^{15}N$ ~167 could not have been changed significantly by atmospheric escape over time with the most likely initial value being ~166-172. This also indicates that Titan's original building blocks must have been different from those of the Earth's N_2. While the latter originated from primitive meteorites, Titan's N_2 likely resulted from NH_3 and complex organics within cometary ices having $^{14}N/^{15}N$ ratios comparable to Titan's initial value. The N-bearing molecules were decomposed in Titan's interior and subsequently outgassed to form its present atmosphere.

Scherf et al., Space Sci. Rev., 216, 123, 2020.

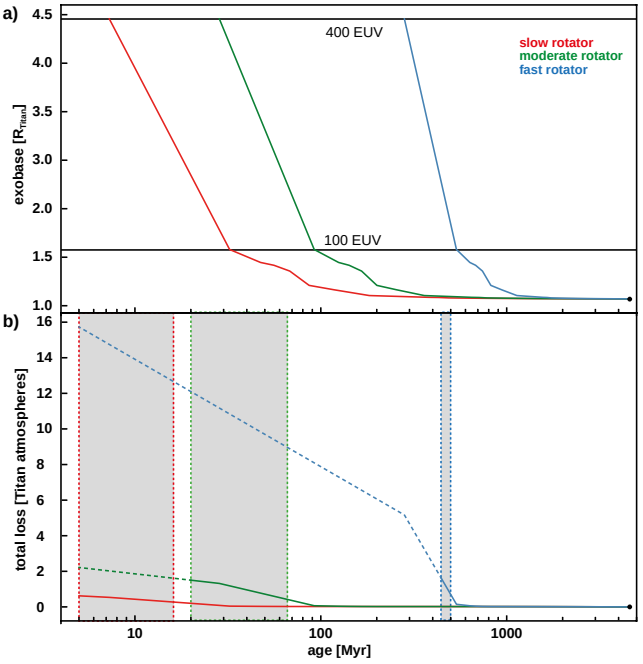

Panel a: Titan's exobase level over time for a slow, moderate and fast rotator. Panel b: The loss of nitrogen over time. The gray areas indicate the earliest possible origin of Titan's atmosphere for the different solar rotators.

COMETS AND DUST

Comets and dust are the remains of the proto-planetary cloud surrounding the new-born Sun, from which the planets were created. Although, dust can also be created at a later stage through collisions of e.g. asteroids. After the groundbreaking *Rosetta* mission ESA's first fast (F-class) mission *Comet Interceptor* has kicked off.

COMET INTERCEPTOR

Comet Interceptor's primary science goal is to characterize, for the first time, a dynamically-new comet or interstellar object, including its surface composition, shape, structure, and the composition of its coma. It will consist of three spacecraft, which will give a unique, multi-point "snapshot" measurement of the comet solar wind interaction region, complementing single spacecraft observations made at other comets.

A new comet, fresh from the Kuiper belt or the Oort cloud, is to be spotted by Earthbound telescopes, its ephemeris determined and then selected as a target if it crosses the ecliptic at an appropriate distance from the Earth. If available, an interstellar object like 1I/'Oumuamua or 2I/Borisov, can also be defined as a target.

Comet Interceptor will be launched with ESA's *ARIEL* spacecraft in 2029. It will be a multi-element spacecraft comprising a primary platform (*A*), which also acts as the communications hub, and two sub-spacecraft (*B1* built by JAXA and *B2* built by ESA), allowing multi-point observations around the target.

IWF will build the DPU for the *MANIaC* package on the primary platform and is involved in the *Dust-Field-Plasma (DFP)* package, for which it will contribute the front-end electronics for the magnetometer on the *B2* spacecraft. In 2020, the work for both instruments was focused on establishing the instrument, performance and interface requirements, which has led to successful completions of the Preliminary Requirements Reviews by the end of the year.

Artist's impression of *Comet Interceptor* (© OHB Italia).

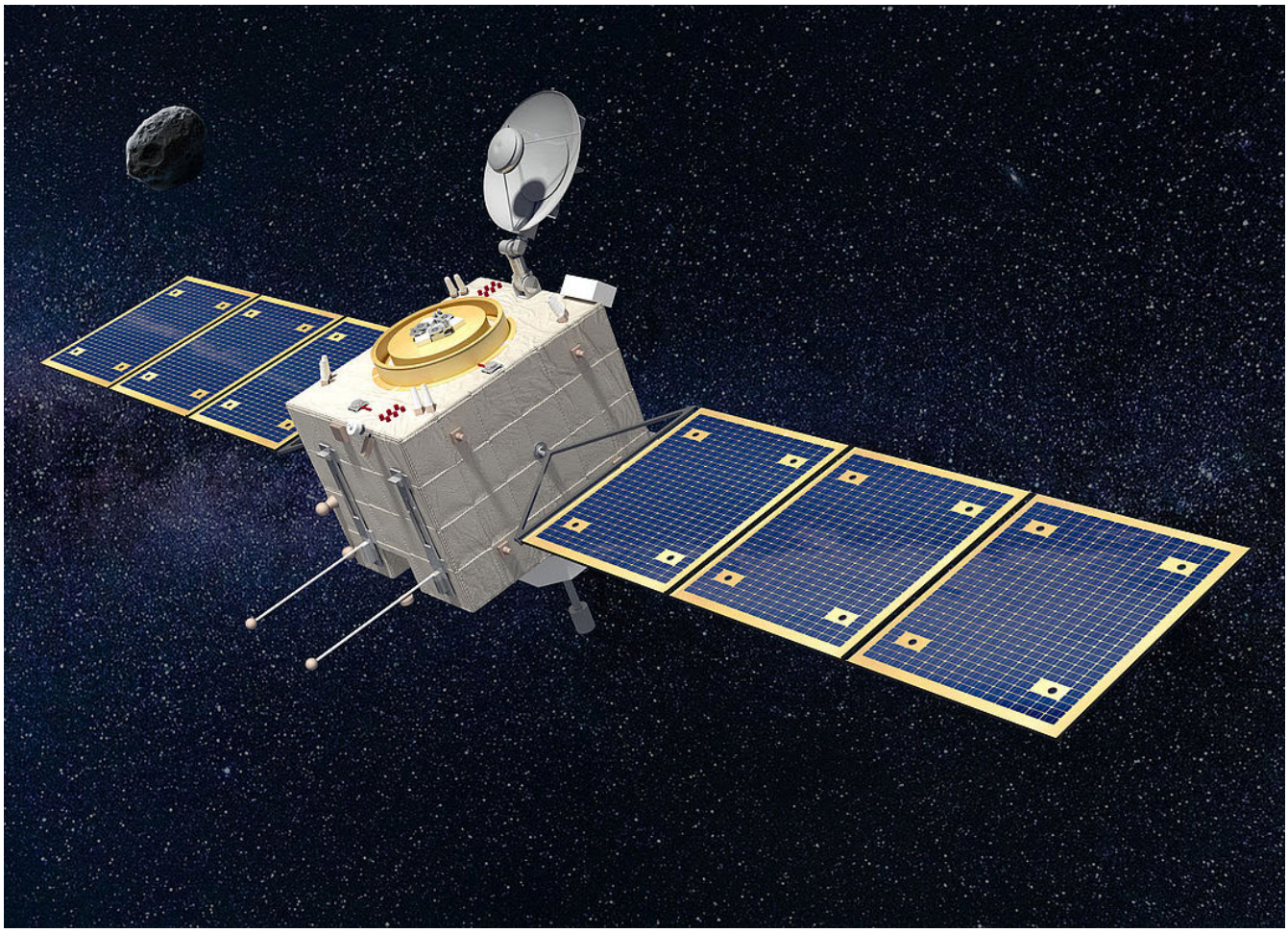

COPHYLAB

CoPhyLab started as a joint project a joint German, Austrian, and Swiss research project between TU Braunschweig, the University of Bern, and IWF to investigate cometary processes in space simulation laboratories. Later on, the following external partners joined: the Max-Planck Institute for Solar System Research (MPS), DLR Berlin, the University of Stirling, and the Qian Xuesen Laboratory of Space Technology in China.

The project aims to increase the understanding of the *Rosetta* mission results by conducting selected experiments in a controlled environment. The campaign is organized in a set of Small (S), Medium (M), and Large (L) experiments. It's core is the Large Chamber, currently being built in Braunschweig, where L-experiments are designed. These will involve the participation of all project partners and run usually for two or three weeks. IWF participates in the design of the L-Chamber and provides hardware components like the solar simulator, a large glass viewport for its light beam, the sample manipulation device, and parts of the sample lifting device.

IWF concentrated mostly on gas flow measurements in granular sample materials. For this purpose experiments in a dedicated vacuum chamber were made. In parallel, a model was developed to simulate the gas flow in such materials based on the experiment results. This simulation is done in close cooperation with the MPS in Göttingen.

The sample manipulation device, developed at IWF, will provide a mobile sensor platform inside the L-Chamber. The main part is a gantry system, which can precisely operate inside the vacuum chamber at liquid nitrogen temperatures to perform various measurements at the sample materials during the test campaign.

CoPhyLab L-Chamber at TU Braunschweig (© ÖAW/IWF/Kargl).

TIME SCALES AND MAGNITUDES OF CHARGED DUST AND S/C POTENTIALS

Interplanetary dust particles originate from the activity of comets, collisions of asteroids, and contribute to the interplanetary medium. Micron-sized dust grains that reside in the solar wind also interact with spacecraft and the surrounding space plasma. These interactions lead to changes in dust grain and spacecraft potentials as well as to local density variations in the dusty plasma itself. Typical time series during a dust impact event on a *MMS* spacecraft is shown in the upper panel of the figure. The vaporization of the dust during the impact event triggers local changes in the space plasma parameters and affects the time series of the signal.

For the correct interpretation of such measurement data it is crucial to develop suitable mathematical models that allow to reconstruct the physics behind these kind of interactions. Standard models assume the dust grain at rest and Maxwellian velocity distributions in the space plasma environment. Important generalizations of these models were performed to include realistic distribution functions, secondary electron emission, and further physical effects. Special emphasis was made to derive valid estimates of observables, with the aim to predict the magnitudes and charging time scales during dust impact events in space, which can be used in future space missions, e.g. *Comet Interceptor*.

Lhotka et al., Phys. Plasmas, 27, 103704, 2020.

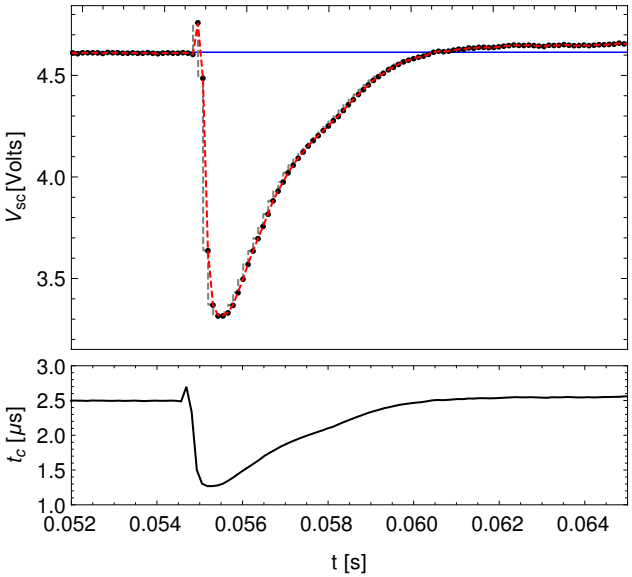

Change of potential during a dust impact event on *MMS* spacecraft and reconstruction of the signal on the basis of mathematical models (red; undisturbed potential in blue) in the top panel, together with estimates of the charging time scales (black) as shown in the bottom panel.

EXOPLANETARY SYSTEMS

The field of exoplanet research (i.e. investigation of planets orbiting stars other than the Sun) has developed strongly in the past decades. Since the discovery of 51 Peg b in 1995, the first detected exoplanet orbiting a Sun-like star, about 4500 exoplanets, most in planetary systems, are now known. Improved instrumentation and analysis techniques have led to the detection of smaller and lighter planets, down to Earth-size, Earth-mass planets, some orbiting in the habitable zone of the cooler stars. However, hot Neptunes and (ultra-)hot Jupiters are still prime targets for atmospheric characterization, mostly because of their larger radii, which indicate the presence of a volatile-rich atmosphere that facilitates observations and analyses.

The main exoplanet missions in which IWF is involved with hardware and/or science are *CHEOPS*, *CUTE*, *PLATO*, *ARIEL*, and *ATHENA*. IWF concentrates on the study and characterization of planetary atmospheres and of the star-planet interaction phenomenon using both theory and observations, focusing particularly on the analysis of exoplanet atmospheric escape and mass-loss processes. The research is based on the collection and analysis of ground- and space-based observations to constrain the models.

CHEOPS data collected during the first stages of science operations have been used to constrain the reflective properties, the day-side temperature, and the planetary orbital obliquity of the hot Jupiter WASP-189b. The data have further demonstrated the excellent quality of *CHEOPS'* photometry.

A tool enabling the use of the cloudy non-local thermodynamic equilibrium radiative transfer code for computing exoplanetary transmission spectra has been developed. It has been demonstrated that the code has a wide applicability range, spanning from Earth-like planets to ultra-hot Jupiters, and that it will be a key tool for interpreting both ground- and space-based transmission spectroscopy observations.

KELT-9b is one of the hottest known exoplanets (Illustration: Harald Ritsch, © ÖAW).

CHEOPS

CHEOPS (CHaracterising ExOPlanet Satellite), successfully launched on 18 December 2019, has started regular science operations on 18 April 2020. The mission aims at studying exoplanets by means of ultra-high precision photometry. The main science goals are to find transits of small planets, known to exist from radial-velocity surveys, measure precise radii for a large sample of planets to study the nature of Neptune- to Earth-sized planets, obtain precise observations of transiting giant planets to study their atmospheric properties, and look for new planets particularly in already known systems. IWF provided the *Back-End-Electronics (BEE)*, one of the two on-board computers, which controls the data flow and the thermal stability of the telescope structure. The institute also developed the mission's signal-to-noise calculator. Within the guaranteed time observations of the *CHEOPS* consortium, IWF is also responsible for two observing programs aiming at improving our understanding of the mass-radius relation of planets and of processes affecting planetary atmospheric evolution.

Between January and April 2020, *CHEOPS* went through its commissioning phase that has culminated in the demonstration of the achievement of the mission requirements. In particular, *CHEOPS* shall be able to detect Earth-size planets transiting G5 dwarf stars (i.e. 0.9 solar radii) in the V = 6-9 magnitude range by achieving a photometric precision of 20 ppm in 6 hours of integration time. In the case of K-type stars (i.e. 0.7 solar radii) in the V = 9-12 magnitude range, *CHEOPS* shall be able to detect transiting Neptune-size planets achieving a photometric precision of 85 ppm in three hours of integration time. To demonstrate the achievement of the science requirements, during commissioning *CHEOPS* observed HD88111, which is a magnitude V = 9.2 G-type star for which *GAIA* provides a radius of 0.9 solar radii. The photometric precision and stability were estimated by finding the transit depth that can be detected with a signal-to-noise ratio of one. For a six hours period of observations, the achieved photometric precision was 15.5 ppm that is well within the requirements. Furthermore, *CHEOPS* observed TYC 5502-1037-1 that is a magnitude V = 11.9 K-type star with a radius of 0.7 solar radii, achieving a 75 ppm precision, compliant with the science requirements. These precisions have been achieved without any detrending, therefore reflecting the intrinsic stability of *CHEOPS*.

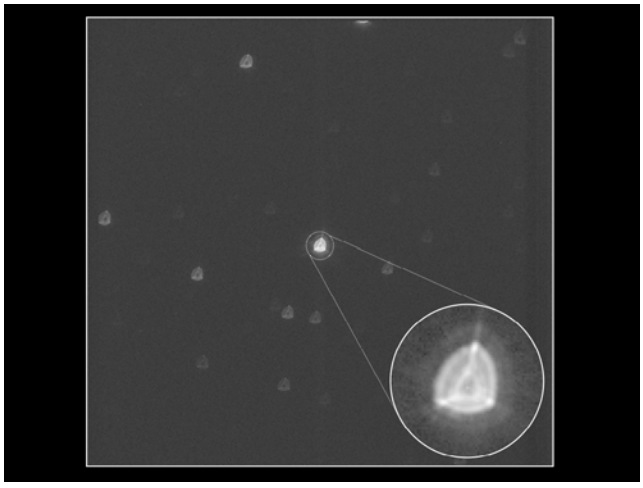

CHEOPS image of its first target star (© ESA/Airbus/*CHEOPS* Mission Consortium).

A few stars known to host planets were also targeted during commissioning as part of the end-to-end validation of the operational process. The giant planet KELT-11b was among these targets. The planet orbits an evolved sub-giant star of magnitude V = 8 in a period of about five days. The data were analyzed employing "pycheops" that is a python code developed by the *CHEOPS* science team specifically for the analysis of *CHEOPS* data. Considering the stellar radius given in the literature, the results of the data analysis led to a planetary radius measurement in agreement with that provided in the literature, but with an about five times smaller uncertainty.

CUTE

CUTE (Colorado Ultraviolet Transit Experiment) is a NASA-funded 6U-form CubeSat led by the University of Colorado and scheduled for launch in September 2021. It will perform low-resolution transmission spectroscopy of transiting exoplanets at near-ultraviolet wavelengths. *CUTE* will study the upper atmosphere of short period exoplanets with the aim of observationally constraining atmospheric escape processes, which are key to understand planetary evolution, and detect heavy metals, which constrain the presence and composition of aerosols in the lower atmosphere. Furthermore, *CUTE*'s continuous temporal coverage of planetary transits will allow to detect transit asymmetries, which are possibly connected with the presence of planetary magnetic fields.

IWF is the only technological contributor to the mission outside of the University of Colorado (Boulder), where *CUTE* is being developed. IWF is responsible for the development of the data simulator, of the data signal-to-noise calculator, of the ground data reduction software, and of the algorithms defining the on-board data reduction software.

In 2020, IWF has finalized the development of the *CUTE* data signal-to-noise calculator and has focused on the development of the data reduction software that will reach completion following laboratory tests on the flight instrument to be performed in 2021 and following the collection of commissioning data right after launch.

PLATO

PLATO (PLAnetary Transits and Oscillations of stars) is ESA's third medium (M-class) mission, led by DLR. Its objective is to find and study a large number of exoplanetary systems, with emphasis on the properties of terrestrial planets in the habitable zone around solar-like stars. *PLATO* has also been designed to investigate seismic activity of stars, enabling the precise characterization of the host star, including its age. IWF takes part in two work packages (one on stellar characterization and one on planetary evolution) aiming at gaining the knowledge and preparing the tools necessary to best exploit the data. The institute contributes to the development of the I*nstrument Controller Unit (ICU)* with the development of the *Router and Data Compression Unit (RDCU)*. Launch is expected in 2026.

PLATO consists of 24 telescopes for nominal and two telescopes for fast observations. Each telescope has its dedicated front-end-electronics, reading and digitizing the CCD content. Twelve nominal and two fast DPUs collect the data from the front-end-electronics and extract the areas of interest. The *RDCU* is a key element in the data processing chain, providing the communication between the DPUs and the *ICU*. The second task of the *RDCU* is the lossless compression of the science data. For performance reasons, the compression algorithm is implemented in an FPGA.

Main tasks in 2020 were the finalization and manufacturing of the *RDCU* engineering models, the continuation of the design of the VHDL code and the finalization of the test environment. The design of the compressor, in particular the communication with the *ICU*, has been completely redesigned to comply with the increased number of imagettes. The latest design of the *RDCU* is compliant with all requirements and can handle 20% more scientific data than actually requested.

ARIEL

ARIEL (Atmospheric Remote-sensing Infrared Exoplanet Large-survey) is ESA's fourth medium (M-class) mission, led by University College London, to be launched in 2028. It will investigate the atmospheres of several hundreds exoplanets to address the fundamental questions on how planetary systems form and evolve. During its four-year mission, *ARIEL* will observe 1000 exoplanets ranging from Jupiter- and Neptune- down to super-Earth-size in the visible and infrared with its meter-class telescope. The analysis of *ARIEL* spectra and photometric data will enable extracting the chemical fingerprints of gases and condensates in planetary atmospheres, including the elemental composition for the most favorable targets, with a particular focus on carbon and oxygen. Thermal and scattering properties of the atmosphere will also be studied.

ARIEL consists of a one meter telescope feeding two infrared low-resolution spectrographs and the fine guiding sensor (FGS), working in the optical. To improve the satellite's pointing stability, the FGS provides optical photometry of the target in three broad bands that are used to control instrumental systematics, measure intrinsic stellar variability, and constrain the presence of high-altitude aerosols in planetary atmospheres. Within the *ARIEL* mission, IWF co-leads the upper atmosphere working group and is heavily involved in testing the mission's performances and advancing the atmospheric retrieval tools.

Artist's impression of ESA's *PLATO* spacecraft. This top view highlights the unique payload that comprises 26 cameras. Two smaller cameras, seen at top in this image, are not part of the payload, but rather startrackers used for navigation (© ESA/ATG medialab).

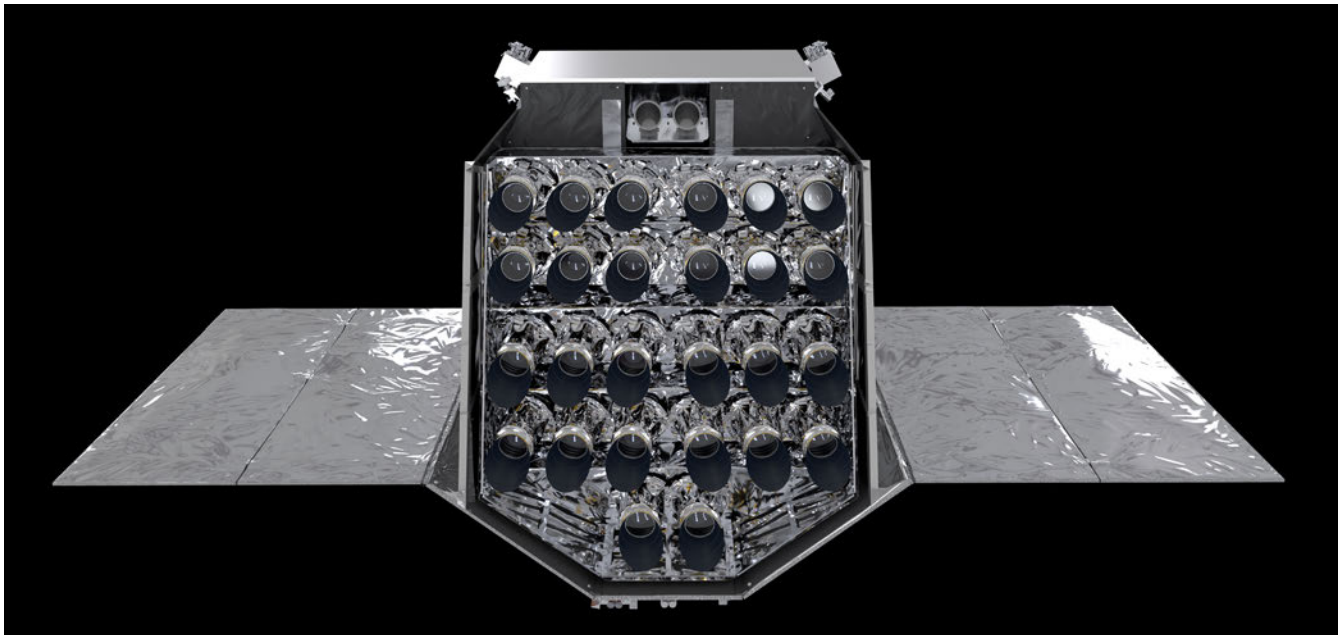

ATHENA

ATHENA (Advanced Telescope for High-ENergy Astrophysics), is ESA's second large (L-class) mission in the Cosmic Vision 2015-2025 plan. Its objective is to study hot gas in clusters and groups of galaxies and the intergalactic medium, to determine how ordinary matter assembles into large-scale structures. The second topic is the growth of black holes and their impact on the universe. The observations in the X-ray range of the electromagnetic spectrum will help to understand the high energetic processes close to the event horizon of black holes and provide more details for the baryonic component, locked in ultra-hot gas.

The institute will contribute to the *Wide Field Imager (WFI)* with the development of the *Central Processing Module (CPM)*. At present, the team is executing a study to classify the performance increase when using the latest processor technology. Key topics are the performance of the processor cores, efficiency of the internal data bus system, the multi-core configuration, but also the communication between the four processor cores.

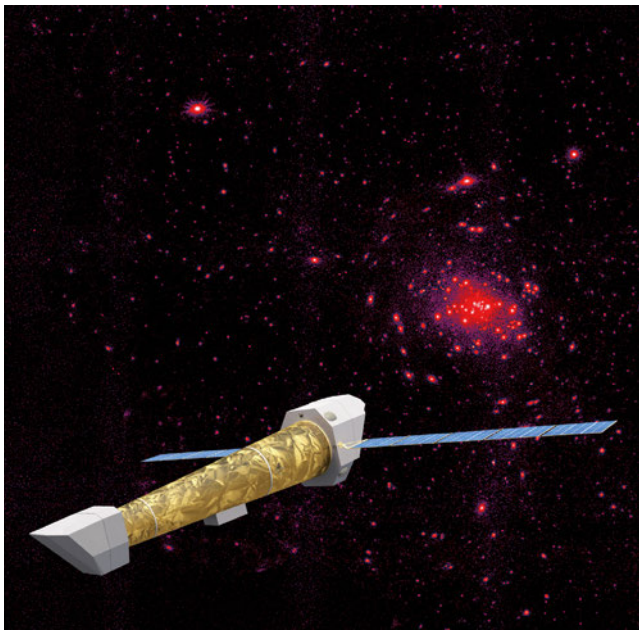

Artistic view of *ATHENA* (© IRAP, CNES & ESA, ACO) looking at the Andromeda Galaxy (© N. Vulic).

HOT DAYSIDE & ASYMMETRIC TRANSIT OF WASP-189B SEEN BY CHEOPS

As *CHEOPS* carries out its observations in a broad optical passband, it can provide insights into the reflected light from exoplanets. It can constrain the short-wavelength thermal emission for the hottest planets by observing occultations and phase curves. Observations of the hot Jupiter WASP-189b, a two Jupiter-masses planet orbiting an A-type star, have been collected with *CHEOPS* during the first stage of science operations. Four occultations of WASP-189b have been detected at high significance in individual measurements resulting to an occultation depth of 87.9±4.3 ppm. Comparisons with model predictions indicate that the occultation measurement is consistent with an unreflective atmosphere heated to a temperature of 3435±27 K, when assuming inefficient heat redistribution. Furthermore, two additional *CHEOPS* transits of WASP-189b reveal an asymmetric shape that is attributed to gravity darkening of the host star caused by its high rotation rate. These measurements have been also used to refine the planetary parameters, finding an about 25% deeper transit compared to literature. Also, the data enabled one to measure a projected orbital obliquity of 86.4+2.9-4.4 deg, in good agreement with a previous spectroscopic measurement, and to derive a true obliquity of 85.4±4.3 deg. The data reveal that for a 6.6 mag star, and using a one-hour binning, *CHEOPS* delivers data with a residual root mean square error between 10 and 17 ppm on the individual light curves, and 5.7 ppm when combining the four transits.

Lendl et al., Astron. Astrophys., 643, A94, 2020.

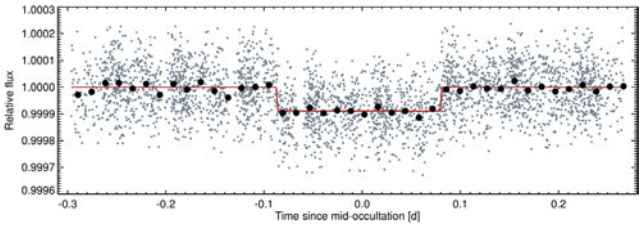

Corrected and phase-folded *CHEOPS* occultation light curve of WASP-189b. Black points show the light curve binned into 20-minute intervals, the red line shows the final occultation model.

MITIGATING FLICKER NOISE IN HIGH-PRECISION PHOTOMETRY

The short-timescale stellar photometric variability ("flicker") can reach amplitudes comparable to the transit depth of Earth-sized planets. Characterizing the statistical properties of flicker noise and quantifying its impact are therefore critical. Solar observations have been used to identify flicker noise and simulate realistic transits across the solar disk to estimate the errors made on the transit parameters due to the presence of real solar noise. *Kepler* observations have been further used to extend the study to a wider parameter range. It was shown that stellar granulation is a stochastic colored noise. Both the flicker correlation timescales and amplitudes increase with the stellar mass and radius. Biases can occur if these correlations are not taken into account, when fitting for the parameters of transiting exoplanets. In particular, errors of up to 10% on the planet-to-star radius ratio have been found for an Earth-sized planet orbiting a Sun-like star. Therefore, flicker will significantly affect the inferred parameters of transits observed at high precision with *CHEOPS* and *PLATO* for F- and G-type stars.

Sulis et al., Astron. Astrophys., 636, A70, 2020.

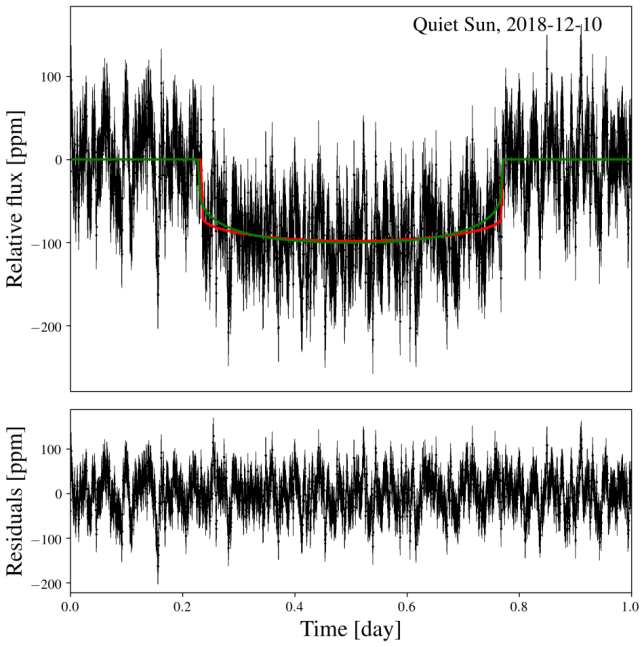

Top: Example of artificial transit of an Earth-sized planet crossing the disk center of the Sun (black). The transit model with the true input parameters is shown in green and the model computed using the inferred parameters in red. The error on the planet-to-star radius ratio is around 2% in this example. Bottom: Residuals based on the inferred transit model.

CaII H&K STELLAR ACTIVITY PARAMETER AS A PROXY FOR STELLAR EUV FLUXES

Atmospheric escape is an important factor shaping the exoplanet population and hence drives our understanding of planet formation. Atmospheric escape from giant planets is driven primarily by the stellar X-ray and extreme-ultraviolet (EUV) radiation. Furthermore, EUV and UV radiation power disequilibrium chemistry. Our understanding of atmospheric escape and chemistry, therefore, depends on our knowledge of the stellar UV fluxes. While the far-ultraviolet fluxes can be observed for some stars, most of the EUV range is unobservable due to the lack of a space telescope with EUV capabilities and, for the more distant stars, due to interstellar medium absorption. Thus it becomes essential to have indirect means for inferring EUV fluxes from features observable at other wavelengths. Analytic functions have been developed for predicting the EUV emission of F-, G-, K-, and M-type stars from the $\log R'_{HK}$ activity parameter that is commonly obtained from ground-based optical observations of the CaII H&K lines. The scaling relations are based on a collection of about 100 nearby stars with published $\log R'_{HK}$ and EUV flux values, where the latter are either direct measurements or inferences from high-quality far-ultraviolet (FUV) spectra. The scaling relations return EUV flux values with an accuracy of about three, which is slightly lower than that of other similar methods based on FUV or X-ray measurements.

Sreejith et al., Astron. Astrophys., 644, A67, 2020.

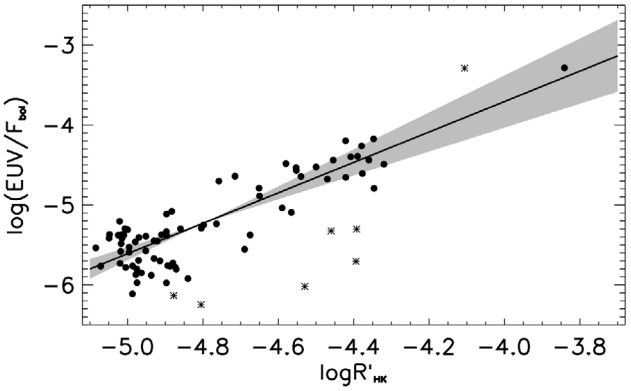

Correlation between the stellar activity index ($\log R'_{HK}$) and EUV flux for F-, G-, and K-type stars. The RMS on $\log(EUV/F_{bol})$ after the fit is 0.40. Stars removed as a result of a sigma clipping algorithm applied to remove outliers are indicated by the asterisks. The gray areas indicate the uncertainties on the fit.

NEAR-ULTRAVIOLET TRANSMISSION SPECTROSCOPY OF HD209458b

The inflated transiting hot Jupiter HD209458b is one of the best studied objects since the beginning of exoplanet characterization. A re-analysis of near-ultraviolet (NUV) transmission observations of HD209458b enabled us to detect ionized iron (FeII) absorption in a 100 Å-wide range around 2370 Å, lying beyond the planetary Roche lobe. However, absorption of equally strong FeII lines expected to be around 2600 Å has not been detected. Neutral magnesium (MgI), ionized magnesium (MgII), and neutral iron (FeI) have also not been detected. These results avoid the conflict with theoretical models present on the basis of previous analyses, which detected MgI but did not detect MgII from this same dataset. The data reveal evidence for the presence of strong hydrodynamic escape that carries atoms as heavy as iron beyond the planetary Roche lobe, even for planets less irradiated than extreme ultra-hot Jupiters such as WASP-12b and KELT-9b. The detection of iron and non-detection of magnesium in the upper atmosphere of HD209458b can be explained by a model in which the lower atmosphere forms (hence, sequesters) primarily magnesium-bearing condensates, rather than iron condensates, as suggested by current microphysical models. The inextricable synergy between upper- and lower-atmosphere properties highlights the value of combining observations that probe both regions.

Cubillos et al., Astrophys. J., 159, 111, 2020.

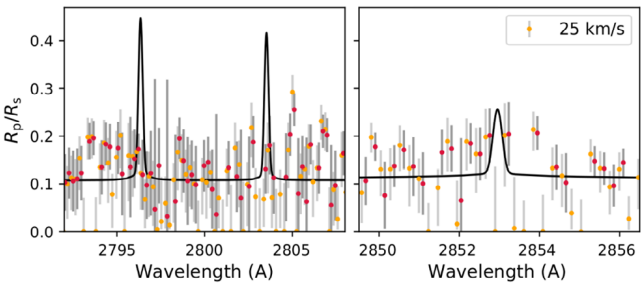

HD209458b transmission spectrum around the MgII h&k (left) and MgI (right) resonance lines at 25 km/s spectral resolution. The yellow and red dots denote the transit depths obtained from two different data analysis methods, the gray lines show the error bar (see legend). A horizontal shift has been implemented for visibility. The black solid lines show the magnesium absorption profiles based on the densities obtained from a recent upper atmosphere model uncapped at the Roche lobe boundary. No significant absorption feature has been detected at the wavelengths of the magnesium lines.

NON-LTE TRANSMISSION SPECTRUM MODELING OF HD209458b

Exoplanetary upper atmospheres are low density environments where radiative processes can compete with collisional ones and introduce non-local thermodynamic equilibrium (NLTE) effects into transmission spectra. A NLTE radiative transfer framework capable of modeling exoplanetary transmission spectra over a wide range of planetary properties has been developed. The NLTE spectral synthesis code Cloudy has been adapted to produce an atmospheric structure and atomic transmission spectrum in both NLTE and local thermodynamic equilibrium (LTE) for the hot Jupiter HD209458b, given a published temperature-pressure profile. Selected spectral features, including Hα, NaI D, HeI 10830 Å, FeI & II ultraviolet (UV) bands, and C, O and Si UV lines, are compared with literature observations and models where available. The strength of NLTE effects are measured for individual spectral lines to identify which features are most strongly affected. The developed modeling framework computing NLTE synthetic spectra reproduces literature results for the HeI 10830 Å triplet, the NaI D lines, and the forest of FeI lines in the optical. Individual spectral lines in the NLTE spectrum exhibit up to 40% stronger absorption relative to the LTE spectrum.

Young et al., Astron. Astrophys., 641, A47, 2020.

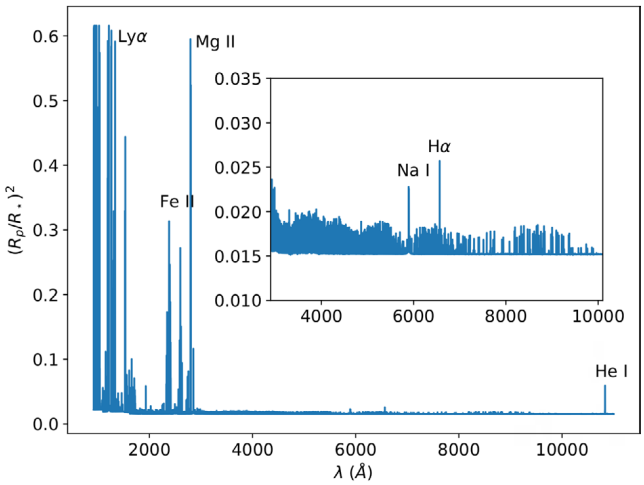

High spectral resolution (R = 100000) synthetic NLTE transmission spectrum of HD209458b at mid-transit. Prominent features include Lyman series lines, FeII packets of lines at 2350 and 2600 Å, the MgII h&k doublet at 2800 Å, NaI D lines at 5890 Å, Hα, and the HeI triplet at 10830 Å. The inset displays the finer details of the 3000-10000 Å range.

CONSTRAINING THE ATMOSPHERIC TEMPERATURE STRUCTURE OF KELT-9b

Observationally constraining the atmospheric temperature-pressure (TP) profile of exoplanets is an important step forward for improving planetary atmosphere models. The observed transmission spectra of the Hα and Hβ lines have been employed to constrain the TP profile of the ultra-hot Jupiter KELT-9b. Almost 150 one-dimensional TP profiles have been constructed varying the lower and upper atmospheric temperatures, as well as the location and gradient of the temperature rise. For each TP profile, transmission spectra of the Hα and Hβ lines have been computed employing the Cloudy radiative transfer code, thus accounting for non-local thermodynamic equilibrium (NLTE) effects. The TP profiles leading to the best fit of the observations are characterized by an upper atmospheric temperature of about 10000 K and by an inverted temperature profile at pressures higher than 10^{-4} bar. The assumption of local thermodynamic equilibrium leads to overestimate the level population of excited hydrogen by several orders of magnitude, and hence to significantly overestimate the strength of the Balmer lines. Modeling the atmospheres of ultra-hot Jupiters requires one to account for metal photo-ionization and NLTE effects.

Fossati et al., Astron. Astrophys., 643, A131, 2020.

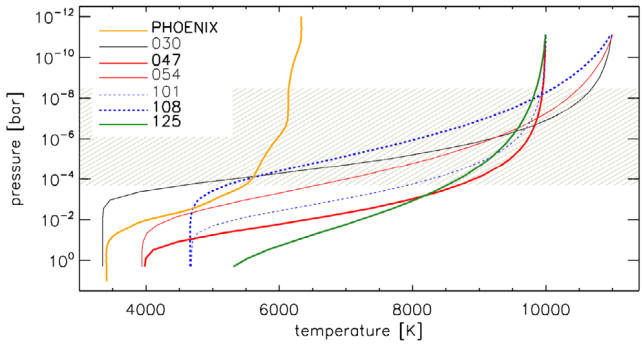

TP profiles (for different runs) best fitting the observed Hα and Hβ lines. The thicker lines indicate the three TP profiles fulfilling stricter conditions set for the line fit. The hatched area shows the main formation region of the Hα and Hβ lines according to the three best fitting models.

UV NI LINES IN THE ATMOSPHERE OF TRANSITING EARTH-LIKE PLANETS

Nitrogen is a biosignature gas that cannot be maintained in its Earth-like ratio with CO_2 under abiotic conditions. It has also proven to be notoriously hard to detect at optical and infrared wavelengths. The ultraviolet region may provide new opportunities to characterize exoplanetary atmospheric nitrogen. The non-local thermodynamic equilibrium spectral synthesis code Cloudy has been used to produce a far-ultraviolet atomic transmission spectrum for an Earth-Sun-like system, and identify nitrogen features. The number of transits required for 1σ and 3σ detections of the planetary NI 1200 Å triplet signal with the G120M grating of the *LUMOS* spectrograph designed for the *LUVOIR* mission, as a function of distance to the system and stellar ultraviolet emission, has been estimated. The resulting minimum number of transit observations are 188 and 1685, respectively, for a system located at a distance of one pc with 100 times the solar ultraviolet flux. Future studies in this direction should therefore focus on Earth-like planets orbiting in the habitable zone of M dwarfs.

Young et al., Astron. Nachr., 341, 879-886, 2020.

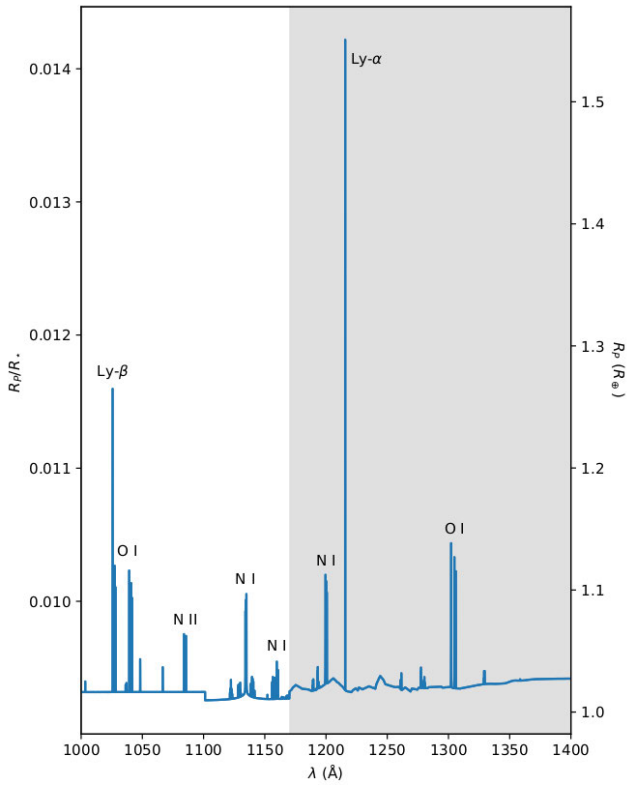

Far-UV transmission spectrum of an Earth-like planet orbiting a Sun-like star. Prominent features are marked. The gray shaded region indicates where the molecular continuum from the literature has been added a posteriori.

VARIABILITY OF TRANSIT LIGHT CURVES OF KEPLER OBJECTS

Hitherto, the study of exoplanetary transit timing and duration variability supposed the transit light curves (TLCs) to be symmetric, suggesting a priori a spherical shape for the transiter. As a result, the independent positions of transit borders are unknown. Using a-quadratic approximation for the independently considered start-, end-, and minimum- parts of the long-cadence phase-folded TLCs of different types of exoplanets, provided by the *Kepler* space telescope, their variability is checked for the first time. Temporal and cross-correlation analysis of the TLCs timing parameters over the whole observation period of *Kepler* (> 3 years) enable detection and diagnostics of the varying transit borders and TLCs' asymmetry. Among the considered TLCs of 98 *Kepler* Objects of Interest (KOIs), 15 confirmed giant exoplanets and five objects with still debatable status (probably non-planets) show variations in their transit timing parameters at timescales from ≈400 to > 1500 days. These variations are especially well manifested as an anti-correlation between the transit start- and end- time, indicating variability in the dimensions of transiting shadows.

Also the objects with well pronounced oscillations of transit border timing and asymmetry were found. The discovered variability of transit timing is an important indicator of the large-scale non-stationary processes in the atmospheres of KOIs, as well as dust and aerosol generation in their upper layers and in their close vicinity. A catalog of the most peculiar objects, which deserve further investigation and detailed modeling was elaborated.

Arkhypov et al., Astron. Astrophys., 638, A143, 2020.

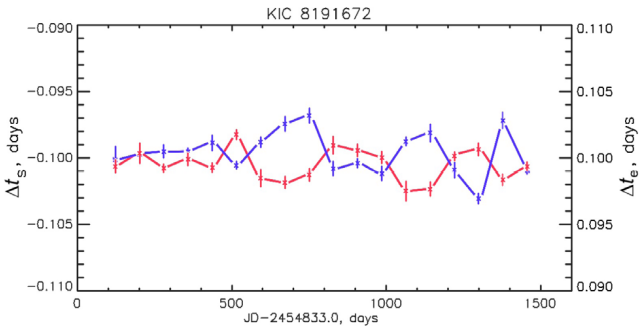

Anti-correlated variations of the start- (Δt_s, red) and end- (Δt_e, blue) time for the KOI 18.01 revealed in the TLC of KIC 8191672.

SATELLITE LASER RANGING

In addition to routinely tracking more than 150 targets, which are equipped with laser retro-reflectors, the Satellite Laser Ranging (SLR) station of IWF is working on various international projects.

Recent highlights include a publication in "Nature Communications" presenting first successful daylight space debris laser ranging, MHz laser ranging with millimeter accuracy both during day and night, and a new technique called quanta photogrammetry to measure unique light curve fingerprints of tumbling satellites and space debris.

DAYLIGHT SPACE DEBRIS LASER RANGING

The daylight space debris laser ranging observation routine consists of the following steps: the tracking of a target is usually started at elevations above 15°. The target is visualized against the blue sky background using a 20 cm piggyback telescope. As soon as the target is detected using a self-developed real-time detection software and the determined offsets are used to correct the inaccurate orbit predictions and to center the target within the field of view of the SLR telescope. Additional across-track offsets are corrected by applying pointing offsets to the receiving telescope. Varying biases are continuously corrected during tracking, primarily by correcting the time bias. Range biases of the target due to two line element (TLE) errors cannot be estimated via image analysis and the only chance to apply corrections to the predictions is by shifting the activation time of the detector. The closer the activation of the detector is to the arrival time of a reflected photon the higher the chances of detection are.

The space debris laser ranging search routine is an iteration process consisting of applying time biases, optically centering the target and experimentally shifting the detector activation times. Four successful space debris passes were measured between March and October 2019. Space debris laser ranging measurements were regarded as daylight passes if the elevation of the Sun was above the horizon. Three different types of SL (Sea Launch) rocket bodies originating from Zenit, Tsyklon or Vostok launches between 1971 and 1995 were observed. The maximum Sun elevation during the measurement was 39° at 10:31 local time on 22 March 2019. The observed-minus-calculated residuals of an SL-16 rocket body relative to the predicted pass (corrected by the real-time time bias applied to center the target) are displayed in the figure. The measurement lasted for approximately 100 s. A slope within the reflected photons indicates that the time bias used to center the target was slightly underestimated, which is related to imperfect alignment of the optical axis of the piggyback telescope. Due to the remaining time bias, the object moves to regions further away from the initial detector activation time and the trace of the debris within the noise would soon disappear. Once recognizing the returns from the object, the observer hence shifts the triggering time towards the returning photons, increasing the detection probability. A correct time bias results in returns appearing as a straight line within the residuals. Applying the time and range biases to the predicted orbit, it is possible to match the measured values to predicted ones resulting in residuals close to zero. Returns coming from the front and the back of the body are statistically detected corresponding to range differences of up to 8 m giving an indication of the size of the rocket body.

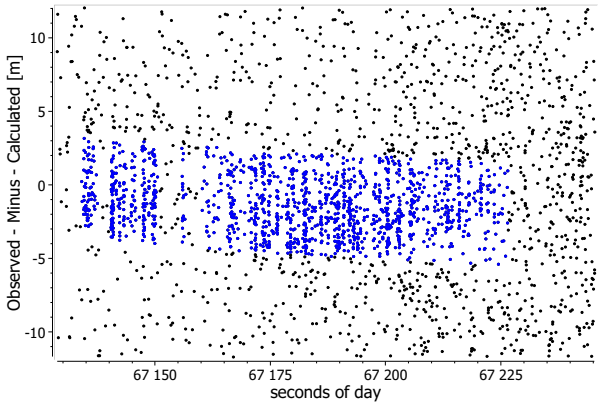

Daylight space debris laser ranging results to an SL-16 upper stage rocket body (NORAD ID: 22803). The figure shows the orbit corrected Observed-Minus-Calculated Residuals [m] vs. the seconds of day on 2019/10/01 at a Sun elevation of 11.5°. Identified photons from the rocket body are highlighted in blue.

These daylight space debris laser ranging results guide the way to significantly increasing potential observation times. Depending on the season, for the Graz SLR station twilight conditions occur for a maximum of 6 h per day while daylight lasts for 8-16 h, increasing potential observation times in Graz up to 22 h. The increased coverage will encourage an observation network of space debris stations to be formed (similar to the International Laser Ranging Service), which could immediately react in case of conjunction warnings targeting a certain object rapidly improving the predictions. Improved predictions are central in decision-making with respect to avoidance maneuvers. In addition to that, highly accurate orbits are crucial for future active removal or laser nudging missions.

Steindorfer et al., Nat. Comm., 11, 3735, 2020.

MHZ LASER RANGING DEMONSTRATION

In the past 20 years, the kHz SLR technology was practiced widely in the International Laser Ranging Service (ILRS) network. Ultra-high repetition rate laser ranging (up to MHz) is the next promising strategy for future SLR. Increased repetition rates, ultra-short pulse width and low pulse energy can significantly improve the performance of SLR in terms of data density, accuracy, precision and stability to further enhance its unique contributions to the International Terrestrial Reference Frame.

In July 2020, the SLR station in Graz demonstrated 1 MHz SLR using a laser with a very low pulse energy of ~7.8 µJ. Targets from low Earth orbits up to inclined geosynchronous orbits were successfully tracked during nighttime up to a maximum slant range of 38,000 km. Among those, a maximum return rate of up to 53% was achieved, equivalent to 265,000 returns per second for the satellite *Swarm-B*. Compared to the conventional 2 kHz SLR system in Graz, the 1 MHz SLR system leads to significantly higher return rates in all orbital regimes. According to the ILRS normal point (NP) algorithm, this will significantly improve the precision of the final NP results in view of statistical errors. Consequently, it will also lead to an increased temporal resolution for distinguishing individual retro-reflector cubes, analyzing the spin rate, spin axis motion, signature and attitude of satellites and space debris objects.

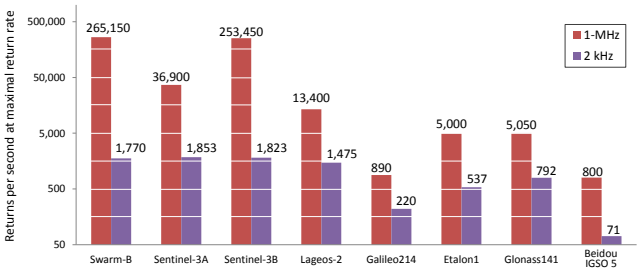

A comparison of returns per second between Graz 2 kHz system (in the year 2020) and the 1 MHz demonstration in different orbits from Low Earth Orbit (LEO) up to Inclined Geosynchronous Orbit (IGSO). It shows that a 1 MHz system improves by up to two magnitudes for some LEO satellites (*Swarm*, *Sentinel*), and up to one magnitude more data for high orbiters (e.g. *Beidou*).

Currently, SLR Graz tracks uncooperative space debris with a 16 Watt, 200 Hz laser ranging. Although the lower pulse energy will decrease the detection probability, this can be compensated by increasing the laser repetition rate. A new MHz laser with increased power will be installed as a next step to further test this potential application.

QUANTA PHOTOGRAMMETRY

The conventional detection of Micro-Meteoroid and Orbital Debris (MMOD) impacts on satellites is based on in-situ sensing or direct, visual inspection of the retrieved surface elements exposed to the particle flux and thus requires active in-orbit operations. Quanta Photogrammetry (QPM) is an optical method for remote detection of surface structural anomalies of passive satellites by measuring solar photon flux reflected off the satellite surface towards the ground detection system.

The light curves of the experimental geodetic satellite *Ajisai* (NORAD 16908, altitude of 1490 km) are collected with a single photon avalanche diode (SPAD) counting system. QPM utilizes the inertial attitude model of the satellite to project the high-rate photometric samples onto the spacecraft body fixed frame. Single-photon light curves collected from October 2015 until January 2018 are used to map the reflectivity of 149 mirror panels on-board of *Ajisai* (approx. sized 20 × 20 cm each).

The superposition of the photometric samples collected over multiple passes reveals the structural details of the reflective surfaces and locates the persistent anomalies. Exemplarily four mirrors are presented in the figure below where plateau-normalized observations are fitted by a low-degree polynomial mesh in order to generate the photogram. Relatively small, irregularly shaped (panel b) and spot-like (panels c, d) anomalies are revealed that can indicate surface degradation due to long-term environmental interactions and MMOD hypervelocity impacts.

Kucharski et al., Acta Astronaut., 174, 24-31, 2020.

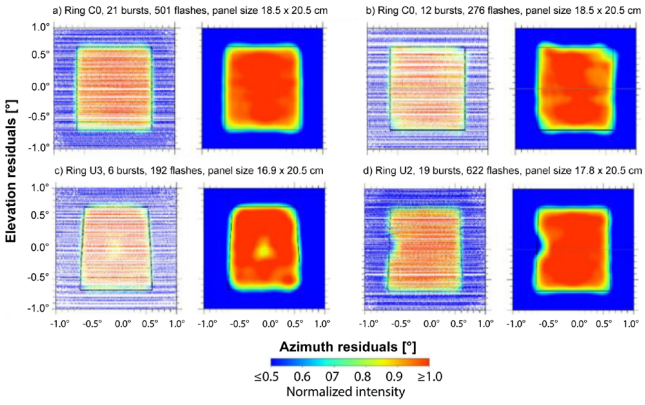

Measured flux and average photogram of four different mirrors of *Ajisai* with different panel sizes. The flux is displayed relative to the angular coordinate system with respect to the central normal N of each mirror. a) an expected reflection pattern of a good quality panel, b) panel with reflectivity irregularities at the edges, c) panel with a central spot-like reflectivity defect, d) panel with a spot-like reflectivity defect at the edge of the mirror.

TECHNOLOGIES

NEW DEVELOPMENTS

One possible aspect to reduce costs of space exploration and hence allowing for more frequent missions is to reduce the spacecraft size and consequently the launch masses. Scientific instruments also have to decrease their resource requirements such as volume, mass, and power, but at the same time achieve at least the same performance as heritage instruments. Therefore, the development of new instrument technologies is essential for competitive and excellent space research.

NEXT GENERATION ASPOC

For future science missions, active spacecraft potential control down to <10 V is crucial to be able to operate sensitive scientific payloads. This does not only apply to large and medium-sized spacecraft, but also to micro- and nano-spacecraft, such as CubeSats. IWF, together with FOTEC, started a two-year technology study with the goal to develop a miniaturized version (50% power, 40% mass) of the *ASPOC* instruments built for NASA's *MMS* mission, which, six years after launch, are still operating flawlessly.

The *ASPOC* instrument as flying aboard NASA's *MMS* mission (left, © ÖAW/IWF) and the electronics box design of the next generation *ASPOC* (right, © ÖAW/IWF/Wallner).

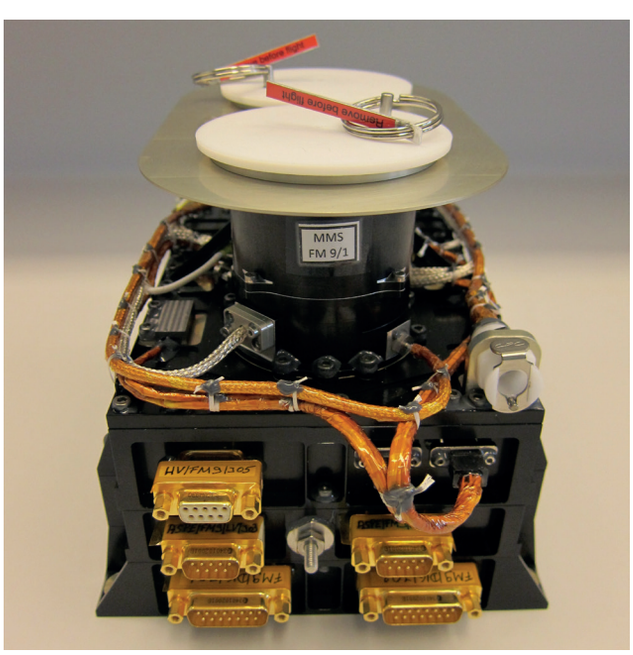

The developed next generation *ASPOC* (*ASPOC-NG*) consists of the following major components:

- Ion or electron emitter module (by FOTEC)
- Power and control electronics box (by IWF)
- On-board software (by IWF)

High voltages are fed through the top plate of the electronics box directly into the base of the emitter module via spring contacts. The reservoir for the ion source is heated by driving a current over a Pt100 temperature sensor.

IWF completed the *ASPOC-NG* vacuum chamber setup and conducted performance and beam divergence tests with an emitter test module from FOTEC. The typical operating voltage for a beam current of 10 µA was 7.70 kV. Successive stability tests at different beam currents ranging from 5 to 80 µA showed an overall good performance. By using a Gallium-Indium alloy as propellant, it was possible to reduce the heating power from 800 mW *(MMS)* to 200 mW *(ASPOC-NG)*.

Concerning the control electronics developed by IWF, the layout of all boards (DPU extension board, filament converter, HV control and HV cascade) was finished. IWF also finalized the grounding scheme, which applies to the *ASPOC* electronics box and the emitter module. Finally, the mechanical design of the electronics box has been completed. In December 2020, IWF also successfully passed the Detailed Design Review with ESA, which allows IWF to continue with assembly, integration and test.

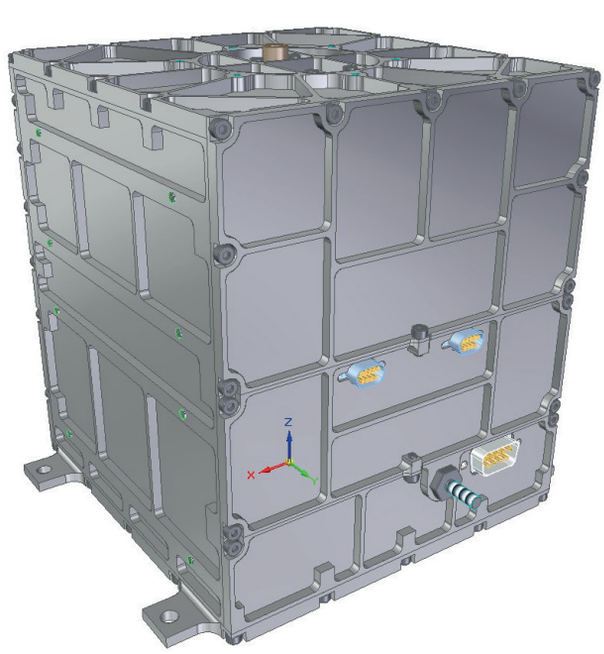

MAGNETOMETER FRONT-END ASIC

IWF and the Institute of Electronics of the Graz University of Technology (TUG) are collaborating on the next generation of the space proven Magnetometer Front-end ASIC (MFA). It features the readout electronics for magnetic field sensors which is optimized in terms of size and power consumption. The next generation Application Specific Integrated Circuit (ASIC) shall overcome dynamic range limitations. It will be space qualified in the frame of the *FORSESAIL* mission.

In 2020, two earlier developed test chips have been further evaluated. The first chip was fabricated in a 180 nm technology by United Microelectronics Corporation (UMC), the second chip by XFAB Silicon Foundries. The first chip contains a single axis of the required feedback path including a single-bit digital-to-analog converter, which combines delta-sigma modulation with the benefits of pulse width modulation. Measurement results have shown that all developed building blocks have a signal-to-noise ratio of over 100 dB.

The digital-to-analog converter on the second test chip consists of 64 current steering cells, dynamic element matching and a digital delta-sigma modulator. In order to meet the requirements regarding low power consumption and high linearity a two-stage cascaded delta-sigma modulator with current output was implemented. Each noise shaper was realized as a third-order modulator with a current-steering cell. Evaluation results indicated an effective number of 17 bits for a given bandwidth of 512 Hz.

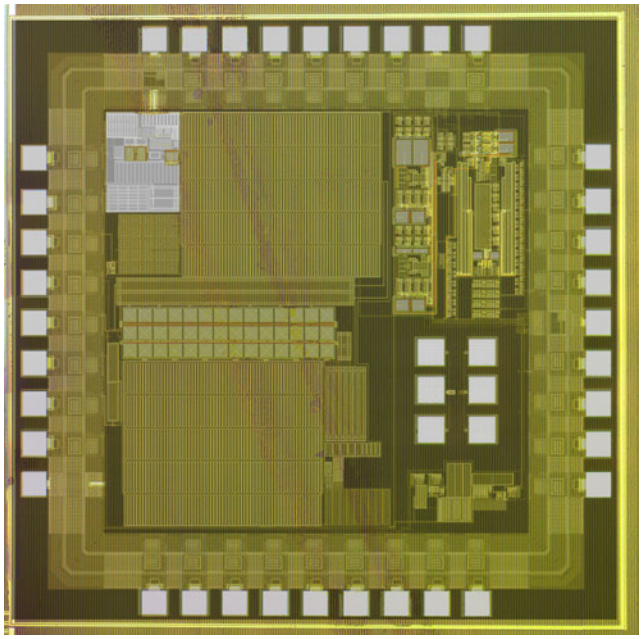

Microchip fabricated in a 180 nm technology by UMC for early performance demonstration. The implemented feedback path including a digital-to-analog converter features a signal-to-noise ratio of over 100 dB (© TUG/IHF).

OPTICAL FIBERS

The *J-MAG* instrument on board ESA's *JUICE* mission to the icy moons of Jupiter is going to perform magnetic field measurements with the help of two vector (fluxgate) sensors and one optical scalar sensor *(MAGSCA)*, which provides very accurate reference measurements for the in-flight-calibration of the fluxgate sensors. *MAGSCA* uses light fields produced by a modulated laser to excite electrons in Rubidium atoms for measuring the magnitude of the surrounding magnetic field. The optical sensor is located at the tip of a 10.5 m long boom, whereas the light source and the photodetector are part of the *J-MAG* instrument electronics located within the *JUICE* satellite. Two optical fibers, with a routed length of nearly 20 meters each, are needed to transmit the laser light from the instrument electronics to the sensor and back. A 50 µm graded-index multi-mode fiber was selected for the outbound optical transmission whereas the return path has been realized with a 400 µm step index multi-mode fiber.

A 400 µm step index multi-mode fiber with non-magnetic connectors and a polymer jacket, which protects the fiber over a wide temperature range from -190 °C to +120 °C (© ÖAW/IWF/Pollinger).

Due to the *JUICE* mission's harsh environmental conditions in terms of particle radiation (several Mrad of total ionizing dose) and low temperature (-190 °C) as well as the need for a fully non-magnetic design, a set of customized fiber assemblies had to be designed and qualified. This challenging development could be finished in 2020 based on an excellent teamwork between industry (Airbus Defense & Space, Schaefter + Kirchhoff GmbH, and Linden Photonics, Inc.), ESA, Fraunhofer INT, the Institute of Experimental Physics of TUG, and IWF.

ON-BOARD COMPUTER

The institute is involved in several missions with the development of digital processing units. IWF started to work with the latest generation of the LEON-type processors, the quad core GR740. This new processor type is based on the fourth generation, the LEON4 core. The primary goal is to find the optimal configuration in terms of system clock, memory configuration, wait states and usage of the processor-inbuilt cache memory. Another topic is to run tasks simultaneously on all four cores to study their interaction when accessing same memory areas, the impact of the cache pre-fetch strategy, bus load, etc.

The typical tasks for Digital Processing Units are the interpretation and execution of tele-commands, packing of telemetry data and execution of pre-programmed timelines. A growing aspect is data compression to maximize the amount of science data for a limited telemetry channel, thus improving instrument performance but also science output. The compression algorithms are designed and optimized for the actual application or instrument. Starting points are either physical parameters, e.g. the calculation of plasma parameters instead of transmitting the measured distribution function, or classical compression algorithm, like classical lossless compression algorithms as used for imaging detectors.

In the frame of the development of *PLATO's Router and Data Compression Unit (RDCU)*, IWF designed an IP core to implement a SpaceWire interface in FPGA logic. This core was used to build a SpaceWire to USB/Ethernet interface unit, based on a commercial single board computer. The first application, an instrument simulator for the *SMILE Soft-X-ray Imager*, is based on a Raspberry Pi board. An in-house developed HAT (Hardware Attached to the Top) provides an FPGA containing the SpaceWire IP core and the LVDS driver components. This design is rather cheap in comparison to commercially available SpaceWire-USB, very compact and versatile due to the software running at the Raspberry Pi. However, the data rate is limited, since the Raspberry Pi does not provide direct access to the data bus. A future design may be based on a more powerful industrial version of a single board computer.

Engineering Model of *PLATO's Router and Data Compression Unit* (© ÖAW/IWF/Steller).

INFRASTRUCTURE

Instruments aboard spacecraft are exposed to harsh environments, e.g., vacuum, large temperature ranges, radiation, and high mechanical loads during launch. Furthermore, these instruments are expected to be highly reliable, providing full functionality over the entire mission time, which could last for more than a decade.

IWF owns several test facilities and special infrastructure for the production of flight hardware. A high-performance computer helps the scientists to cope with the enormous data, which have to be analyzed for space missions.

MICROSCOPE WORKPLACES

Due to the ever-smaller components required for the design of miniaturized space qualified electronics, it has become necessary to increase the number of microscope workplaces in the IWF electronics laboratories. Almost all microscopes now have swiveling eyepieces, making it easier to work ergonomically. The working distance between the microscope and the electronics can also be changed quickly and easily using special attachment lenses.

For further information on the IWF infrastructure refer to www.oeaw.ac.at/en/iwf/institute/infrastructure.

Microscope-based workplace in an electronics laboratory (© ÖAW/Klaus Pichler).

LAST BUT NOT LEAST

PUBLIC OUTREACH

IWF is actively engaged in science education and public outreach.

During the *Solar Orbiter* Launch Event in the early morning hours of 10 February, about 50 space enthusiasts listened to the talks of Christian Möstl and Philippe Bourdin and followed a flawless lift-off of ESA's new Sun-exploring spacecraft aboard a US Atlas V rocket from NASA's Kennedy Space Center in Cape Canaveral, Florida.

Solar Orbiter Launch Event at IWF Graz (© ÖAW/IWF/Scherr).

After March 2020, no visitors could be guided through the labs and most events (Fifteen Seconds Festival, the Space exhibition during the Graz fair, etc.) had to be canceled due to Covid-19. However, IWF found new ways to bring science to the public.

In the frame of ÖAW's Science Bites series, Tanja Amerstorfer gave an interview about solar storms, which was recorded and presented at YouTube. On the ÖAW website, Günter Kargl discussed the possibility and risks of going on vacation in outer space. Last but not least, Manfred Steller answered the "ÖAW Forschungsfrage" in a video about the development of space-borne instruments.

Most seminars were given virtually. In the "Magnetosphere Online Seminar Series" organized by different US hosts, international speakers, including two scientists from IWF, gave insights into the magnetosphere's mysteries. On 15 May, Ferdinand Plaschke talked about the magnetosheath and on 22 June, Takuma Nakamura explained the low latitude boundary layer.

The "Game Changers" series of the International Space Science Institute (ISSI) explain how missions change(d) our view of the solar system. On 15 October, Rumi Nakamura talked about the results of NASA's *MMS* mission and showed how magnetic field lines around Earth break and reconnect.

On 9 October, the Austrian "Lange Nacht der Forschung" (LNF) was held online for the first time. The whole program was available until the end of the year. IWF participated with videos about different topics for both younger and adult audience.

Future scientists during the shooting of the LNF video about how to make magnetic putty (© ÖAW/IWF/Scherr).

In the same month, Manuel Scherf reported about news from Mars and Wolfgang Voller told about the autumn sky at URANIA Steiermark in Graz. In November, Ute Amerstorfer gave a lecture about space weather at Planetarium Wien.

The European Researchers Night took place on 27 November and also presented its program online. Tanja Amerstorfer talked about how to predict the arrival of solar storms and junior scientist Andreas Weiss interacted in a "Science Flash" with young people, who were interested in his educational and professional background.

During summer time, eight high-school students performed an internship at IWF under the "Talente-Praktika" program of FFG. They worked on magnetometer microchips, measurement of analog

signals, boot-software and load simulator for *SMILE*, historic Sun spots observations, magnetic field data of *BepiColombo* and *CSES* as well as aurora phenomena.

Topics discussed in the space blog of the Austrian newspaper "Der Standard" were the launch of *Solar Orbiter* and machine learning as basis for efficient data analysis.

The Servus TV show "P.M. Wissen" interviewed Luca Fossati about the exoplanet mission *CHEOPS* and Manuel Scherf about life on Mars.

Luca Fossati next to a bright star, explaining the transit method for discovering exoplanets during the video shooting of P.M. Wissen (© ÖAW/IWF/Scherr).

RECOGNITION

IWF reached the top five nominations for the Styrian WKO (Austrian Economic Chambers) PR Panther in the category "science" with the project "Klappe auf für *CHEOPS*".

Luca Fossati was among the Falling Walls finalists and presented his science breakthrough of the year 2020 in the category "Physical Sciences".

LECTURING

In summer 2020 and in winter term 2020/2021 IWF members gave (online) lectures at the University of Graz, Graz University of Technology, University of Vienna, TU Braunschweig, FH Joanneum, and FH Wiener Neustadt.

NEW PROJECTS

In 2020, the following third party projects with a budget greater than 100,000 EUR were acquired:

Project	Lead
ESA - *Rosetta*/*MIDAS*: Cometary Dust Analysis	T. Mannel
ESA - Tumbling Motion of Space Debris Objects	M. Steindorfer
ESA - *Galileo* Attitude Determination using mm SLR	M. Steindorfer
EU - Europlanet 2024 - Research Infrastructure	G. Kargl
FFG - High Precision Magnetometer Front-end-ASIC	W. Magnes
FFG - Assembly and Test of the *MAGSCA* Spare Model	W. Magnes
FWF - Fine Structures in Auroral Radio Emissions	G. Fischer
FWF - Energy Transfer Magnetosph. Boundary Layers	T. Nakamura

MEETINGS

T. Amerstorfer, M.Y. Boudjada, G. Kargl, R. Nakamura, M.A. Reiss, O.W. Roberts, M. Scherf, and M. Volwerk were members of scientific program and/or organizing committees at four international conferences.

THESES

Besides lecturing, members of the institute are supervising Bachelor, Diploma, Master and Doctoral Theses. In 2020, the following supervised theses have been completed:

Blasl, K.A.: In-situ spacecraft observations of surface waves at Earth's magnetopause during periods of southward interplanetary magnetic field Diploma Thesis, Universität Graz, 100 pages, 2020.

de Spiegeleer, A.: There and back again ... An Earth magneto-tale - Understanding plasma flows in the magnetotail, Doctoral Thesis, Umea University, 71 pages, 2020.

Schweighart, M.: Gas Flow Through Porous Media With Regard to Comets and Asteroids, Diploma Thesis, Universität Graz, 64 pages, 2020.

PUBLICATIONS

REFEREED ARTICLES

Acton, J.S., M.R. Goad, L. Raynard, S.L. Casewell, J.A.G. Jackman, R.D. Alexander, D.R. Anderson, D. Bayliss, E.M. Bryant, M.R. Burleigh, C. Belardi, B.F. Cooke, P. Eigmuller, S. Gill, J.S. Jenkins, M. Lendl, T. Louden, J. McCormac, M. Moyano, L.D. Nielsen, R.H. Tilbrook, S. Udry, C.A. Watson, R.G. West, P.J. Wheatley, J.I. Vines: NGTS J214358.5-380102 - NGTS discovery of the most eccentric known eclipsing M-dwarf binary system, *MNRAS*, **494**, 3950-3961, 2020.

Aplin, K.L., G. Fischer, T.A. Nordheim, A. Konovalenko, V. Zakharenko, P. Zarka: Atmospheric electricity at the ice giants, *Space Sci. Rev.*, **216**, 26, 2020.

Arkhypov, O.V., M.L. Khodachenko, A. Hanslmeier: Variability of transit light curves of Kepler objects of interest, *Astron. Astrophys.*, **638**, A143, 2020.

Armstrong, D.J., T.A. Lopez, V. Adibekyan, R.A. Booth, E.M. Bryant, K.A. Collins, M. Deleuil, A. Emsenhuber, C.X. Huang, G.W. King, J. Lillo-Box, J.J. Lissauer, E. Matthews, O. Mousis, L.D. Nielsen, H. Osborn, J. Otegi, N.C. Santos, S.G. Sousa, K.G. Stassun, D. Veras, C. Ziegler, J.S. Acton, J.M. Almenara, D.R. Anderson, D. Barrado, S.C.C. Barros, D. Bayliss, C. Belardi, F Bouchy, C. Briceño, M. Brogi, D.J.A. Brown, M.R. Burleigh, S.L. Casewell, A. Chaushev, D.R. Ciardi, K.I. Collins, K.D. Colón, B.F. Cooke, I.J.M. Crossfield, R.F. Díaz, E. Delgado Mena, O.D.S. Demangeon, C. Dorn, X. Dumusque, P. Eigmüller, M. Fausnaugh, P. Figueira, T. Gan, S. Gandhi, S. Gill, E.J. Gonzales, M.R. Goad, M.N. Günther, R. Helled, S. Hojjatpanah, S.B. Howell, J. Jackman, J.S. Jenkins, J.M. Jenkins, E.L.N. Jensen, G.M. Kennedy, D.W. Latham, N. Law, M. Lendl, M. Lozovsky, A.W. Mann, M. Moyano, J. McCormac, F. Meru, C. Mordasini, A. Osborn, D. Pollacco, D. Queloz, L. Raynard, G.R. Ricker, P. Rowden, A. Santerne, J.E. Schlieder, S. Seager, L. Sha, T.-G. Tan, R.H. Tilbrook, E. Ting, S. Udry, R. Vanderspek, C.A. Watson, R.G. West, P.A. Wilson, J.N. Winn, P. Wheatley, J. Noel Villasenor, J.I. Vines, Z. Zhan: A remnant planetary core in the hot-Neptune desert, *Nature*, **583**, 39-42, 2020.

Bailey, R.L., C. Möstl, M.A. Reiss, A.J. Weiss, U.V. Amerstorfer, T. Amerstorfer, J. Hinterreiter, W. Magnes, R. Leonhardt: Prediction of Dst during solar minimum using in situ measurements at L5, *Space Weather*, **18**, e2019SW002424, 2020.

Banerdt, W.B., S.E. Smrekar, D. Banfield, D. Giardini, M. Golombek, C.L. Johnson, P. Lognonné, A. Spiga, T. Spohn, C. Perrin, S.C. Stähler, D. Antonangeli, S. Asmar, C. Beghein, N. Bowles, E. Bozdag, P. Chi, U. Christensen, J. Clinton, G.S. Collins, I. Daubar, V. Dehant, M. Drilleau, M. Fillingim, W. Folkner, R.F. Garcia, J. Garvin, J. Grant, M. Grott, J. Grygorczuk, T. Hudson, J.C.E. Irving, G. Kargl, T. Kawamura, S. Kedar, S. King, B. Knapmeyer-Endrun, M. Knapmeyer, M. Lemmon, R. Lorenz, J.N. Maki, L. Margerin, S.M. McLennan, C. Michaut, D. Mimoun, A. Mittelholz, A. Mocquet, P. Morgan, N.T. Mueller, N. Murdoch, S. Nagihara, C. Newman, F. Nimmo, M. Panning, W.T. Pike, A.-C. Plesa, S. Rodriguez, J.A. Rodriguez-Manfredi, C.T. Russell, N. Schmerr, M. Siegler, S. Stanley, E. Stutzmann, N. Teanby, J. Tromp, M. van Driel, N. Warner, R. Weber, M. Wieczorek: Initial results from the InSight mission on Mars, *Nat. Geosci.*, **13**, 183-189, 2020.

Barnes, D., J.A. Davies, R.A. Harrison, J.P. Byrne, C.H. Perry, V. Bothmer, J.P. Eastwood, P.T. Gallagher, E.K.J. Kilpua, C. Möstl, L. Rodriguez, A.P. Rouillard, D. Odstrcil: CMEs in the heliosphere: III. A statistical analysis of the kinematic properties derived from stereoscopic geometrical modelling techniques applied to CMEs detected in the heliosphere from 2008 to 2014 by STEREO/HI-1, *Solar Phys.*, **295**, 150, 2020.

Barnes, J.R., C.A. Haswell, D. Staab, G. Anglada-Escudé, L. Fossati, J.P.J. Doherty, J. Cooper, J.S. Jenkins, M.R. Díaz, M.G. Soto, P.A. Peña Rojas: An ablating 2.6 $M_{\oplus}$ planet in an eccentric binary from the Dispersed Matter Planet Project, *Nat. Astron.*, **4**, 419–426, 2020.

Baumjohann, W., A. Matsuoka, Y. Narita, W. Magnes, D. Heyner, K.-H. Glassmeier, R. Nakamura, D. Fischer, F. Plaschke, M. Volwerk, T.L. Zhang, H.-U. Auster, I. Richter, A. Balogh, C.M. Carr, M. Dougherty, T.S. Horbury, H. Tsunakawa, M. Matsushima, M. Shinohara, H. Shibuya, T. Nakagawa, M. Hoshino, Y. Tanaka, B.J. Anderson, C.T. Russell, U. Motschmann, F. Takahashi, A. Fujimoto: The BepiColombo-Mio magnetometer en route to Mercury, *Space Sci. Rev.*, **216**, 125, 2020.

Benedikt, M.R., M. Scherf, H. Lammer, E. Marcq, P. Odert, M. Leitzinger, N.V. Erkaev: Escape of rock-forming volatile elements and noble gases from planetary embryos, *Icarus*, **347**, 113772, 2020.

Biber, H., P.S. Szabo, N. Jäggi, M. Wallner, R. Stadlmayr, M.V. Morc, A. Nenning, A Mutzke, K. Mezger, H. Lammer, D. Primetzhofer, J. Fleig, A. Galli, P. Wurz, F. Aumayr: Solar wind Helium ion interaction with Mg and Fe rich pyroxene as Mercury surface analogue, *Nucl. Instrum. Methods Phys. Res. B*, **480**, 10-15, 2020.

Birn, J., M. Chandler, R. Nakamura: Ion beams in the plasma sheet boundary layer: MMS observations and test particle simulations, *J. Geophys. Res.*, **125**, e2019JA027113, 2020.

Blanc, M., O. Prieto-Ballesteros, N. Andre, J. Gomez-Elvira, G. Jones, V. Sterken, W. Desprats, L.I. Gurvits, K. Khurana, G. Balmino, A. Blocker, R. Broquet, E. Bunce, C. Cavel, G. Choblet, G. Colins, M. Coradini, J. Cooper, D. Dirkx, D. Fontaine, P. Garnier, D. Gaudin, P. Hartogh, H. Hussmann, A. Genova, L. Iess, A. Jaggi, S. Kempf, N. Krupp, L. Lara, J. Lasue, V. Lainey, F. Leblanc, J.-P. Lebreton, A. Longobardo, R. Lorenz, P. Martins, Z. Martins, J.-C. Marty,

A. Masters, D. Mimoun, E. Palumba, V. Parro, P. Regnier, J. Saur, A. Schutte, E.C. Sittler, T. Spohn, R. Srama, K. Stephan, K. Szego, F. Tosi, S. Vance, R. Wagner, T. Van Hoolst, M. Volwerk, J.-E. Wahlund, F. Westall, P. Wurz: Joint Europa Mission (JEM): A multi-scale study of Europa to characterize its habitability and search for extant life, *Planet. Space Sci.*, **193**, 104960, 2020.

Blanco-Cano, X., L. Preisser, P. Kajdic, D. Rojas-Castillo: Magnetosheath microstructure: Mirror mode waves and jets during southward IP magnetic field, *J. Geophys. Res.*, **125**, e2020JA027940, 2020.

Boudjada, M.Y., A. Abou el-Fadl, P.H.M. Galopeau, E. Al-Haddad, H. Lammer: Observations of solar type III radio bursts by Cassini/RPWS experiment, *Adv. Radio Sci.*, **18**, 83-87, 2020.

Boudjada, M.Y., P.H.M. Galopeau, S. Sawas, V. Denisenko, K. Schwingenschuh, H. Lammer, H.U. Eichelberger, W. Magnes, B.P. Besser: Low-altitude frequency-banded equatorial emissions observed below the electron cyclotron frequency, *Ann. Geophys.*, **38**, 765-774, 2020.

Bourdin, Ph.-A.: Driving solar coronal MHD simulations on high-performance computers, *Geophys. Astro. Fluid Dyn.*, **114**, 235-260, 2020.

Bryant, E.M., D. Bayliss, J. McCormac, P.J. Wheatley, J.S. Acton, D.R. Anderson, D.J. Armstrong, F. Bouchy, C. Belardi, M.R. Burleigh, R.H. Tilbrook, S.L. Casewell, B.F. Cooke, S. Gill, M.R. Goad, J.S. Jenkins, M. Lendl, D. Pollacco, D. Queloz, L. Raynard, A.M.S. Smith, J.I. Vines, R.G. West, S. Udry: Simultaneous TESS and NGTS transit observations of WASP-166 b, *MNRAS*, **494**, 5872-5881, 2020.

Capitanio, L., M. Bartylak, M. Cui, B. Engegaard, M. Gassner, S.G. Heinemann, G. Kargl, S.T. Latzko, P.G. Madonia, A.J. May, A. Postel, J. Rodriguez Munoz, G.J. Schwarzkop, R.F. Shipman, R. Skalidis, V. Trivino Herrero, K. Wikman: EREBUS: the EuRopean Extinction BUmp Survey, *Exp. Astron.*, **50**, 145-158, 2020.

Carleo, I., D. Gandolfi, O. Barragán, J.H. Livingston, C.M. Persson, K.W.F. Lam, A. Vidotto, M.B. Lund, C. Villarreal D'Angelo, K.A. Collins, L. Fossati, A.W. Howard, D. Kubyshkina, R. Brahm, A. Oklopčić, P. Mollière, S. Redfield, L.M. Serrano, F. Dai, M. Fridlund, F. Borsa, J. Korth, M. Esposito, M.R. Díaz, L. Dyregaard Nielsen, C. Hellier, S. Mathur, H.J. Deeg, A.P. Hatzes, S. Benatti, F. Rodler, J. Alarcon, L. Spina, Â.R.G. Santos, I. Georgieva, R.A. García, L. González-Cuesta, G.R. Ricker, R. Vanderspek, D.W. Latham, S. Seager, J.N. Winn, J.M. Jenkins, S. Albrecht, N.M. Batalha, C. Beard, P.T. Boyd, F. Bouchy, J.A. Burt, R.P. Butler, J. Cabrera, A. Chontos, D.R. Ciardi, W.D. Cochran, K.I. Collins, J.D. Crane, I. Crossfield, S. Csizmadia, D. Dragomir, C. Dressing, P. Eigmüller, M. Endl, A. Erikson, N. Espinoza, M. Fausnaugh, F. Feng, E. Flowers, B. Fulton, E.J. Gonzales, N. Grieves, S. Grziwa, E.W. Guenther, N.M. Guerrero, T. Henning, D. Hidalgo, T. Hirano, M. Hjorth, D. Huber, H. Isaacson, M. Jones, A. Jordán, P. Kabáth, S.R. Kane, E. Knudstrup, J. Lubin, R. Luque, I. Mireles, N. Narita, D. Nespral, P. Niraula, G. Nowak, E. Palle, M. Pätzold, E.A. Petigura, J. Prieto-Arranz, H. Rauer, P. Robertson, M.E. Rose, A. Roy, P. Sarkis, J.E. Schlieder, D. Ségransan, S. Shectman, M. Skarka, A.M.S. Smith, J.C. Smith, K. Stassun, J. Teske, J.D. Twicken, V. Van Eylen, S. Wang, L.M. Weiss, A. Wyttenbach: The multiplanet system TOI-421: A warm Neptune and a super puffy mini-Neptune transiting a G9 V star in a visual binary, *Astron. J.*, **160**, 114, 2020.

Celletti, A., C. Gales, C. Lhotka: Resonances in the Earth's space environment, *Commun. Nonlinear Sci. Numer. Simulat.*, **84**, 105185, 2020.

Chang, Q., X. Xu, Q. Xu, J. Wang, J. Xu, Y. Ye, T.L. Zhang: The demagnetization of the Venusian ionosphere under nearly flow-aligned interplanetary magnetic fields, *Astrophys. J.*, **900**, 63, 2020.

Chen, L.-J., S. Wang, O. Le Contel, A. Rager, M. Hesse, J. Drake, J. Dorelli, J. Ng, N. Bessho, D. Graham, L.B.Wilson III, T. Moore, B. Giles, W. Paterson, B. Lavraud, K. Genestreti, R. Nakamura, Yu.V. Khotyaintsev, R.E. Ergun, R.B. Torbert, J. Burch, C. Pollock, C.T. Russell, P.-A. Lindqvist, L. Avanov: Lower-hybrid drift waves driving electron nongyrotropic heating and vortical flows in a magnetic reconnection layer, *Phys. Rev. Lett.*, **125**, 025103, 2020.

Collinson, G., D. Sibeck, N. Omidi, R. Frahm, T.L. Zhang, D. Mitchell, J. Halekas, J. Espley, Y. Futaana, B. Jakosky: Foreshock cavities at Venus and Mars, *J. Geophys. Res.*, **125**, e2020JA028023, 2020.

Comisel, H., Y. Narita, U. Motschmann: Alfvén wave evolution into magnetic filaments in 3-D space plasma, *Earth Planets Space*, **72**, 32, 2020.

Constantinescu, O.D., H.-U. Auster, M. Delva, O. Hillenmaier, W. Magnes, F. Plaschke: Maximum-variance gradiometer technique for removal of spacecraft-generated disturbances from magnetic field data, *Geosci. Instrum. Method. Data Syst.*, **9**, 451–469, 2020.

Cooke, B.F., D. Pollacco, M. Lendl, T. Kuntzer, A. Fortier: CHEOPS observations of TESS primary mission monotransits, *MNRAS*, **494**, 736-742, 2020.

Cubillos, P.E., L. Fossati, T. Koskinen, M.E. Young, M. Salz, K. France, A.G. Sreejith, C.A. Haswell: Near-ultraviolet transmission spectroscopy of HD 209458b: Evidence of ionized iron beyond the planetary Roche lobe, *Astrophys. J.*, **159**, 111, 2020.

Dai, L., C. Wang, Z. Cai, W. Gonzalez, M. Hesse, P. Escoubet, T. Phan, V. Vasyliunas, Q. Lu, L. Li, L. Kong, M. Dunlop, R. Nakamura, J. He, H. Fu, M. Zhou, S. Huang, R. Wang, Y. Khotyaintsev, D. Graham, A. Retino, L. Zelenyi, E.E. Grigorenko, A. Runov, V. Angelopoulos, L. Kepko, K.-J. Hwang, Y. Zhang: AME: A cross-scale constellation of CubeSats to explore magnetic reconnection in the solar-terrestrial relation, *Front. Physics*, **8**, 89, 2020.

Dalba, P.A., A.F. Gupta, J.E. Rodriguez, D. Dragomir, C.X. Huang, S.R. Kane, S.N. Quinn, A. Bieryla, G.A. Esquerdo, B.J. Fulton, N. Scarsdale, N.M. Batalha, C. Beard, A. Behmard, A. Chontos, I.J.M. Crossfield, C.D. Dressing, S. Giacalone, M.L. Hill, L.A. Hirsch, A.W. Howard, D. Huber, H. Isaacson, M. Kosiarek, J. Lubin, A.W. Mayo, T. Mocnik, J.M.A. Murphy, E.A. Petigura, P. Robertson, L.J. Rosenthal, A. Roy, R.A. Rubenzahl, J. Van Zandt, L.M.

Weiss, E. Knudstrup, M.F. Andersen, F. Grundahl, X.Y. Yao, J. Pepper, S. Villanueva, D.R. Ciardi, R. Cloutier, T.L. Jacobs, M.H. Kristiansen, D.M. LaCourse, M. Lendl, H.P. Osborn, E. Palle, K.G. Stassun, D.J. Stevens, G.R. Ricker, R. Vanderspek, D.W. Latham, S. Seager, J.N. Winn, J.M. Jenkins, D.A. Caldwell, T. Daylan, W. Fong, R.F. Goeke, M.E. Rose, P. Rowden, J.E. Schlieder, J.C. Smith, A. Vanderburg: The TESS-Keck survey. I. A warm sub-Saturn-mass planet and a caution about stray light in TESS cameras, *Astron. J.*, **159**, 241, 2020.

Dandouras, I., M. Blanc, L. Fossati, M. Gerasimov, E.W. Guenther, K.G. Kislyakova, H. Lammer, Y. Lin, B. Marty, C. Mazelle, S. Rugheimer, M. Scherf, C. Sotin, L. Sproß, S. Tachibana, P. Wurz, M. Yamauchi: Future missions related to the determination of the elemental and isotopic composition of Earth, Moon and the terrestrial planets, *Space Sci. Rev.*, **216**, 121, 2020.

Debrecht, A., J. Carroll-Nellenback, A. Frank, E.G. Blackman, G. Eric, L. Fossati, J. McCann, R. Murray-Clay: Effects of radiation pressure on the evaporative wind of HD 209458b, *MNRAS*, **493**, 1292-1305, 2020.

Denton, R.E., R.B. Torbert, H. Hasegawa, I. Dors, K.J. Genestreti, M.R. Argall, D. Gershman, O. Le Contel, J.L. Burch, C.T. Russell, R.J. Strangeway, B.L. Giles, D. Fischer: Polynomial reconstruction of the reconnection magnetic field observed by multiple spacecraft, *J. Geophys. Res.*, **125**, e2019JA027481, 2020.

Dikpati, M., P.A. Gilman, S. Chatterjee, S.W. McIntosh, T.V. Zaqarashvili: Physics of magnetohydrodynamic Rossby waves in the Sun, *Astrophys. J.*, **896**, 141, 2020.

Du, A.M., Y. Zhang, H.Y. Li, D.H. Qiao, Z. Yi, T.L. Zhang, L.F. Meng, Y.S. Ge, H. Luo, L. Zhao, S.Q. Sun, J.M. Ou, Z. Li, X. Feng, J.L. Dai: The Chinese Mars ROVER fluxgate magnetometers, *Space Sci. Rev.*, **216**, 135, 2020.

Dumbadze, G., B. Shergelashvili: Oscillations of ellipsoidal solar active regions, *Astrophys.*, **63**, 108-113, 2020.

Dumbovic, M., B. Vršnak, J. Guo, B. Heber, Ka. Dissauer, F. Carcaboso, M. Temmer, A. Veronig, T. Podladchikova, C. Möstl, T. Amerstorfer, A. Kirin: Evolution of Coronal Mass Ejections and the corresponding Forbush decreases: Modeling vs. multi-spacecraft observations, *Solar Phys.*, **295**, 104, 2020.

Ehrenreich, D., C. Lovis, R. Allart, M. Rosa, Z. Osorio, F. Pepe, S. Cristiani, R. Rebolo, N.C. Santos, F. Borsa, O. Demangeon, X. Dumusque, J.I. González Hernández, N. Casasayas-Barris, D. Ségransan, S. Sousa, M. Abreu, V. Adibekyan, M. Affolter, C. Allende Prieto, Y. Alibert, M. Aliverti, D. Alves, M. Amate, G. Avila, V. Baldini, T. Bandy, W. Benz, A. Bianco, É. Bolmont, F. Bouchy, V. Bourrier, C. Broeg, A. Cabral, G. Calderone, E. Pallé, H.M. Cegla, R. Cirami, J.M.P. Coelho, P. Conconi, I. Coretti, C. Cumani, G. Cupani, H. Dekker, B. Delabre, S. Deiries, V. D'Odorico, P. Di Marcantonio, P. Figueira, A. Fragoso, L. Genolet, M. Genoni, R. Génova Santos, N. Hara, I. Hughes, O. Iwert, F. Kerber, J. Knudstrup, M. Landoni, B. Lavie, J.-L. Lizon, M. Lendl, G. Lo Curto, C. Maire, A. Manescau, C.J.A.P. Martins, D. Mégevand, A. Mehner, G. Micela, A. Modigliani, P. Molaro, M. Monteiro, M. Monteiro, M. Moschetti, E. Müller, N. Nunes, L. Oggioni, A. Oliveira, G. Pariani, L. Pasquini, E. Poretti, J.L. Rasilla, E. Redaelli, M. Riva, S. Santana Tschudi, P. Santin, P. Santos, A. Segovia Milla, J.V. Seidel, D. Sosnowska, A. Sozzetti, P. Spanò, A. Suárez Mascareño, H. Tabernero, F. Tenegi, S. Udry, A. Zanutta, F. Zerbi: Nightside condensation of iron in an ultrahot giant exoplanet, *Nature*, **580**, 597-601, 2020.

Ergun, R.E., N. Ahmadi, L. Kromyda, S.J. Schwartz, A. Chasapis, S. Hoilijoki, F.D. Wilder, J.E. Stawarz, K.A. Goodrich, D.L. Turner, I.J. Cohen, S.T. Bingham, J.C. Holmes, R. Nakamura, F. Pucci, R.B. Torbert, J.L. Burch, P.-A. Lindqvist, R.J. Strangeway, O. Le Contel, B.L. Giles: Observations of particle acceleration in magnetic reconnection-driven turbulence, *Astrophys. J.*, **898**, 154, 2020.

Escoubet, C.P., K.-J. Hwang, S. Toledo-Redondo, L. Turc, S.E. Haaland, N. Aunai, J. Dargent, J.P. Eastwood, R.C. Fear, H. Fu, K.J. Genestreti, D.B. Graham, Yu.V. Khotyaintsev, G. Lapenta, B. Lavraud, C. Norgren, D.G. Sibeck, A. Varsani, J. Berchem, A.P. Dimmock, G. Paschmann, M. Dunlop, Y.V. Bogdanova, O. Roberts, H. Laakso, A. Masson, M.G.G.T. Taylor, P. Kajdic, C. Carr, I. Dandouras. A. Fazakerley, R. Nakamura, J.L. Burch, B.L. Giles, C. Pollock, C.T. Russell, R.B. Torbert: Cluster and MMS simultaneous observations of magnetosheath high speed jets and their impact on the magnetopause, *Front. Astron. Space Sci.*, **6**, 78, 2020.

Fischer, G., W.M. Farrell, D.A. Gurnett, W.S. Kurth: Nondetection of radio emissions from Titan lightning by Cassini RPWS, *J. Geophys. Res.*, **125**, e2020JE006496, 2020.

Folsom, C.P., D.O. Fionnagáin, L. Fossati, A.A. Vidotto, C. Moutou, P. Petit, D. Dragomir, J.-F. Donati: Circumstellar environment of 55 Cancri. The super-Earth 55 Cnc e as a primary target for star-planet interactions, *Astron. Astrophys.*, **633**, A48, 2020.

Fossati, L., D. Shulyak, A.G. Sreejith, T. Koskinen, M.E. Young, P.E. Cubillos, L.M. Lara, K. France, M. Rengel, P.W. Cauley, J.D. Turner, A. Wyttenbach, F. Yan: A data-driven approach to constraining the atmospheric temperature structure of the ultra-hot Jupiter KELT-9b, *Astron. Astrophys.*, **643**, A131, 2020.

Franci, L., J.E. Stawarz, E. Papini, P. Hellinger, T.K.M. Nakamura, D. Burgess, S. Landi, A. Verdini, L. Matteini, R. Ergun, O. Le Contel, P.-A. Lindqvist: Modeling MMS observations at the Earth's magnetopause with hybrid simulations of Alfvénic turbulence, *Astrophys. J.*, **898**, 175, 2020.

Franco, A.M.S., M. Fränz, E. Echer, M.J.A. Bolzan, T.L. Zhang: The correlation length of ULF waves around Venus: VEX observations, *Planet. Space Sci.*, **180**, 104761, 2020.

Futyan, D., A. Fortier, M. Beck, D. Ehrenreich, A. Bekkelien, W. Benz, N. Billot, V. Bourrier, C. Broeg, A. Collier Cameron, A. Deline, T. Kuntzer, M. Lendl, D. Queloz, R. Rohlfs, A.E. Simon, F. Wildi: Expected performances of the Characterising Exoplanet Satellite (CHEOPS). II. The CHEOPS simulator, *Astron. Astrophys.*, **635**, A23, 2020.

Gebauer, S., J.L. Grenfell, H. Lammer, J.-P. Paul de Vera, L. Sproß, V.S. Airapetian, M. Sinnhuber, H. Rauer: Atmospheric nitrogen when life evolved on Earth, *Astrobiol.*, **20**, 1413-1426, 2020.

Gibson, N.P., S. Merritt, S.K. Nugroho, P.E. Cubillos, E.J.W. de Mooij, T. Mikal-Evans, L. Fossati, J. Lothringer, N. Nikolov, D.K. Sing, J.J. Spake, C.A. Watson, J. Wilson: Detection of Fe I in the atmosphere of the ultra-hot Jupiter WASP-121b, and a new likelihood-based approach for Doppler-resolved spectroscopy, *MNRAS*, **493**, 2215–2228, 2020.

Gill, S., B.F. Cooke, D. Bayliss, L.D. Nielson, M. Lendl, P.J. Wheatley, D.R. Anderson, M. Moyano, E.M. Bryant, J.S. Acton, C. Belardi, F. Bouchy, M.R. Burleigh, S.L. Casewell, A. Chausev, M.R. Goad, J.A.G. Jackman, J.S. Jenkins, J. McCormac, M.N. Gunther, H.P. Osborn, D. Pollaco, L. Raynard, A.M.S. Smith, R.H. Tillbrook, O. Turner, S. Udry, J.I. Vines, C.A. Watson, R.G. West: A longperiod (P=61.8 d M5V dwarf eclipsing a Sun-like star from TESS and NGTS, *MNRAS*, **495**, 2713-2719, 2020.

Gill, S., D. Bayliss, B.F. Cooke, P.J. Wheatley, L.D. Nielsen, M. Lendl, J. McCormac, E.M. Bryant, J.S. Acton, D.R. Anderson, C. Belardi, F. Bouchy, M.R. Burleigh, A.C. Cameron, S.L. Casewell, A. Chaushev, M.R. Goad, M.N. Günther, C. Hellier, J.A.G. Jackman, J.S. Jenkins, M. Moyano, D. Pollacco, L. Raynard, A.M.S Smith, R.H. Tilbrook, O. Turner, S. Udry, R.G. West: NGTS and WASP photometric recovery of a single-transit candidate from TESS, *MNRAS*, **491**, 1548-1553, 2020.

Gill, S., P.J. Wheatley, B.F. Cooke, A. Jordán, L.D. Nielsen, D. Bayliss, D.R. Anderson, J.I. Vines, M. Lendl, J.S. Acton, D.J. Armstrong, F. Bouchy, R. Brahm, E.M. Bryant, M.R. Burleigh, S.L. Casewell, P. Eigmüller, N. Espinoza, E. Gillen, M.R. Goad, N. Grieves, M.N. Günther, T. Henning, M.J. Hobson, A. Hogan, J.S. Jenkins, J. McCormac, M. Moyano, H.P. Osborn, D. Pollacco, D. Queloz, H. Rauer, L. Raynard, F. Rojas, P. Sarkis, A.M.S. Smith, M. Tala Pinto, R.H. Tilbrook, S. Udry, C.A. Watson, R.G. West: NGTS-11 b (TOI-1847 b): A transiting warm Saturn recovered from a TESS single-transit event, *Astrophys. J. Lett.*, **898**, L11, 2020.

Goetz, C., F. Plaschke, M.G.G.T. Taylor: Singing comet waves in a solar wind convective electric field frame, *Geophys. Res. Lett.*, **47**, e2020GL087418, 2020.

Goldstein, J., P.W. Valek, D.J. McComas, J. Redfern, H. Spence, R.M. Skoug, B.A. Larsen, G.D. Reeves, R. Nakamura: Global ENA imaging and in situ observations of substorm dipolarization on 10 August 2016, *J. Geophys. Res.*, **125**, e2019JA027733, 2020.

Grigorenko, E.E., A.Y. Malykhin, D.R. Shklyar, S. Fadanelli, B. Lavraud, E.V. Panov, L. Avanov, B. Giles, O. Le Contel: Investigation of electron distribution functions associated with whistler waves at dipolarization fronts in the Earth's magnetotail: MMS observations, *J. Geophys. Res.*, **125**, e2020JA028268, 2020.

Gronoff, G., P. Arras, S. Baraka, J.M. Bell, G. Cessateur, O. Cohen, S.M. Curry, J.J. Drake, M. Elrod, J. Erwin, K. Garcia-Sage, C. Garraffo, A. Glocer, N.G. Heavens, K. Lovato, R. Maggiolo, C.D. Parkinson, C. Simon Wedlund, D.R. Weimer, W.B. Moore: Atmospheric escape processes and planetary atmospheric evolution, *J. Geophys. Res.*, **125**, e2019JA027639, 2020.

Guilluy, G., V. Andretta, F. Borsa, P. Giacobbe, A. Sozzetti, E. Covino, V. Bourrier, L. Fossati, A.S. Bonomo, M. Esposito, M.S. Giampapa, A. Harutyunyan, M. Rainer, M. Brogi, G. Bruno, R. Claudi, G. Frustagli, A.F. Lanza, L. Mancini, L. Pino, E. Poretti, G. Scandariato, L. Affer, C. Baffa, A. Baruffolo, S. Benatti, K. Biazzo, A. Bignamini, W. Boschin, I. Carleo, M. Cecconi, R. Cosentino, M. Damasso, S. Desidera, G. Falcini, A.F. Martinez Fiorenzano, A. Ghedina, E. González-Álvarez, J. Guerra, N. Hernandez, G. Leto, A. Maggio, L. Malavolta, J. Maldonado, G. Micela, E. Molinari, V. Nascimbeni, I. Pagano, M. Pedani, G. Piotto, A. Reiners: The GAPS programme at TNG. XXII. The GIARPS view of the extended helium atmosphere of HD189733 b accounting for stellar activity, *Astron. Astrophys.*, **639**, A49, 2020.

Hartman, J.D., A. Jordán, D. Bayliss, G.Á. Bakos, J. Bento, W. Bhatti, R. Brahm, Z. Csubry, N. Espinoza, Th. Henning, L. Mancini, K. Penev, M. Rabus, P. Sarkis, V. Suc, M. de Val-Borro, G. Zhou, J.D. Crane, S. Shectman, J.K. Teske, S. X. Wang, R.P. Butler, J. Lázár, I. Papp, P. Sári, D.R. Anderson, C. Hellier, R.G. West, K. Barkaoui, F.J. Pozuelos, E. Jehin, M. Gillon, L. Nielsen, M. Lendl, S. Udry, G.R. Ricker, R. Vanderspek, D.W. Latham, S. Seager, J.N. Winn, J. Christiansen, I.J.M. Crossfield, C.E. Henze, J.M. Jenkins, J.C. Smith, E.B. Ting: HATS-47b, HATS-48Ab, HATS-49b, and HATS-72b: Four warm giant planets transiting K dwarfs, *Astrophys. J.*, **159**, 173, 2020.

Hasegawa, H., T.K.M. Nakamura, D.J. Gershman, Y. Nariyuki, A.F.- Vinas, B.L. Giles, B. Lavraud, C.T. Russell, Y.V. Khotyaintsev, R.E. Ergun, Y. Saito: Generation of turbulence in Kelvin-Helmholtz vortices at the Earth's magnetopause: Magnetospheric Multiscale observations, *J. Geophys. Res.*, **125**, e2019JA027595, 2020.

Haswell, C.A., D. Staab, J.R. Barnes, G. Anglada-Escudé, L. Fossati, J.S. Jenkins, A.J. Norton, J.P.J. Doherty, J. Cooper: Dispersed Matter Planet Project discoveries of ablating planets orbiting nearby bright stars, *Nat. Astron.*, **4**, 408–418, 2020.

Hayakawa, H., B.P. Besser, T. Iju, R. Arlt, S. Uneme, S. Imada, P.-A. Bourdin, A. Kraml: Thaddäus Derfflinger's sunspot observations during 1802-1824: A primary reference to understand the Dalton Minimum, *Astrophys. J.*, **890**, 98, 2020.

Horbury, T.S., H. O'Brien, I. Carrasco Blazquez, M. Bendyk, P. Brown, R. Hudson, V. Evans, T.M. Oddy, C.M. Carr, T.J. Beek, E. Cupido, S. Bhattacharya, J.-A. Dominguez, L. Matthews, V.R. Myklebust, B. Whiteside, S.D. Bale, W. Baumjohann, D. Burgess, V. Carbone, P. Cargill, J. Eastwood, G. Erdös, L. Fletcher, R. Forsyth, J. Giacalone, K.-H. Glassmeier, M.L. Goldstein, T. Hoeksema, M. Lockwood, W. Magnes, M. Maksimovic, E. Marsch, W. H. Matthaeus, N. Murphy, V.M. Nakariakov, C.J. Owen, M. Owens, J. Rodriguez-Pacheco, I. Richter, P. Riley, C.T. Russell, S. Schwartz, R. Vainio, M. Velli, S. Vennerstrom, R.

Walsh, R.F. Wimmer-Schweingruber, G. Zank, D. Müller, I. Zouganelis, A.P. Walsh: The Solar Orbiter magnetometer, *Astron. Astrophys.*, **642**, A9, 2020.

Hwang, K.-J., K. Dokgo, E. Choi, J.L. Burch, D.G. Sibeck, B.L. Giles, H. Hasegawa, H.S. Fu, Y. Liu, Z. Wang, T.K.M. Nakamura, X. Ma, R.C. Fear, Y. Khotyaintsev, D.B. Graham, Q.Q. Shi, C.P. Escoubet, D.J. Gershman, W.R. Paterson, C.J. Pollock, R.E. Ergun, R.B. Torbert, J.C. Dorelli, L. Avanov, C.T. Russell, R.J. Strangeway: Magnetic reconnection inside a flux rope induced by Kelvin-Helmholtz vortices, *J. Geophys. Res.*, **125**, e2019JA027665, 2020.

Kasaba, Y., T. Takashima, S. Matsuda, S. Eguchi, M. Endo, T. Miyabara, M. Taeda, Y. Kuroda, Y. Kasahara, T. Imachi, H. Kojima, S. Yagitani, M. Moncuquet, J.-E. Wahlund, A. Kumamoto, A. Matsuoka, W. Baumjohann, S. Yokota, K. Asamura, Y. Saito, D. Delcourt,· M. Hirahara, S. Barabash, N. Andre, M. Kobayashi, I. Yoshikawa, G. Murakam, H. Hayakawa: Mission data processor aboard the BepiColombo Mio spacecraft: Design and scientific operation concept, *Space Sci. Rev.*, **216**, 34, 2020.

Keles, E., D. Kitzmann, M. Mallonn, X. Alexoudi, L. Fossati, L. Pino, J.V. Seidel, T.A. Carroll, M. Steffen, I. Ilyin, K. Poppenhäger, K.G. Strassmeier, C.von Essen, V. Nascimbeni, J.D. Turner: Probing the atmosphere of HD189733b with the Na I and K I lines, *MNRAS*, **498**, 1023-1033, 2020.

Kislyakova, K.G., C.P. Johnstone, M. Scherf, M. Holmström, I.I. Alexeev, H. Lammer, M.L. Khodachenko, M. Güdel: Evolution of the Earth's polar outflow from mid-archean to present, *J. Geophys. Res.*, **125**, e2020JA027837, 2020.

Korovinskiy, D.B., A.V. Divin, V.S. Semenov, N.V. Erkaev, S.A. Kiehas, I.V. Kubyshkin: Grad-Shafranov reconstruction of the magnetic configuration in the reconnection X-point vicinity in compressible plasma, *Phys. Plasmas*, **27**, 082905, 2020.

Krauss, S., S. Behzadpour, M. Temmer, C. Lhotka: Exploring thermospheric variations triggered by severe geomagnetic storm on 26 August 2018 using GRACE Follow-On Data, *J. Geophys. Res.*, **127**, e2019JA027731, 2020.

Krticka, J., A. Kawka, Z. Mikulášek, L. Fossati, I. Krticková, M. Prvák, J. Janík, M. Skarka, R. Liptaj: Understanding the rotational variability of K2 targets. HgMn star KIC 250152017 and blue horizontal branch star KIC 249660366, *Astron. Astrophys.*, **639**, A8, 2020.

Kubyshkina, D., A.A. Vidotto, L. Fossati, E. Farrell: Coupling thermal evolution of planets and hydrodynamic atmospheric escape in MESA, *MNRAS*, **499**, 77-88, 2020.

Kucharski, D., G. Kirchner, T. Otsubo, S.K. Flegel, H. Kunimori, M.K. Jah, F. Koidl, J.C. Bennett, M. Steindorfer, P. Wang: Quanta photogrammetry of experimental geodetic satellite for remote detection of micrometeoroid and orbital debris impacts, *Acta Astronaut.*, **174**, 24-31, 2020.

Lammer, H., M. Leitzinger, M. Scherf, P. Odert, C. Burger, D. Kubyshkina, C. Johnstone, T. Maindl, C.M. Schäfer, M. Güdel, N. Tosi, A. Nikolaou, E. Marcq, N.V. Erkaev, L. Noack, K.G. Kislyakova, L. Fossati, E. Pilat-Lohinger, F. Ragossnig, E.A. Dorfi: Constraining the early evolution of Venus and Earth through atmospheric Ar, Ne isotope and bulk K/U ratios, *Icarus*, **339**, 113551, 2020.

Lammer, H., M. Scherf, H. Kurokawa, Y. Ueno, C. Burger, T. Maindl, C.P. Johnstone, M. Leizinger, M. Benedikt, L. Fossati, K.G. Kislyakova, B. Marty, G. Avice, B. Fegley, P. Odert: Loss and fractionation of noble gas isotopes and moderately volatile elements from planetary embryos and early Venus, Earth and Mars, *Space Sci. Rev.*, **216**, 74, 2020.

Langer, N., C. Schürmann, K. Stoll, P. Marchant, D.J. Lennon, L. Mahy, S.E. de Mink, M. Quast, W. Riedel, H. Sana, P. Schneider, A. Schootemeijer, C. Wang, L.A. Almeida, J.M. Bestenlehner, J. Bodensteiner, N. Castro, S. Clark, P.A. Crowther, P. Dufton, C.J. Evans, L. Fossati, G. Gräfener, L. Grassitelli, N. Grin, B. Hastings, A. Herrero, A. de Koter, A. Menon, L. Patrick, J. Puls, M. Renzo, A.A.C. Sander, F.R.N. Schneider, K. Sen, T. Shenar, S. Simón-Días, T.M. Tauris, F. Tramper, J.S. Vink, X.-T. Xu: Properties of OB star-black hole systems derived from detailed binary evolution models, *Astron. Astrophys.*, **638**, A39, 2020.

Leitzinger, M., P. Odert, R. Greimel, K. Vida, L. Kriskovics, E.W. Guenther, H. Korhonen, F. Koller, A. Hanslmeier, Z. Kovari, H. Lammer: A census of coronal mass ejections on solar-like stars, *MNRAS*, **493**, 4570-4589, 2020.

Lendl, M., F. Bouchy, S. Gill, L.D. Nielsen, O. Turner, K. Stassun, J.S. Acton, D.R. Anderson, D.J. Armstrong, D. Bayliss, C. Belardi, E.M. Bryant, M.R. Burleigh, A. Chaushev, S.L. Casewell, B.F. Cooke, P. Eigmüller, E. Gillen, M.R. Goad, M.N. Günther, J. Hagelberg, J.S. Jenkins, T. Louden, M. Marmier, J. McCormac, M. Moyano, D. Pollacco, L. Raynard, R.H. Tilbrook, S. Udry, J.I. Vines, R.G. West, P.J. Wheatley, G. Ricker, R. Vanderspek, D.W. Latham, S. Seager, J. Winn, J.M. Jenkins, B. Addison, C. Briceño, R. Brahm, D.A. Caldwell, J. Doty, N. Espinoza, B. Goeke, T. Henning, A. Jordán, A. Krishnamurthy, N. Law, R. Morris, J. Okumura, A.W. Mann, J.E. Rodriguez, P. Sarkis, J. Schlieder, J.D. Twicken, S. Villanueva, R.A. Wittenmyer, D.J. Wright, C. Ziegler: TOI-222: A single-transit TESS candidate revealed to be a 34-d eclipsing binary with CORALIE, EulerCam, and NGTS, *MNRAS*, **492**, 1761-1769, 2020.

Lendl, M., Sz. Csizmadia, A. Deline, L. Fossati, D. Kitzmann, K. Heng, S. Hoyer, S. Salmon, W. Benz, C. Broeg, D. Ehrenreich, A. Fortier, D. Queloz, A. Bonfanti, A. Brandeker, A. Collier Cameron, L. Delrez, A. Garcia Muñoz, M. J. Hooton, P.F.L. Maxted, B.M. Morris, V. Van Grootel, T.G. Wilson, Y. Alibert, R. Alonso, J. Asquier, T. Bandy, T. Bárczy, D. Barrado, S.C.C. Barros, W. Baumjohann, M. Beck, T. Beck, A. Bekkelien, M. Bergomi, N. Billot, F. Biondi, X. Bonfils, V. Bourrier, M.-D. Busch, J. Cabrera, V. Cessa, S. Charnoz, B. Chazelas, C. Corral Van Damme, M.B. Davies, M. Deleuil, O.D.S. Demangeon, B.-O. Demory, A. Erikson, J. Farinato, M. Fridlund, D. Futyan, D. Gandolfi, M. Gillon, P. Guterman, J. Hasiba, E. Hernandez, K.G. Isaak, L. Kiss, T. Kuntzer, A. Lecavelier des Etangs, T. Lüftinger, J. Laskar, C. Lovis, D. Magrin, L. Malvasio, L. Marafatto, H. Michaelis, M. Munari, V. Nascimbeni, G. Olofsson, H. Ottacher, R. Ottensamer, I. Pagano, E. Pallé, G. Peter, D. Piazza, G. Piotto, D. Pollacco, F. Ratti, H. Rauer,

R. Ragazzoni, N. Rando, I. Ribas, M. Rieder, R. Rohlfs, F. Safa, N.C. Santos, G. Scandariato, D. Ségransan, A.E. Simon, V. Singh, A.M.S. Smith, M. Sordet, S.G. Sousa, M. Steller, Gy.M. Szabó, N. Thomas, M. Tschentscher, S. Udry, V. Viotto, I. Walter, N.A. Walton, F. Wildi, D. Wolter: The hot dayside and asymmetric transit of WASP-189 b seen by CHEOPS, *Astron. Astrophys.*, **643**, A94, 2020.

Leto, P., C. Trigilio, C.S. Buemi, F. Leone, I. Pillitteri, L. Fossati, F. Cavallaro, L.M. Oskinova, R. Ignace, J. Krtička, G. Umana, G. Catanzaro, A. Ingallinera, F. Bufano, S. Riggi, L. Cerrigone, S. Loru, F. Schilliró, C. Agliozzo, N.M. Phillips, M. Giarrusso, J. Robrade: The auroral radio emission of the magnetic B-type star ϱ OphC, *MNRAS Letters*, **499**, L72-L76, 2020.

Leto, P., C. Trigilio, F. Leone, I. Pillitteri, C.S. Buemi, L. Fossati, F. Cavallaro, L.M. Oskinova, R. Ignace, J. Krticka, G. Umana, G. Catanzaro, A. Ingallinera, F. Bufano, C. Agliozzo, N.M. Phillips, L. Cerrigone, S. Riggi, S. Loru, M. Munari, M. Gangi, M. Giarrusso, J. Robrade: Evidence for radio and X-ray auroral emissions from the magnetic B-type star rho Oph A, *MNRAS*, **493**, 4657-4676, 2020.

Lhotka,C., N. Rubab, O.W. Roberts, J.C. Holmes, K. Torkar, R. Nakamura: Charging time scales and magnitudes of dust and spacecraft potentials in space plasma scenarios, *Phys. Plasmas*, **27**, 103704, 2020.

Li, W.Y., D.B. Graham, Yu.V. Khotyaintsev, A. Vaivads, M. André, K. Min, K. Liu, B.B. Tang, C. Wang, K. Fujimoto, C. Norgren, S. Toledo-Redondo, P.-A. Lindqvist, R.E. Ergun, R.B. Torbert, A.C. Rager, J.C. Dorelli, D.J. Gershman, B.L. Giles, B. Lavraud, F. Plaschke, W. Magnes, O. Le Contel, C.T. Russell, J.L. Burch: Electron Bernstein waves driven by electron crescents near the electron diffusion region, *Nat. Comm.*, **11**, 141, 2020.

Liu, K., X.J. Hao, Y.R. Li, T.L. Zhang, Z.H. Pan, M.M. Chen, X.W. Hu, X. Li, C.L. Shen, Y.M. Wang: Mars Orbiter magnetometer of China's first Mars mission Tianwen-1, *Earth Planet. Phys.*, **4**, 384-389, 2020.

Liu, T.Z., H. Hietala, V. Angelopoulos, Y. Omelchenko, R. Vainio, F. Plaschke: Statistical study of magnetosheath jet-driven bow waves, *J. Geophys. Res.*, **125**, e2019JA027710, 2020.

Longobardo, A., V. Della Corte, A. Rotundi, M. Fulle, G. Rinaldi, M. Formisano, V. Zakharov, S. Ivanovski, T. Mannel, M. Ciarniello, L. Inno, M. Rubin, E. Palomba, H. Cottin, F. Dirri, P. Palumbo, C. Güttler, S. Merouane, C. Tubiana, B. Pestoni, Z. Dionnet: 67P/Churyumov-Gerasimenko's dust activity from pre- to post-perihelion as detected by Rosetta/GIADA, *MNRAS*, **496**, 125-137, 2020.

Lu, S., R. Wang, Q. Lu, V. Angelopoulos, R. Nakamura, A.V. Artemyev, P.L. Pritchett, T.Z. Liu, X.-J. Zhang, W. Baumjohann, W. Gonzalez, A.C. Rager, R.B. Torbert, B.L. Giles, D.J. Gershman, C.T. Russell, R.J. Strangeway, Y. Qi, R.E. Ergun, P.-A. Lindqvist, J.L. Burch, S. Wang: Magnetotail reconnection onset caused by electron kinetics with a strong external driver, *Nat. Comm.*, **11**, 5049, 2020.

Lukin, A.S., E.V. Panov, A.V. Artemyev, A.A. Petrukovich, S. Haaland, R. Nakamura, V. Angelopoulos, A. Runov, E.V. Yushkov, L.A. Avanov, B.L. Giles, C.T. Russell, R.J. Strangeway: Comparison of the flank magnetopause at near-Earth and Lunar distances: MMS and ARTEMIS observations, *J. Geophys. Res.*, **125**, e2020JA028406, 2020.

Magnes, W., O. Hillenmaier, H.-U. Auster, P. Brown, S. Kraft, J. Seon, M. Delva, A. Valavanoglou, S. Leitner, D. Fischer, G. Berghofer, Y. Narita, F. Plaschke, M. Volwerk, J. Wilfinger, C. Strauch, J. Ludwig, D. Constantinescu, K.-H. Fornacon, K. Gebauer, D. Hercik, I. Richter, J.P. Eastwood, J.P. Luntama, A. Hilgers, M. Heil, G.W. Na, C.H. Lee: Space weather magnetometer aboard GEO-KOMPSAT-2A, *Space Sci. Rev.*, **216**, 119, 2020.

Maksimovic, D., S.D. Bale, T. Chust, Y. Khotyaintsev, V. Krasnoselskikh, M. Kretzschmar, D. Plettemeier, H.O. Rucker, J. Soucek, M. Steller, Š. Štverák, P. Trávnícek, A. Vaivads, S. Chaintreuil, M. Dekkali, O. Alexandrova, P.-A. Astier, G. Barbary, D. Bérard, X. Bonnin, K. Boughedada, B. Cecconi, F. Chapron, M. Chariet, C. Collin, Y. de Conchy, D. Dias, L. Guéguen, L. Lamy, V. Leray, S. Lion, L.R. Malac-Allain, L. Matteini, Q.N. Nguyen, F. Pantellini, J. Parisot, P. Plasson, S. Thijs, A. Vecchio, I. Fratter, E. Bellouard, E. Lorfèvre, P. Danto, S. Julien, E. Guilhem, C. Fiachetti, J. Sanisidro, C. Laffaye, F. Gonzalez, B. Pontet, N. Quéruel, G. Jannet, P. Fergeau, J.-Y. Brochot, G. Cassam-Chenai, T. Dudok de Wit, M. Timofeeva, T. Vincent, C. Agrapart, G.T. Delory, P. Turin, A. Jeandet, P. Leroy, J.-C. Pellion, V. Bouzid, B. Katra, R. Piberne, W. Recart, O. Santolík, I. Kolmašová, V. Krupar, O. Kruparová, D. Píša, L. Uhlír, R. Lán, J. Baše, L. Ahlèn, M. André, L. Bylander, V. Cripps, C. Cully, A. Eriksson, S.-E. Jansson, E.P.G. Johansson, T. Karlsson, W. Puccio, J. Brínek, H. Ottacher, M. Panchenko, M. Berthomier, K. Goetz, P. Hellinger, T.S. Horbury, K. Issautier, E. Kontar, S. Krucker, O. Le Contel, P. Louarn, M. Martinovic, C.J. Owen, A. Retino, J. Rodríguez-Pacheco, F. Sahraoui, R.F. Wimmer-Schweingruber, A. Zaslavsky, I. Zouganelis: The Solar Orbiter Radio and Plasma Waves (RPW) instrument, *Astron. Astrophys.*, **642**, A12, 2020.

Marsch, E., Y. Narita: Dirac equation based on the vector Lorentz group, *Eur. Phys. J. Plus*, **135**, 782, 2020.

Marshall, A.T., J.L. Burch, P.H. Reiff, J.M. Webster, R.B. Torbert, R.E. Ergun, C.T. Russell, R.J. Strangeway, B.L. Giles, R. Nakamura, K.-J. Hwang, K.J. Genestreti: Asymmetric reconnection within a flux rope-type dipolarization front, *J. Geophys. Res.*, **125**, e2019JA027296, 2020.

McCormac, J., E. Gillen, J.A.G. Jackman, D.J.A. Brown, D. Bayliss, P.J. Wheatley, D.R. Anderson, D.J. Armstrong, F. Bouchy, J.T. Briega, M.R. Burleigh, J. Cabrera, S.L. Casewell, A. Chaushev, B. Chazelas, P. Chote, B.F. Cooke, J.C. Costes, S. Csizmadia, P. Eigmüller, A. Erikson, E. Foxell, B.T. Gänsicke, M.R. Goad, M.N. Günther, S.T. Hodgkin, M.J. Hooton, J.S. Jenkins, G. Lambert, M. Lendl, E. Longstaff, T. Louden, M. Moyano, L.D. Nielsen, D. Pollacco, D. Queloz, H. Rauer, L. Raynard, A.M.S. Smith, B. Smalley, M. Soto, O. Turner, S. Udry, J.I. Vines, S.R. Walker, C.A. Watson, R.G. West: NGTS-10b: The shortest period hot Jupiter yet discovered, *MNRAS*, **493**, 126-140, 2020.

Mdzinarishvili, T.G., B.M. Shergelashvili, D.R. Japaridze, B.B. Chargeishvili, A.G. Kosovichev, S.Poedts: Determination of the solar rotation parameters via orthogonal polynomials, *Adv. Space Res.*, **65**, 1843-1851, 2020.

Mecina, M., B. Aringer, W. Nowotny, M.A.T. Groenewegen, F. Kerschbaum, M. Brunner, H.-P. Gail: Extended view on the dust shells around two carbon stars, *Astron. Astrophys.*, **644**, A66, 2020.

Melnik, V.N., H.O. Rucker, A.I. Brazhenko, M. Panchenko, A.A. Konovalenko, A.V. Frantsuzenko3, V.V. Dorovskyy, M.V. Shevchuk: Radio signature of a distant behind-the-limb CME on 2017 September 6, *Astrophys. J.*, **905**, 10, 2020.

Milillo, A., M. Fujimoto, G. Murakami, J. Benkhoff, J. Zender, S. Aizawa, M. Dósa, L. Griton, D. Heyner, G. Ho, S.M. Imber, X. Jia, T. Karlsson, R.M. Killen, M. Laurenza, S.T. Lindsay, S. McKenna-Lawlor, A. Mura, J.M. Raines, D.A. Rothery, N. André, W. Baumjohann, A. Berezhnoy, P.A. Bourdin, E.J. Bunce, F. Califano, J. Deca, S. de la Fuente, C. Dong, C. Grava, S. Fatemi, P. Henri, S.L. Ivanovski, B.V. Jackson, M. James, E. Kallio, Y. Kasaba, E. Kilpua, M. Kobayashi, B. Langlais, F. Leblanc, C. Lhotka, V. Mangano, A. Martindale, S. Massetti, A. Masters, M. Morooka, Y. Narita, J.S. Oliveira, D. Odstrcil, S. Orsini, M.G. Pelizzo, C. Plainaki, F. Plaschke, F. Sahraoui, K. Seki, J.A. Slavin, R. Vainio, P. Wurz, S. Barabash, C.M. Carr, D. Delcourt, K.-H. Glassmeier, M. Grande, M. Hirahara, J. Huovelin, O. Korablev, H. Kojima, H.I.M. Lichtenegger, S. Livi, A. Matsuoka, R. Moiss, M. Moncuquet, K. Muinonen, E. Quèmerais, Y. Saito, S. Yagitani, I. Yoshikawa, J.-E. Wahlund: Investigating Mercury's environment with the two-spacecraft BepiColombo Mission, *Space Sci. Rev.*, **216**, 93, 2020.

Möstl, C., A.J. Weiss, R.L. Bailey, M.A. Reiss, T. Amerstorfer, J. Hinterreiter, M. Bauer, S.W. McIntosh, N. Lugaz, D. Stansby: Prediction of the in situ coronal mass ejection rate for solar cycle 25: Implications for Parker Solar Probe in situ observations, *Astrophys. J.*, **903**, 92, 2020.

Munoz, A.G., A. Youngblood, L. Fossati, D. Gandolfi, J. Cabrera, H. Rauer: Is pi Men c's atmosphere hydrogen-dominated? Insights from a non-detection of H i Ly α absorption, *Astrophys. J. Lett.*, 888, L21, 2020.

Murakami, G., H. Hayakawa, H. Ogawa, S. Matsuda, T. Seki, Y. Kasaba, Y. Saito, I. Yoshikawa, M. Kobayashi, W. Baumjohann, A. Matsuoka, H. Kojima, S. Yagitani, M. Moncuquet, J.-E. Wahlund, D. Delcourt, M. Hirahara, S. Barabash, O. Korablev, M. Fujimoto: Mio - First comprehensive exploration of Mercury's space environment: Mission overview, *Space Sci. Rev.*, **216**, 113, 2020.

Nakamura, T.K.M., F. Plaschke, H. Hasegawa, Y.-H. Liu, K.-J. Hwang, K.A. Blasl, R. Nakamura: Decay of Kelvin-Helmholtz vortices at the Earth's magnetopause under pure southward IMF conditions, *Geophys. Res. Lett.*, **47**, e2020GL087574, 2020.

Nakamura, T.K.M., J.E. Stawarz, H. Hasegawa, Y. Narita, L. Franci, F.D. Wilder, R. Nakamura, W.D. Nystrom: Effects of fluctuating magnetic field on the growth of the Kelvin-Helmholtz instability at the Earth's magnetopause, *J. Geophys. Res.*, **125**, e2019JA027515, 2020.

Narita, Y., O.W. Roberts, Z. Vörös, M. Hoshino: Transport ratios of the kinetic Alfvén mode in space plasmas, *Front. Physics*, **8**, 166, 2020.

Nielsen, L.D., R. Brahm, F. Bouchy, N. Espinoza, O. Turner, S. Rappaport, L. Pearce, G. Ricker, R. Vanderspek, D.W. Latham, S. Seager, J.N. Winn, J.M. Jenkins, J.S. Acton, G. Bakos, T. Barclay, K. Barkaoui, W. Bhatti, C. Briceño, E.M. Bryant, M.R. Burleigh, D.R. Ciardi, K.A. Collins, K.I. Collins, B.F. Cooke, Z. Csubry, L.A. dos Santos, Ph. Eigmüller, M.M. Fausnaugh, T. Gan, M. Gillon, M.R. Goad, N. Guerrero, J. Hagelberg, R. Hart, T. Henning, C.X. Huang, E. Jehin, J.S. Jenkins, A. Jordán, J.F. Kielkopf, D. Kossakowski, B. Lavie, N. Law, M. Lendl, J.P. de Leon, C. Lovis, A.W. Mann, M. Marmier, J. McCormac, M. Mori, M. Moyano, N. Narita, D. Osip, J.F. Otegi, F. Pepe, F.J. Pozuelos, L. Raynard, H.M. Relles, P. Sarkis, D. Ségransan, J.V. Seidel, A. Shporer, M. Stalport, C. Stockdale, V. Suc, M. Tamura, T.G. Tan, R.H. Tilbrook, E.B. Ting, T. Trifonov, S. Udry, A. Vanderburg, P.J. Wheatley, G. Wingham, Z. Zhan, C. Ziegler: Three short-period Jupiters from TESS. HIP 65Ab, TOI-157b, and TOI-169b, *Astron. Astrophys.*, **639**, A76, 2020.

Norgren, C., M. Hesse, D.B. Graham, Yu.V. Khotyaintsev, P. Tenfjord, A. Vaivads, K. Steinvall, Y. Xu, D.J. Gershman, P.-A. Lindqvist, F. Plaschke, J.L. Burch: Electron acceleration and thermalization at magnetotail separatrices, *J. Geophys. Res.*, **125**, e2019JA027440, 2020.

Odert, P., N.V. Erkaev, K.G. Kislyakova, H. Lammer, A.V. Mezentsev, V.A. Ivanov, L. Fossati, M. Leitzinger, D. Kubyshkina, M. Holmström: Modeling the Ly α transit absorption of the hot Jupiter HD 189733b, *Astron. Astrophys.*, **638**, A49, 2020.

Owen, C.J., R. Bruno, S. Livi, P. Louarn, K. Al Janabi, F. Allegrini, C. Amoros, R. Baruah, A. Barthe, M. Berthomier, S. Bordon, C. Brockley-Blatt, C. Brysbaert, G. Capuano, M. Collier, R. DeMarco, A. Fedorov, J. Ford, V. Fortunato, I. Fratter, A.B. Galvin, B. Hancock, D. Heirtzler, D. Kataria, L. Kistler, S.T. Lepri, G. Lewis, C. Loeffer, W. Marty, R. Mathon, A. Mayall, G. Mele, K. Ogasawara, M. Orlandi, A. Pacros, E. Penou, S. Persyn, M. Petiot, M. Phillips, L. Prech, J.M. Raines, M. Reden, A.P. Rouillard, A. Rousseau, J. Rubiella, H. Seran, A. Spencer, J.W. Thomas, J. Trevino, D. Verscharen, P. Wurz, A. Alapide, L. Amoruso, N. André, C. Anekallu, V. Arciuli, K.L. Arnett, R. Ascolese, C. Bancroft, P. Bland, M. Brysch, R. Calvanese, M. Castronuovo, I. Cermák, D. Chornay, S. Clemens, J. Coker, G. Collinson, R. D'Amicis, I. Dandouras, R. Darnley, D. Davies, G. Davison, A. De Los Santos, P. Devoto, G. Dirks, E. Edlund, A. Fazakerley, M. Ferris, C. Frost, G. Fruit, C. Garat, V. Génot, W. Gibson, J.A. Gilbert, V. de Giosa, S. Gradone, M. Hailey, T.S. Horbury, T. Hunt, C. Jacquey, M. Johnson, B. Lavraud, A. Lawrenson, F. Leblanc, W. Lockhart, M. Maksimovic, A. Malpus, F. Marcucci, C. Mazelle, F. Monti, S. Myers, T. Nguyen, J. Rodriguez-Pacheco, I. Phillips, M. Popecki, K. Rees, S.A. Rogacki, K. Ruane, D. Rust, M. Salatti, J.A. Sauvaud, M.O. Stakhiv, J. Stange, T. Stubbs, T. Taylor, J.-D. Techer, G. Terrier, R. Thibodeaux, C. Urdiales, A. Varsani, A.P. Walsh, G. Watson, P. Wheeler, G. Willis, R. F. Wimmer-Schweingruber, B. Winter, J. Yardley, I. Zouganelis: The Solar Orbiter Solar Wind Analyser (SWA) suite, *Astron. Astrophys.*, **642**, A16, 2020.

Owen, J.E., I.F. Shaikhislamov, H. Lammer, L. Fossati, M.L. Khodachenko: Hydrogen dominated atmospheres on terrestrial mass planets: Evidence, origin and evolution, *Space Sci. Rev.*, **216**, 129, 2020.

Owens, M., M. Lang, L. Barnard, P. Riley, M. Ben-Nun, C.J. Scott, M. Lockwood, M.A. Reiss, C.N. Arge, S. Gonzi: A computationally efficient, time-dependent model of the solar wind for use as a surrogate to three-dimensional numerical magnetohydrodynamic simulations, *Solar Phys.*, **295**, 43, 2020.

Panov, E.V., S. Lu, P.L. Pritchett: Understanding spacecraft trajectories through detached magnetotail interchange heads, *J. Geophys. Res.*, **125**, e2020JA027930, 2020.

Perri, S., D. Perrone, E. Yordanova, L. Sorriso-Valvo, W.R. Paterson, D.J. Gershman, B.L. Giles, C.J. Pollock, J.C. Dorelli, L.A. Avanov, B. Lavraud, Y. Saito, R. Nakamura, D. Fischer, W. Baumjohann, F. Plaschke, Y. Narita, W. Magnes, C.T. Russell, R.J. Strangeway, O. Le Contel, Y. Khotyaintsev, F. Valentini: On the deviation from Maxwellian of the ion velocity distribution functions in the turbulent magnetosheath, *J. Plasma Phys.*, **86**, 905860108, 2020.

Pino, L., J.-M. Désert, M. Brogi, L. Malavolta, A. Wyttenbach, M. Line, J. Hoeijmakers, L. Fossati, A.S. Bonomo, V. Nascimbeni, V. Panwar, L. Affer, S. Benatti, K. Biazzo, A. Bignamini, F. Borsa, I. Carleo, R. Claudi, R. Cosentino, E. Covino, M. Damasso, S. Desidera, P. Giacobbe, A. Harutyunyan, A.F. Lanza, G. Leto, A. Maggio, J. Maldonado, L. Mancini, G. Micela, E. Molinari, I. Pagano, G. Piotto, E. Poretti, M. Rainer, G. Scandariato, A. Sozzetti, R. Allart, L. Borsato, G. Bruno, L. Di Fabrizio, D. Ehrenreich, A. Fiorenzano, G. Frustagli, B. Lavie, C. Lovis, A. Magazzù, D. Nardiello, M. Pedani, R. Smareglia: Neutral iron emission lines from the dayside of KELT-9b: The GAPS program with HARPS-N at TNG XX, *Astrophys. J. Lett.*, **894**, L27, 2020.

Plaschke, F., H. Hietala, Z. Vörös: Scale sizes in magnetosheath jets, *J. Geophys. Res.*, **125**, e2020JA027962, 2020.

Plaschke, F., M. Jernej, H. Hietala, L. Vuorinen: On the alignment of velocity and magnetic fields within magnetosheath jets, *Ann. Geophys.*, **38**, 287-296, 2020.

Pollinger, A., C. Amtmann, A. Betzler, B. Cheng, M. Ellmeier, C. Hagen, I. Jernej, R. Lammegger, B. Zhou, W. Magnes: In-orbit results of the Coupled Dark State Magnetometer aboard the China Seismo-Electromagnetic Satellite, *Geosci. Instrum. Method. Data Syst.*, **9**, 275-291, 2020.

Pozuelos, F.J., J.C. Suárez, G.C. de Elía, Z.M. Berdiñas, A. Bonfanti, A. Dugaro, M. Gillon, E. Jehin, M.N. Günther, V. Van Grootel, L.J. Garcia, A. Thuillier, L. Delrez, J.R. Rodón: GJ 273: On the formation, dynamical evolution, and habitability of a planetary system hosted by an M dwarf at 3.75 parsec, *Astron. Astrophys.*, **641**, A23, 2020.

Qin, P., Y. Ge, A. Du, C. Huang, Y. Zhang, H. Luo, J. Ou, T.L. Zhang, L. Shan: Coupling between the magnetospheric dipolarization front and the Earth's ionosphere by ultralow-frequency waves, *Astrophys. J. Lett.*, **895**, L13, 2020.

Raptis, S., T. Karlsson, F. Plaschke, A. Kullen, P.-A. Lindqvist: Classifying magnetosheath jets using MMS: statistical properties, *J. Geophys. Res.*, **125**, e2019JA027754, 2020.

Reiss, M.A., P.J. MacNeice, K. Muglach, C.N. Arge, C. Möstl, P. Riley, J. Hinterreiter, R.L. Bailey, A.J. Weiss, M.J. Owens, T. Amerstorfer, U. Amerstorfer: Forecasting the ambient solar wind with numerical models. II. An adaptive prediction system for specifying solar wind speed near the sun, *Astrophys. J.*, **891**, 165, 2020.

Roberts, O.W., D. Verscharen, Y. Narita, R. Nakamura, Z. Vörös, F. Plaschke: Possible coexistence of kinetic Alfvén and ion Bernstein modes in sub-ion scale compressive turbulence in the solar wind, *Phys. Rev. Research*, **2**, 043253, 2020.

Roberts, O.W., J. Thwaites, L. Sorriso-Valvo, R. Nakamura, Z. Vörös: Higher-order statistics in compressive solar wind plasma turbulence: High-resolution density observations from the Magnetospheric MultiScale mission, *Front. Physics*, **8**, 584063, 2020.

Roberts, O.W., R. Nakamura, K. Torkar, D.B. Graham, D.J. Gershman, J.C. Holmes, A. Varsani, C.P. Escoubet, Z. Vörös, S.Wellenzohn, Y. Khotyaintsev, R.E. Ergun, B.L. Giles: Estimation of the electron density from spacecraft potential during high-frequency electric field fluctuations, *J. Geophys. Res.*, **125**, e2020JA027854, 2020.

Roberts, O.W., R. Nakamura, K. Torkar, Y. Narita, J.C. Holmes, Z. Vörös1, C. Lhotka, C.P. Escoubet, D.B. Graham, D.J. Gershman, Y. Khotyaintsev, P.-A. Lindqvist: Sub-ion scale compressive turbulence in the solar wind: MMS spacecraft potential observations, *Astrophys. J. Suppl. Ser.*, **250**, 35, 2020.

Scherf, M., H. Lammer, N.V. Erkaev, K.E. Mandt, S.E. Thaller, B. Marty: Nitrogen atmospheres of the icy bodies in the solar system, *Space Sci. Rev.*, **216**, 123, 2020.

Schmid, D., F. Plaschke, Y. Narita, D. Heyner, J.Z.D. Mieth, B.J. Anderson, M. Volwerk, A. Matsuoka, W. Baumjohann: Magnetometer in-flight offset accuracy for the BepiColombo spacecraft, *Ann. Geophys.*, **38**, 823-832, 2020.

Schneider, A., N. Stoira, A. Refregier, A.J. Weiss, M. Knabenhans, J. Stadel, R. Teyssier: Baryonic effects for weak lensing. Part I. Power spectrum and covariance matrix, *JCAP*, **2020**, 019, 2020.

Seidel, J.V., D. Ehrenreich, V. Bourrier, R. Allart, O. Attia, H.J. Hoeijmakers, M. Lendl, E. Linder, A. Wyttenbach, N. Astudillo-Defru, D. Bayliss, H.M. Cegla, K. Heng, B. Lavie, C. Lovis, C. Melo, F. Pepe, L.A. dos Santos, D. Ségransan, S. Udry: Hot Exoplanet Atmospheres Resolved with Transit Spectroscopy (HEARTS): V. Detection of sodium on the bloated super-Neptune WASP-166b, *Astron. Astrophys.*, **641**, L7, 2020.

Shaikhislamov, I.F., L. Fossati, M.L. Khodachenko, H. Lammer, A. García Muñoz, A. Youngblood, N.K. Dwivedi, M.S. Rumenskikh: Three-dimensional hydrodynamic simulations of the upper atmosphere of π Men c: Comparison with Ly α transit observations, *Astron. Astrophys.*, **639**, A109, 2020.

Shaikhislamov, I.F., M.L. Khodachenko, H. Lammer, A.G. Berezutsky, I.B. Miroshnichenko, M. Rumenskikh: Three-dimensional modelling of absorption by various species for hot Jupiter HD 209458b, *MNRAS*, **491**, 3435–3447, 2020.

Shergelashvili, B.M., V.N. Melnik, G. Dididze, H. Fichtner, G. Brenn, S. Poedts, H. Foysi, M.L. Khodachenko, T.V. Zaqarashvili: A new class of discontinuous solar wind solutions, *MNRAS*, **496**, 1023-1034, 2020.

Sorathia, K.A., V.G. Merkin, E.V. Panov, B. Zhang, J.G. Lyon, J. Garretson, A.Y. Ukhorskiy, S. Ohtani, M. Sitnov, M. Wiltberger: Ballooning-interchange instability in the near-Earth plasma sheet and auroral beads: Global magnetospheric modeling at the limit of the MHD approximation, *Geophys. Res. Lett.*, **47**, e2020GL088227, 2020.

Sreejith, A.G., L. Fossati, A. Youngblood, K. France, S. Ambily: Ca II H&K stellar activity parameter: A proxy for extreme ultraviolet stellar fluxes, *Astron. Astrophys.*, **644**, A67, 2020.

Staab, D., C.A. Haswell, J.R. Barnes, G. Anglada-Escudé, L. Fossati, J.P.J. Doherty, J. Cooper, J.S. Jenkins, M.R. Díaz, M.G. Soto: A compact multi-planet system around a bright nearby star from the Dispersed Matter Planet Project, *Nat. Astron.*, **4**, 399-407, 2020.

Staples, F.A., I.J. Rae, C. Forsyth, A.R.A. Smith, K.R. Murphy, K.M. Raymer, F. Plaschke, N.A. Case, C.J. Rodger, J.A. Wild, S.E. Milan, S.M. Imber: Do statistical models capture the dynamics of the magnetopause during sudden magnetospheric compressions?, *J. Geophys. Res.*, **125**, e2019JA027289, 2020.

Steindorfer, M.A., G. Kirchner, F. Koidl, P. Wang, B. Jilete, T. Flohrer: Daylight space debris laser ranging, *Nat. Comm.*, **11**, 3735, 2020.

Stüeken, E.E., S.M. Som, M. Claire, S. Rugheimer, M. Scherf, L. Sproß, N. Tosi, Y. Ueno, H. Lammer: Correction to: Mission to planet Earth: The first two billion years, *Space Sci. Rev.*, **216**, 41, 2020.

Stüeken, E.E., S.M. Som, M. Claire, S. Rugheimer, M. Scherf, L. Sproß, N. Tosi, Y. Ueno, H. Lammer: Mission to planet Earth: The first two billion years, *Space Sci. Rev.*, **216**, 31, 2020.

Sulis, S., D. Mary, L. Bigot: 3D magneto-hydrodynamical simulations of stellar convective noise for improved exoplanet detection. I. Case of regularly sampled radial velocity observations, *Astron. Astrophys.*, **635**, A146, 2020.

Sulis, S., M. Lendl, S. Hofmeister, A. Veronig, L. Fossati, P. Cubillos, V. Van Grootel: Mitigating flicker noise in high-precision photometry. I. Characterization of the noise structure, impact on the inferred transit parameters, and predictions for CHEOPS observations, *Astron. Astrophys.*, **636**, A70, 2020.

Szabo, P.S., H. Biber, N. Jaggi, M. Brenner, D. Weichselbaum, A. Niggas, R. Stadlmayr, D. Primetzhofer, A. Nenning, A. Mutzke, M. Sauer, J. Fleig, A. Foelske-Schmitz, K. Mezger, H. Lammer, A. Galli, P. Wurz, F. Aumayr: Dynamic potential sputtering of Lunar analog material by solar wind ions, *Astrophys. J.*, **891**, 100, 2020.

Szabo, P.S., H. Biber, N. Jäggi, M. Wappl, R. Stadlmayr, D. Primetzhofer, A. Nenning, A. Mutzke, J. Fleig, K. Mezger, H. Lammer, A. Galli, P. Wurz, F. Aumayr: Experimental insights into space weathering of Phobos: Laboratory investigation of sputtering by atomic and molecular planetary ions, *J. Geophys. Res. Planets*, **125**, e2020JE006583, 2020.

Toepfer, S., Y. Narita, D. Heyner, P. Kolhey, U. Motschmann: Mathematical foundation of Capon's method for planetary magnetic field analysis, *Geosci. Instrum. Method. Data Syst.*, **9**, 471–481, 2020.

Toepfer, S., Y. Narita, D. Heyner, U. Motschmann: The Capon Method for Mercury's magnetic field analysis, *Front. Physics*, **8**, 249, 2020.

Treumann, R.A., W. Baumjohann: Auroral Kilometric Radiation and electron pairing, *Front. Physics*, **8**, 386, 2020.

Treumann, R.A., W. Baumjohann: Lorentzian entropies and Olbert's κ - distribution, *Front. Physics*, **8**, 221, 2020.

Treumann, R.A., W. Baumjohann: Olbertian partition function in scalar field theory, *Front. Physics*, **8**, 610625, 2020.

Treumann, R.A., W. Baumjohann: Topside reconnection, *Front. Physics*, **8**, 586082, 2020.

Turner, J.D., E.J.W. de Mooij, R. Jayawardhana, M.E. Young, L. Fossati, T. Koskinen, J.D. Lothringer, R. Karjalainen, M. Karjalainen: Detection of ionized calcium in the atmosphere of the ultra-hot Jupiter KELT-9b, *Astrophys. J. Lett.*, **888**, L13, 2020.

Uchava, E.S., A.G. Tevzadze, B.M. Shergelashvili, N.S. Dzhalilov, S. Poedts: Fire-hose instability of inhomogeneous plasma flows with heat fluxes, *Phys. Plasmas*, **27**, 112901, 2020.

Venot, O., V. Parmentier, J. Blecic, P.E. Cubillos, I.P. Waldmann, Q. Changeat, J.I. Moses, P. Tremblin, N. Crouzet, P. Gao, D. Powell, P.-O. Lagage, I. Dobbs-Dixon, M.E. Steinrueck, L. Kreidberg, N. Batalha, J.L. Bean, K.B. Stevenson, S. Casewell, L. Carone: Global chemistry and thermal structure models for the Hot Jupiter WASP-43b and predictions for JWST, *Astrophys. J.*, **890**, 176, 2020.

Vernisse, Y., B. Lavraud, M. Faganello, S. Fadanelli, M. Sisti, F. Califano, S. Eriksson, D.J. Gershman, J. Dorelli, C. Pollock, B. Giles, L. Avanov, J. Burch, J. Dargent, R.E. Ergun, C.J. Farrugia, V. Génot, H. Hasegawa, C. Jacquey, I. Kacem, R. Kieokaew, M. Kuznetsova, T. Moore, T.K.M. Nakamura, W. Paterson, E. Penou, T.D. Phan, C.T. Russell, Y. Saito, J.-A. Sauvaud, S. Toledo-Redondo: Latitudinal dependence of the Kelvin-Helmholtz instability and beta dependence of vortex-induced high-guide field Magnetic Reconnection, *J. Geophys. Res.*, **125**, e2019JA027333, 2020.

Volwerk, M., C. Goetz, F. Plaschke, T. Karlsson, D. Heyner, B. Anderson: On the magnetic characteristics of magnetic holes in the solar wind between Mercury and Venus, *Ann. Geophys.*, **38**, 51-60, 2020.

Wade, G.A., S. Bagnulo, Z. Keszthelyi, C.P. Folsom, E. Alecian, N. Castro, A. David-Uraz, L. Fossati, V. Petit,

M.E. Shultz, J. Sikora: No evidence of a sudden change of spectral appearance or magnetic field strength of the O9.7V star HD 54879, *MNRAS*, **492**, L1-L5, 2020.

Walsh, A.P., T.S. Horbury, M. Maksimovic, C.J. Owen, J. Rodríguez-Pacheco, R.F. Wimmer-Schweingruber, I. Zouganelis, C. Anekallu, X. Bonnin, R. Bruno, I. Carrasco Blázquez, I. Cernuda, T. Chust, A. De Groof, F. Espinosa Lara, A.N. Fazakerley, H.R. Gilbert, R. Gómez-Herrero, G.C. Ho, S. Krucker, S.T. Lepri, G.R. Lewis, S. Livi, P. Louarn, D. Müller, T. Nieves-Chinchilla, H. O'Brien, P. Osuna, P. Plasson, J.M. Raines, A.P. Rouillard, O.C. St. Cyr, L. Sánchez, J. Soucek, A. Varsani, D. Verscharen, C.J. Watson, G. Watson, D.R. Williams: Coordination of the in situ payload of Solar Orbiter, *Astron. Astrophys.*, **642**, A5, 2020.

Wang, G.Q., M. Volwerk, S.D. Xiao, M.Y. Wu, Y.F. Hao, L.J. Liu, G. Wang, Y.Q. Chen, T.L. Zhang: Three-dimensional geometry of the electron-scale magnetic hole in the solar wind, *Astrophys. J. Lett.*, **904**, L11, 2020.

Wang, G.Q., T.L. Zhang, M.Y. Wu, D. Schmid, Y. Hao, M. Volwerk: Roles of electrons and ions in formation of the current in mirror-mode structures in the terrestrial plasma sheet: Magnetospheric Multiscale observations, *Ann. Geophys.*, **38**, 309-318, 2020.

Wang, G.Q., T.L. Zhang, M.Y. Wu, Y.F. Hao, S.D. Xiao, G. Wang, L.J. Liu, Y.Q. Chen, M. Volwerk: Study of the electron velocity inside sub-ion-scale magnetic holes in the solar wind by MMS observations, *J. Geophys. Res.*, **125**, e2020JA028386, 2020.

Wang, G.Q., T.L. Zhang, S.D. Xiao, M.Y. Wu, G. Wang, L.J. Liu, Y.Q. Chen, M. Volwerk: Statistical properties of sub-ion magnetic holes in the solar wind at 1 AU, *J. Geophys. Res.*, **125**, e2020JA028320, 2020.

Xiao, S.D., M.Y. Wu, G.Q. Wang, G.Wang, Y.Q. Chen, T.L. Zhang: Turbulence in the near-Venusian space: Venus Express observations, *Earth Planet. Phys.*, **4**, 82-87, 2020.

Xiao, S.D., M.Y. Wu, G.Q. Wang, Y.Q. Chen, T.L. Zhang: Survey of 1-Hz waves in the near-Venusian space: Venus Express observations, *Planet. Space Sci.*, **187**, 104933, 2020.

Xiao, S.D., T.L. Zhang, Z. Vörös, M.Y. Wu, G.Q. Wang, Y.Q. Chen: Turbulence near the Venusian bow shock: Venus Express observations, *J. Geophys. Res.*, **125**, e2019JA027190, 2020.

Xu, Y.B., L.Y. Zhou, C. Lhotka, W.H. Ip: Asteroid migration due to the Yarkovsky effect and the distribution of the Eos family, *MNRAS*, **493**, 1447-1460, 2020.

Yang, Z., Y.D. Liu, A. Johlander, G.K. Parks, B. Lavraud, E. Lee, W. Baumjohann, R. Wang, J.L. Burch: MMS direct observations of kinetic-scale shock self-reformation, *Astrophys. J. Lett.*, **901**, L6, 2020.

Yordanova, E., Z. Vörös, S. Raptis, T. Karlsson: Current sheet statistics in the magnetosheath, *Front. Astron. Space Sci.*, **7**, 2, 2020.

Young, M.E., L. Fossati, C. Johnstone, M. Salz, H.I.M. Lichtenegger, K. France, H. Lammer, P.E. Cubillos: Observability of ultraviolet NI lines in the atmosphere of transiting Earth-like planets, *Astron. Nachr.*, **341**, 879-886, 2020.

Young, M.E., L. Fossati, T.T. Koskinen, M. Salz, P.E. Cubillos, K. France: Non-local thermodynamic equilibrium transmission spectrum modelling of HD209458b, *Astron. Astrophys.*, **641**, A47, 2020.

Zhang, L.Q., A.T.Y. Lui, W. Baumjohann, C. Wang, J.L. Burch, Yu.V. Khotyaintsev: Anisotropic vorticity within bursty bulk flow turbulence, *J. Geophys. Res.*, **125**, e2020JA028255, 2020.

Zhang, L.Q., W. Baumjohann, Yu.V. Khotyaintsev, J.L. Burch, J. Webster, J.Y. Wang, C. Wang, L. Dai, C.Y. Zhang: BBF deceleration down-tail of X −15 RE from MMS observation, *J. Geophys. Res.*, **125**, e2019JA026837, 2020.

Zhang, X., Y. Wang, M.Y. Boudjada, J. Liu, W. Magnes, Y. Zhou, X. Du: Multi-experiment observations of ionospheric disturbances as precursory effects of the Indonesian Ms6.9 earthquake on August 05, 2018, *Remote Sens.*, **12**, 4050, 2020.

Zhao, S., M. Steindorfer, G. Kirchner, Y. Zheng, F. Koidl, P. Wang, W. Shang, J. Zhang, T. Li: Attitude analysis of space debris using SLR and light curve data measured with single-photon detector, *Adv. Space Res.*, **65**, 1518-1527, 2020.

Zouganelis, I., A. De Groof, A.P. Walsh, D.R. Williams, D. Müller, O.C. St Cyr, F. Auchère, D. Berghmans, A. Fludra, T.S. Horbury, R.A. Howard, S. Krucker, M. Maksimovic, C.J. Owen, J. Rodríguez-Pacheco, M. Romoli, S.K. Solanki, C. Watson, L. Sanchez, J. Lefort, P. Osuna, H.R. Gilbert, T. Nieves-Chinchilla, L. Abbo, O. Alexandrova, A. Anastasiadis, V. Andretta, E. Antonucci, T. Appourchaux, A. Aran, C.N. Arge, G. Aulanier, D. Baker, S.D. Bale, M. Battaglia, L. Bellot Rubio, A. Bemporad, M. Berthomier, K. Bocchialini, X. Bonnin, A.S. Brun, R. Bruno, E. Buchlin, J. Büchner, R. Bucik, F. Carcaboso, R. Carr, I. Carrasco-Blázquez, B. Cecconi, I. Cernuda Cangas, C.H.K. Chen, L.P. Chitta, T. Chust, K. Dalmasse, R.D'Amicis, V. Da Deppo, R. De Marco, S. Dolei, L. Dolla, T. Dudok de Wit, L. van Driel-Gesztelyi, J.P. Eastwood, F. Espinosa Lara, L. Etesi, A. Fedorov, F. Félix-Redondo, S. Fineschi, B. Fleck, D. Fontaine, N.J. Fox, A. Gandorfer, V. Génot, M.K. Georgoulis, S. Gissot, A. Giunta, L. Gizon, R. Gómez-Herrero, C. Gontikakis, G. Graham, L. Green, T. Grundy, M. Haberreiter, L.K. Harra, D. M. Hassler, J. Hirzberger, G.C. Ho, G. Hurford, D. Innes, K. Issautier, A.W. James, N. Janitzek, M. Janvier, N. Jeffrey, J. Jenkins, Y. Khotyaintsev, K.-L. Klein, E.P. Kontar, I. Kontogiannis, C. Krafft, V. Krasnoselskikh, M. Kretzschmar, N. Labrosse, A. Lagg, F. Landini, B. Lavraud, I. Leon, S.T. Lepri, G.R. Lewis, P. Liewer, J. Linker, S. Livi, D.M. Long, P. Louarn, O. Malandraki, S. Maloney, V. Martinez-Pillet, M. Martinovic, A. Masson, S. Matthews, L. Matteini, N. Meyer-Vernet, K. Moraitis, R.J. Morton, S. Musset, G. Nicolaou, A. Nindos, H. O'Brien, D. Orozco Suarez, M. Owens, M. Pancrazzi, A. Papaioannou, S. Parenti, E. Pariat, S. Patsourakos, D. Perrone, H. Peter, R.F. Pinto, C. Plainaki, D. Plettemeier, S.P. Plunkett, J.M. Raines, N. Raouafi, H. Reid, A. Retino, L. Rezeau, P. Rochus, L. Rodriguez, L. Rodriguez-Garcia, M. Roth, A.P. Rouillard, F. Sahraoui, C. Sasso, J. Schou,

U. Schühle, L. Sorriso-Valvo, J. Soucek, D. Spadaro, M. Stangalini, D. Stansby, M. Steller, A. Strugarek, Š. Štverák, R. Susino, D. Telloni, C. Terasa, L. Teriaca, S. Toledo-Redondo, J.C. del Toro Iniesta, G. Tsiropoula, A. Tsounis, K. Tziotziou, F. Valentini, A. Vaivads, A. Vecchio, M. Velli, C. Verbeeck, A. Verdini, D. Verscharen, N. Vilmer, A. Vourlidas, R. Wicks, R.F. Wimmer-Schweingruber, T. Wiegelmann, P.R. Young, A.N. Zhukov: The Solar Orbiter science activity plan. Translating solar and heliospheric physics questions into action, *Astron. Astrophys.*, **642**, A3, 2020.

BOOKS

Zhiming C., S. Duan, M. Dunlop, P. Escoubet, H. Fu, K. Fujimoto, W. Gonzalez, D. Graham, J. He, M. Hesse, S. Huang, K.-J. Hwang, L. Kepko, Y. Khotyaintsev, G. Lapenta, H. Li, M. Li, Q. Lu, R. Nakamura, T. Phan, A. Retino, V. Angelopoulos, V. Vasyliunas, C. Wang, R. Wang, H. Zhang, and M. Zhou, Cross-Scale Measurements Of Space Plasmas To Explore Magnetic Reconnection, Ed. L. Baldis, International Space Science Institute, Beijing, 66 p., 2020.

PROCEEDINGS & BOOK CHAPTERS

Besser B.P., M.Y. Boudjada, M.E. Lippitsch, and S. Draxler, Graz and Kepler - working, living, and commemoration, In: *Harmony and Symmetry. Celestial Regularities Shaping Human Culture. Proceedings of the SEAC 2018 Conference in Graz*, Eds. S. Draxler, M.E. Lippitsch, and G. Wolfschmidt, tredition, Hamburg, 276-282, 2020.

Besser B.P., Raketentechnik, Naturwissenschaft und Schuld, In: *Schuld. Interdisziplinäre Perspektiven auf ein Konstitutivum des Menschseins*, Eds. S.M. Bachhiesl, C. Bachhiesl und S. Köchel, Velbrück Wissenschaft, Weilerswist-Metternich, 81-91, 2020.

Nesterov S.A., V.V. Denisenko, M.Y. Boudjada, and H. Lammer, The models of the quasistationary electric field penetration from the ground to the middle latitudes ionosphere, In: *Proceedings VII International Conference "Atmosphere, Ionosphere, Safety" (AIS-2020)*, Eds. O.P. Borchevkina, M.G. Golubkov, and I.V. Karpov, Kaliningrad, 76-78, 2020.

Thermal stress test of black surface coating in liquid nitrogen (© ÖAW/Klaus Pichler).

PERSONNEL

Acaro Narvaez, Andrea Stefania, BSc
Agú, Martin A., Dipl.-Ing.
Aickara Gopinathan, Sreejith, Dr.
Amerstorfer, Tanja, Dr.
Amerstorfer, Ute, Dr.
Aydogar, Özer, Dipl.-Ing.
Bauer, Maike, BSc
Baumjohann, Wolfgang, Prof.
Berghofer, Gerhard, Ing.
Besser, Bruno P., Dr.
Bonfanti, Andrea, Dr.
Boudjada, Mohammed Y., Dr.
Cordelli, Emiliano, PhD
Cubillos, Patricio E., Dr.
Dionatos, Odyssefs, Dr.
Eichelberger, Hans U., Dr.
Fabian, Peter
Fischer, David, Dipl.-Ing.
Fischer, Georg, Dr.
Flock, Barbara, Mag.
Fossati, Luca, Doz.
Fremuth, Gerhard, Dipl.-Ing.
Giner, Franz, Dipl.-Ing.
Graf, Christian, Ing.
Gratzer, Alexander J.
Grill, Claudia
Hagen, Christian, Dipl.-Ing.
Hasiba, Johann, Dipl.-Ing.
Hinterreiter, Jürgen, Dipl.-Ing.
Höck, Eduard, Dipl.-Ing.
Hofmann, Karl, Dipl.-Ing.
Hofwimmer, Thomas, Ing.
Hosner, Martin, MSc
Hradecky, Doris
Jernej, Irmgard, Ing.
Jeszenszky, Harald, Dipl.-Ing.
Kargl, Günter, Dr.
Kaufmann, Erika, Dr.
Khodachenko, Maxim L., Dr.
Kiehas, Stefan, Dr.
Kirchner, Georg, Dr.
Koidl, Franz, Ing.
Kürbisch, Christoph, Ing.
Laky, Gunter, Dipl.-Ing.
Lammer, Helmut, Doz.
Leichtfried, Mario, Ing.
Leitner, Stefan, Dipl.-Ing.
Lichtenegger, Herbert I.M., Dr.
Macher, Wolfgang, Dr.
Magnes, Werner, Dr.
Mannel, Thurid, Dr.
Mautner, David
Mecina, Marko, Mag.
Möstl, Christian, Dr.
Muck, Cosima
Nakamura, Rumi, Doz.
Narita, Yasuhito, Doz.
Neukirchner, Sonja, Ing.
Nischelwitzer-Fennes, Ute, Ing.
Ottacher, Harald, Dipl.-Ing.
Pitterle, Martin
Plaschke, Ferdinand, Dr.
Pollinger, Andreas, Dr.
Posch, Oliver F.
Reiss, Martin A., Dr.
Roberts, Owen W., Dr.
Scherf, Manuel, Mag.
Scherr, Alexandra, Mag.
Scherzer, Maximilian, MSc
Schirninger, Christoph, BSc
Schmid, Daniel, Dr.
Simon Wedlund, Cyril Laurent, Dr.
Stachel, Manfred, Dipl.-Ing.
Steinberger, Michael, Dipl.-Ing.
Steindorfer, Michael, Dr.
Steller, Manfred B., Dr.
Stieninger, Reinhard, Ing.
Teubenbacher, Daniel, BSc
Tonfat Seclen, Jorge L., Dr.
Tschachler, Elvira, Mag.
Tschernitz, Raphael, BSc
Valavanoglou, Aris, Dipl.-Ing.
Varsani, Ali, Dr.
Voller, Wolfgang G., Mag.
Volwerk, Martin, Dr.
Vörös, Zoltan, Dr.
Wallner, Robert, Ing.
Wang, Peiyuan, MSc
Weiss, Andreas J., MSc
Wilfinger, Josef, BSc
Zhang, Tie-Long, Prof.

As of 31 December 2020

IMPRESSUM

PUBLISHER

Wolfgang Baumjohann, Director
Institut für Weltraumforschung (IWF)
Österreichische Akademie der Wissenschaften (ÖAW)
Schmiedlstraße 6, 8042 Graz, Austria
www.oeaw.ac.at/iwf
Twitter: @IWF_oeaw

EDITORS

Bruno Besser, Alexandra Scherr, Martin Volwerk

DESIGN

Alexandra Scherr
pr.iwf@oeaw.ac.at

PRINT

Servicebetrieb ÖH-Uni Graz GmbH


ÖAW IWF